7-25-2012

Microstructure of Systems with Competition

Saurish Chakrabarty
Washington University in St. Louis

WASHINGTON UNIVERSITY IN ST. LOUIS

Department of Physics

Dissertation Examination Committee:
Zohar Nussinov, Chair
Kenneth F. Kelton
Ronald Lovett
Michael C. Ogilvie
Alexander Seidel
Jung-Tsung Shen

Microstructure of Systems with Competition

by

Saurish Chakrabarty

A dissertation presented to the
Graduate School of Arts and Sciences
of Washington University in
partial fulfillment of the
requirements for the degree
of Doctor of Philosophy

August 2012

Saint Louis, Missouri

ABSTRACT OF THE DISSERTATION

Microstructure of Systems with Competition

by

Saurish Chakrabarty

Doctor of Philosophy in Physics

Washington University in St. Louis, 2012

Professor Zohar Nussinov, Chairperson

The micro-structure of systems with competition often exhibits many universal features. In this thesis, we study certain aspects of these structural features as well as the microscopic interactions using disparate exact and approximate techniques. This thesis can be broadly divided into two parts.

In the first part, we use statistical mechanics arguments to make general statements about length and timescales in systems with two-point interactions. We demonstrate that at high temperatures, the correlation function of general $O(n)$ systems exhibits a universal form. This form enables the extraction of microscopic interaction potentials from the high temperature correlation functions. In systems with long range interactions, we find that the largest correlation length diverges in the limit of high temperatures. We derive an exact form for the correlation function in large-n systems with general two-point interactions at finite temperatures. From this, we obtain some features of the correlation and modulation lengths in general systems in the large-n limit. We derive a new exponent characterizing modulation lengths (or times) in systems in which the modulation length (or time) either diverges or becomes

constant as a parameter, such as temperature exceeds a threshold value.

In the second part of this thesis, we study the micro-structure of a metallic glass system using molecular dynamics simulations. We use both classical and first principles simulation to obtain atomic configurations in the liquid as well as the glassy phase. We analyze these using standard methods of local structure analysis – calculation of pair correlation function and structure factor, Voronoi construction, calculation of bond orientational order parameters and calculation of Honeycutt indices. We show the enhancement of icosahedral order in the glassy phase. Apart from this, we also use the techniques of community detection to obtain the inherent structures in the system using an algorithm which allows us to look at arbitrary length-scales.

Acknowledgements

First of all, I would like to thank my father Tapan Kumar Chakrabarty, my mother Dipa Chakrabarty and my sister Patrali Chakrabarty for providing great support and encouragement. I also thank Dida, Jethu, Mama, Mani and Mamoni.

My roommates Manojit and Poulomi made living in St Louis a lot of fun along with Shatadal, Tanika, Satyaki, Mrinmoyda, Maitrayee, Somendra, Satya, Pinaki, Nidhi, Debajit, Sudeshna and Kumar and my classmates Adam Hajari, Ben Burch, Narelle, David Shane, Hiromichi, Seth, Dimitris, Dihui, Wei, Amber and Jason. I thank the physics mentors of 2006-07 for frequently taking us out for free food. Special thanks to the "Mesh" members – Subhadip, Zoheb and Mainak Mukherjee. Many thanks to Rudresh, Santi, Mainak Das, Shradha, Aditi, Krishanu, Sanhita, Mithun and Girish.

I thank my past teachers S. K. Bhattacharyya and Ananda Dasgupta for inspiring me to pursue a career in physics.

Thanks to all my committee members – Ken Kelton, Ronald Lovett, Mike Ogilvie, Alex Seidel and JT Shen.

I thank Mike Widom and Marek Mihalkovič for teaching me numerous computational methods. I also thank Mike for his hospitality during my stay at Pittsburgh.

I thank my group members – Peter, Dandan and Patrick, my former group members Matt, Adam Eggebrecht, Sebastian, Jing, Shouting and Blake, and my former adviser Ralf Wessel.

Special thanks to Julia and Sarah. Sai has taught me a lot of Linux tricks and I thank him greatly for that.

My office was a great place to work in. For that I thank Seth, Mark, Hiromichi, Zhenyu, Julia, Shouting, Dan, Hossein and Sophia.

Lastly, I thank my adviser Zohar Nussinov for being a great inspiration. With his great versatility, he can come up with a new research idea every time a student meets him.

To my father, mother and sister.

Contents

List of Figures

List of Tables

Chapter 1

Introduction

The understanding of the internal structure of systems is one of the important goals in multiple branches of physics. The study of correlation functions of a relevant field forms one of the means to achieve this goal. Fortunately, there lies a lot of universality in such findings.[10–12] This universality could relate to the form which the correlation function takes, its behavior as some parameter defining the system is varied, the length or time scales which characterize it, or in some other property that may be important depending on the system being studied.

This thesis focuses on the structural features of a variety of systems, mainly by studying the behavior of relevant correlation functions both in real and Fourier spaces.

1.1 Correlation functions

Typically, the first step in studying a physical system is the recognition of a suitable order parameter $\phi(\vec{x})$. In the study of most[13] phase transitions, for example, this order parameter is chosen in such a way that its thermodynamic expectation value vanishes on one side of the phase transition. Calculating the expectation value of the order parameter is, however, not always enough when we are interested in properties of a system in situations in which it is not undergoing a phase transition. The correlation function is one of the most straightforward quantities that can be calculated to quantify, in general, order that is present in a system.

The correlation function could be studied in many contexts. First, there is the two-point correlation function $G(\vec{x}) \equiv \langle \phi(0)\phi(\vec{x}) \rangle$ which in translationally invariant systems (e.g., liquids and various lattice systems in the absence of disorder), is associated with the correlation between sites separated by $\vec{x}$. Second, there is the pair correlation function $g(r)$ describing the average atomic number densities at a distance r away from a chosen atom in systems such as liquids. The propagator in $\mathcal{G}(\vec{x}, t)$ in quantum mechanics also represents the correlation between states at two space-time points separated by $(\vec{x}, t)$. Other forms of the correlation function which are not discussed in this thesis, have been used in disparate arenas. Many of our results, however, pertain to general correlation functions and may apply to various systems which we do not discuss in detail. In this thesis, we will be interested in studying the

first two kinds of correlation functions [i.e., $G(\vec{x})$ and $g(r)$]. The work in Chapters 3, 4 and 5 relates to the two-point correlation function $G(\vec{x})$. The configurations of metallic glasses studied in Chapters 6 and 7 can be studied by looking at the pair correlation function $g(r)$ and a related Fourier space quantity $S(q)$.

1.2 Structural features and universality

In statistical physics, models with short range interactions have been at the focus of much study for many decades. Perhaps one of the best known examples are the Ising ferromagnet and the anti-ferromagnet.[14] In nature, long range interactions are equally abundant.[15] Systems in which both long and short range interactions co-exist constitute fascinating problems. Such competing interactions can lead to a wealth of interesting patterns – stripes, bubbles, etc.[16–21] Realizations are found in numerous fields – quantum Hall systems,[22] adatoms on metallic surfaces, amphiphilic systems,[23–26] interacting elastic defects (dislocations and disclinations) in solids,[27] interactions amongst vortices in fluid mechanics[28] and superconductors,[29] crumpled membrane systems,[2] wave-particle interactions,[30, 31] interactions amongst holes in cuprate superconductors,[32–36] arsenide superconductors,[37] manganates and nickelates,[38, 39] some theories of structural glasses,[40–44] colloidal systems,[45, 46] and many more. Much of the work to date focused on the character of the transitions in these systems and the subtle thermodynamics

that is often observed (e.g., the equivalence between different ensembles in many such systems is no longer as obvious, nor always correct, as it is in the canonical short range case.[47]) Other very interesting aspects of different systems have been addressed in Ref. [48].

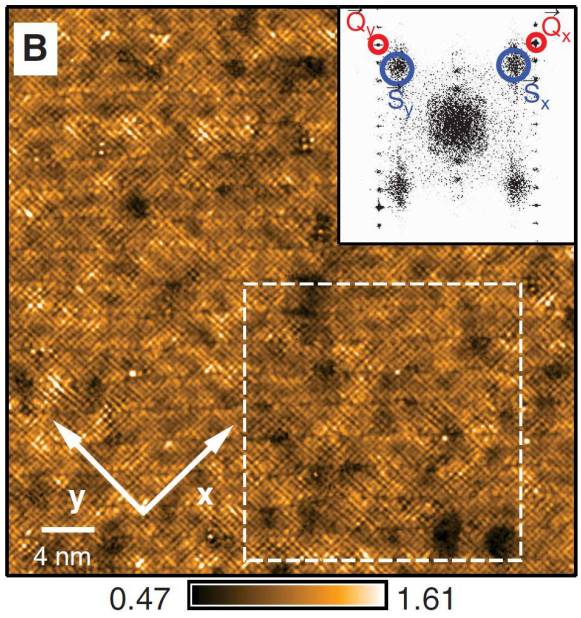

Figure 1.1: Sub-unit-cell resolution image of the electronic structure of a cuprate superconductor at the pseudo-gap energy. Inset shows Fourier space image of the same figure. Nematic and smectic phases are highlighted using the red and blue circles respectively. The nematic phase is characterized by commensurate wave-vectors $\vec{Q}$. The smectic wave-vector, on the other hand takes incommensurate values, $\vec{S}$ which is dependent on the amount of doping, albeit weakly. (From Ref. [1]. Reprinted with permission from AAAS.)

In complex systems, there are, in general, possibly many important length and

time scales that characterize correlations. Aside from correlation lengths describing the exponential decay of correlations, in some materials there are length scales that characterize periodic spatial modulations or other spatially non-uniform properties as in Fig. 1.1.

1.3 Structure of liquids and glasses

In many situations, the study of two-point correlation functions fails to give us the complete picture. Gauge theories (for which the two-point correlation function is trivially zero [49, 50]) as well as numerous systems with "topological order" fall into this category.[51, 52] In the systems of interest in this work, the structural details of the system often have features which are not evident in the pair correlation function. One such example is the liquid-to-glass transition. The pair correlation function of a liquid system looks very similar to that of a glass. This does not mean that there is no structural difference between liquids and glasses. Frank, in 1952, hypothesized that metallic glasses have increased icosahedral order as compared with liquids.[53] However, to be able to notice these (subtle) differences one must go beyond pair-correlation-function-studies. Higher order correlation functions (e.g., four-point correlation functions in space-time [54]) sometimes may capture these differences. The techniques we use to analyze the structure in liquids and glasses is more direct. We take various approaches to study the structure of the liquid and glassy systems. These

are listed below.

- ***Bond-orientational order parameter*** W_6**.** The orientation of bonds around atoms in liquids and glasses is different.[55] For example, in many metallic glass systems, there is an increase in icosahedral order as the liquid is vitrified. The quantity W_6 (which will be defined in Chapter 6) provides us a strong measure of viable icosahedral order.

- ***Voronoi analysis.*** This is a method to obtain the region of space which is closer to a chosen atom than any other atom.[56] The shapes of such regions characterizes the kind of structural order present in a given system. In crystals, the Voronoi cells are uniform (and are termed Wigner-Seitz cells) and are of great importance in understanding electronic and other properties. We will use this as one of our means to quantify icosahedral order in a system.

- ***Honeycutt-Anderson analysis*** Honeycutt-Anderson analysis is a way to look at the local environment around bonds in a system.[57] This will also be used to characterize local order in the liquid and glassy systems which we will study.

- ***Community detection.*** This is a new method that we have introduced. We will use the techniques of multi-resolution community detection[6] to obtain pertinent structures at various resolutions in liquid and glassy systems. The optimum resolutions for our systems will also be computed using such methods.

1.4 Outline

In Chapter 2, we introduce the translationally invariant systems which we focus on in Chapters 3, 4 and 5.

In Chapter 3, we examine correlation functions in the high temperature limit. We derive a universal form of the correlation function of $O(n)$ systems and use it to obtain some interesting results. The material presented in this chapter has been published.[58]

In Chapter 4, we derive a universal form of the Fourier space correlation function in the large-n limit (spherical model) and from it extract general behaviors of length scales at finite temperatures. The material presented in this chapter has been published.[59]

In Chapter 5, we discuss the presence of a universal exponent characterizing various crossovers in systems where the correlation function changes from exhibiting fixed wavelength modulations to continuously varying modulation lengths as the temperature (or some other general parameter λ) is varied.

In Chapter 6, we study a metallic glass system through molecular dynamics simulations. We look at the local structure and observe the change in icosahedral order in high and low temperature systems, corresponding respectively to liquid and glassy phases.

In Chapter 7, we use the techniques of community detection to find out the per-

tinent length scales in a metallic glass system and look at the local structure of the liquid and glassy systems at those resolutions. The material presented in this chapter has been published.[60, 61]

Chapter 2

Systems of study

2.1 Introduction

This chapter contains a general introduction to the systems we study along with the definitions of the various terms we use. These will be used in chapters 3, 4 and 5 of this thesis.

2.2 Systems of study

In the bulk of this thesis, we will be interested in translationally invariant systems whose Hamiltonian, in general, takes the form,

$$H = \frac{1}{2} \sum_{\vec{x} \neq \vec{y}} V(|\vec{x} - \vec{y}|) \vec{S}(\vec{x}) \cdot \vec{S}(\vec{y}). \tag{2.1}$$

In the continuum, this takes the form,

$$H = \frac{1}{2} \int d^d x \; d^d y \; V(|\vec{x} - \vec{y}|) \; \vec{S}(\vec{x}) \cdot \vec{S}(\vec{y}). \tag{2.2}$$

The quantities $\{\vec{S}(\vec{x})\}$ portray n-component spins or fields. The sites $\vec{x}$ and $\vec{y}$ lie on a d-dimensional hypercubic lattice with unit lattice constant. The number of sites is N.

The two point correlation function for the system in Eq. (2.1) is defined as,

$$G(\vec{x}) = \frac{1}{n} \langle \vec{S}(0) \cdot \vec{S}(\vec{x}) \rangle. \tag{2.3}$$

For large distances $x = |\vec{x}|$, the correlation function typically behaves as,

$$G(x) \approx \sum_i f_i(x) \cos\left(\frac{2\pi x}{L_D^{(i)}}\right) e^{-x/\xi_i}, \tag{2.4}$$

where for the i-th term, $f_i(x)$ is an algebraic prefactor, $L_D^{(i)}$ is the modulation length and ξ_i is the corresponding correlation length. There can be multiple correlation and modulation lengths.

Fourier space variables

We will use $v(k)$ and $\vec{s}(\vec{k})$ to denote the Fourier transforms of $V(|\vec{x} - \vec{y}|)$ and $\vec{S}(\vec{x})$ respectively. The Fourier transform convention used here is that,

$$\begin{aligned} a(\vec{k}) &= \sum_{\vec{x}} A(\vec{x}) e^{i\vec{k}\cdot\vec{x}}, \text{ and} \\ A(\vec{x}) &= \frac{1}{N} \sum_{\vec{k}} a(\vec{k}) e^{-i\vec{k}\cdot\vec{x}}. \end{aligned} \tag{2.5}$$

The Hamiltonian in Eq. (2.1) can be rewritten as,

$$H = \frac{1}{2N} \sum_{\vec{k}} v(k) \vec{s}(\vec{k}) \cdot \vec{s}(-\vec{k}). \tag{2.6}$$

When $v(\vec{k})$ is analytic in all momentum space coordinates, it is a function of $|\vec{k}|^2 = k^2$ (and not a general function of $k \equiv \sqrt{\sum_{l=1}^{d} k_l^2}$ with $\{k_l\}$ being the Cartesian components of $\vec{k}$). This is so as $|\vec{k}|$ has branch cuts when viewed as a function of a particular k_l (with all other $k_{l' \neq l}$ held fixed). The lattice Laplacian that links nearest neighbors sites in real space becomes

$$\Delta_{\vec{k}} = 2 \sum_{l=1}^{d} (1 - \cos k_l) \tag{2.7}$$

in k-space. $\Delta_{\vec{k}}$ veers towards $|\vec{k}|^2$ in the continuum (small k) limit.

In the Fourier space, the correlation function takes the form,

$$G(\vec{k}) = \frac{1}{Nn} \langle \vec{s}(\vec{k}) \cdot \vec{s}(-\vec{k}) \rangle. \tag{2.8}$$

The modulation and correlation lengths can be obtained respectively from the real and imaginary parts of the singularities (poles and branch points) of $G(\vec{k})$ in the complex k-plane.

2.3 *O(n)* systems and the large-*n* limit

Heisenberg spins or $O(n)$ spins refer to n-component spins whose magnitude is constrained to be a constant. This constraint makes the calculation of the correlation

function (and hence other related physical quantities) much easier to handle. We choose the normalization adopted by Stanley in Ref. [62].

$$\vec{S}(\vec{x}) \cdot \vec{S}(\vec{x}) = n. \tag{2.9}$$

For Ising spins, $n = 1$. For XY spins, $n = 2$, and so on.

The large n limit of the $O(n)$ spins is equivalent to the spherical model first introduced by Berlin and Kac [63]. This equivalence was established in the work of Stanley [62].

The single component spherical model is given by the Hamiltonian,

$$H = \frac{1}{2} \sum_{\vec{x} \neq \vec{y}} V(|\vec{x} - \vec{y}|) S(\vec{x}) S(\vec{y}). \tag{2.10}$$

The spins in Eq.(2.10) satisfy a single global ("spherical") constraint,

$$\sum_{\vec{x}} S^2(\vec{x}) = N. \tag{2.11}$$

The results that will be derived in this work apply to a variety of systems. These include theories with trivial n-component generalizations of Eq. (2.1). In the bulk of this work, the Hamiltonian has a bilinear form in the spins. We will however, later on, study "soft" spin model with explicit finite quartic terms as we now expand on. An n-component generalization of Eq. (2.1) is given by the Hamiltonian

$$\begin{aligned} H &= \frac{1}{2} \sum_{\vec{x} \neq \vec{y}} V(|\vec{x} - \vec{y}|) \vec{S}(\vec{x}) \cdot \vec{S}(\vec{y}) + \\ &\quad \frac{u}{4} \sum_{\vec{x}} \left(\vec{S}(\vec{x}) \cdot \vec{S}(\vec{x}) - n \right)^2. \end{aligned} \tag{2.12}$$

Such a Hamiltonian represents standard (or "hard") spin or $O(n)$ systems if $u \gg 1$ in the large u limit, the quartic term enforces a "hard" normalization constraint of the particular form $\vec{S}(\vec{x}) \cdot \vec{S}(\vec{x}) = n$. For finite (or small) u, Equation (2.12) describes "soft"-spin systems wherein the normalization constraint is not strictly enforced.

2.4 Obtaining correlation and modulation lengths from the momentum space correlation function

The correlation function in d-dimensional position space, $G(\vec{x})$ is related to that in the momentum space, $G(\vec{k})$ by,

$$G(\vec{x}) = \frac{1}{N} \sum_{\vec{k}} G(\vec{k})\ e^{-i\vec{k}\cdot\vec{x}}. \tag{2.13}$$

In the continuum, this takes the form,

$$G(\vec{x}) = \int \frac{d^d k}{(2\pi)^d} G(\vec{k}) e^{-i\vec{k}\cdot\vec{x}}. \tag{2.14}$$

For spherically symmetric systems, i.e., $G(\vec{k}) = G(k)$, we have,

$$G(x) \;\; = \;\; \int_0^\infty \frac{k^{d-1} dk}{(2\pi)^{d/2}} \frac{\mathrm{J}_{d/2-1}(kx)}{(kx)^{d/2-1}} G(k), \tag{2.15}$$

and $\mathrm{J}_\nu(x)$ is a Bessel function of order ν. The above integral can be evaluated by choosing an appropriate contour in the complex k-plane. The contour can be closed

along a circular arc of radius $R \to \infty$. The contribution from this curved part of the contour is zero if,

$$|G(k)| \lesssim k^{-\frac{d+1}{2}}, \text{ as } k \to \infty. \tag{2.16}$$

After the integral is evaluated, we get terms in the position space correlation function which are the residues associated with the poles of the momentum space correlation function as well as contributions from its branch points. Together, we can summarize that all characteristic lengthscales in position space are determined by,

$$\boxed{\frac{1}{G^{(m)}(K)} = 0}, \tag{2.17}$$

where K is complex and $0 \leq m < \infty$ is the smallest order of the derivative of $G(k)$ which diverges at $k = K$. Eq. (2.17) is a way of including all points of nonanalyticity of the k-space correlation function in the complex k-plane. [Note: $m = 0$ for the poles of $G(k)$ and $m \geq 0$ for the branch points.] The correlation and modulation lengths in the system are determined respectively by the imaginary and real parts of such Ks.

The arguments made here hold for systems defined in the continuum. Extensions to lattice systems is straightforward.

Chapter 3

High temperature correlation functions

3.1 Introduction

All systems veer towards a disordered fixed point in the limit of high temperatures. There are a lot of interesting physics observed at temperatures close to various transitions. As such, a lot of research has been devoted to studying the behavior of disparate systems at and in the vicinity of these finite temperature transitions.

In this chapter, we will focus on high temperature behavior and illustrate that a simple form of the two-point correlation function is universally exact for rather general systems. This will enable us to make several striking observations. In particular, we will demonstrate that in contrast to common intuition, general systems with long

range interactions have a correlation length that increases monotonically with temperature as $T \to \infty$. As they must, however, the correlations decay monotonically with temperature (as the corresponding amplitudes decay algebraically with temperature). There have been no earlier reports of diverging correlation lengths at high temperature. A thermally increasing length-scale of a seemingly very different sort appears in plasmas [64]. The Debye length λ_D, the distance over which screening occurs in a plasma, diverges, at high temperature, as $\lambda_D \propto \sqrt{T}$. We introduce the notion of a *generalized Debye length* associated with disparate long range interactions (including confining interactions) and show that such screening lengths are rather general.

Many early works investigated the high temperature disordered phase via a high temperature series expansion [65, 66] with an eye towards systems with short range interactions. In this chapter, we report on our universal result for the Fourier transformed correlation function for systems with general pair interactions. As it must, for nearest neighbor interactions, our correlation function agrees with what is suggested by standard approximate methods (e.g., the Ornstein-Zernike (OZ) correlation function that may be derived by many approximate schemes [67]). This work places such approximate results on a more rigorous footing and, perhaps most notably, enables us to go far beyond standard short range interactions to find rather surprising results. Our derivations will be done for spin and other general lattice systems with multi-component fields. However, as illustrated later, our results also pertain to continuum

theories.

3.2 The universal form of the high temperature correlation functions

We now derive a universal form for the correlation function at high temperature. As in any other calculation with Boltzmann weights, the high temperature limit is synonymous with weak coupling. Initially, we follow standard procedures and examine a continuous but exact dual theory. High T (or weak coupling) in the original theory corresponds to strong coupling in the dual theory. We will then proceed to examine the consequences of the dual theory at high temperature where the strong coupling interaction term dominates over other non-universal terms that depend, e.g., on the number of components in the original theory. This enables an analysis with general results. Unlike most treatments that focus on the character of various phases and intervening transitions, our interest here is strictly in the *high temperature limit of the correlation functions* in rather general theories of Eq. (2.1). Our aims are **(i)** to make conclusions concerning systems with long range interactions rigorous and **(ii)** to extract microscopic interactions from measurements. It is notable that due to convergence time constraints many numerical approaches, e.g., Ref. [68], compare candidate potentials with experimental data at high temperature (above the melting temperatures) where the approach that we will outline is best suited. We will perform

a transformation to a continuous but exact dual theory where the high temperature character of the original theory can be directly examined.

We augment the right hand side of Eq. (2.1) by $[-\sum_{\vec{x}} \vec{h}(\vec{x})\cdot\vec{S}(\vec{x})]$ and differentiate in the limit $\vec{h}\to 0$ to obtain correlation functions in the usual way.

$$\begin{aligned} G(\vec{x}-\vec{y}) &= \frac{1}{n}\left\langle \vec{S}(\vec{x})\cdot\vec{S}(\vec{y})\right\rangle \\ &= \lim_{h\to 0}\frac{1}{n\beta^2 Z}\sum_{i=1}^{n}\frac{\delta^2 Z}{\delta h_i(\vec{x})\delta h_i(\vec{y})}, \end{aligned} \tag{3.1}$$

with Z the partition function in the presence of the external field $\vec{h}$. By spin normalization, $G(\vec{x})=1$ for $\vec{x}=0$. The index $i=1,2,...,n$ labels the n internal spin (or field) components. The partition function

$$Z = \mathrm{Tr}_S\left[\exp\left(-\frac{\beta}{2N}\sum_{\vec{k}} v(\vec{k})|\vec{s}(\vec{k})|^2+\beta\sum_{\vec{x}}\vec{h}(\vec{x})\cdot\vec{S}(\vec{x})\right)\right]. \tag{3.2}$$

The subscript S denotes the trace with respect to the spins. Using the Hubbard-Stratonovich (HS) transformation, [69–71] we introduce the dual variables $\{\vec{\eta}(\vec{x})\}$ and rewrite the partition function as

$$\begin{aligned} Z = \mathrm{Tr}_S\Bigg[\prod_{\vec{k},i}\Big([2\pi(-v(\vec{k}))]^{-1/2}\ \times \\ \int_{-\infty}^{\infty} d\eta_i(\vec{k}) e^{\frac{N}{2\beta v(\vec{k})}\left|\eta_i(\vec{k})\right|^2+\eta_i(\vec{k})s_i(-\vec{k})}\Big)\prod_{\vec{x}} e^{\beta\vec{h}(\vec{x})\cdot\vec{S}(\vec{x})}\Bigg] \end{aligned} \tag{3.3}$$

$$\begin{aligned} = \mathcal{N}\ \mathrm{Tr}_S\left[\int d^{Nn}\eta \exp\left(\frac{N^2}{2\beta}\sum_{\vec{x},\vec{y}} V^{-1}(\vec{x}-\vec{y})\vec{\eta}(\vec{x})\cdot\vec{\eta}(\vec{y})\right.\right. \\ \left.\left. +\ N\sum_{\vec{x}}\vec{\eta}(\vec{x})\cdot\vec{S}(\vec{x})+\beta\sum_{\vec{x}}\vec{h}(\vec{x})\cdot\vec{S}(\vec{x})\right)\right], \end{aligned} \tag{3.4}$$

with $V^{-1}(\vec{x})$ the inverse Fourier transform of $1/v(\vec{k})$ and $\mathcal{N}$ a numerical prefactor. The physical motivation in performing the duality to the HS variables is that we wish to retain the exact character of the theory [i.e., the exact form of the interactions and the $O(n)$ constraints concerning the spin normalization at all lattice sites]. It is for this reason that we do not resort to a continuum approximation (such as that of the canonical ϕ^4 theory that we will discuss for comparison later on) where normalization is not present. Another reason to choose to work in the dual space is the correspondence with field theories which, in the dual space, becomes clearer in the high temperature limit (in which the quartic term of the ϕ^4 theories becomes irrelevant). Further details are in Ref. [72]. For $O(n)$ spins,

$$\begin{aligned} Z &= \mathcal{N}' \int d^{Nn}\eta \\ &\quad \left[\exp\left(\frac{N^2}{2\beta} \sum_{\vec{x},\vec{y}} V^{-1}(\vec{x}-\vec{y}) \vec{\eta}(\vec{x}) \cdot \vec{\eta}(\vec{y}) \right) \times \right. \\ &\quad \left. \prod_{\vec{x}} \frac{I_{n/2-1}(\sqrt{n}|N\vec{\eta}(\vec{x}) + \beta\vec{h}(\vec{x})|)}{(\sqrt{n}|N\vec{\eta}(\vec{x}) + \beta\vec{h}(\vec{x})|)^{n/2-1}} \right]. \end{aligned} \tag{3.5}$$

The second factor in Eq. (3.5) originates from the trace over the spins and as such embodies the $O(n)$ constraints (the trace in Eq. (3.4) is performed over all configurations with $[\vec{S}(\vec{x})]^2 = n$ at all sites $\vec{x}$). Here, $I_\nu(x)$ is the modified Bessel function of the first kind. In the Ising ($n = 1$) case, the argument of the product in Eq. (3.5) is a hyperbolic cosine. Up to an innocuous additive constant, Eq. (3.5) corresponds to

the dual Hamiltonian,

$$\begin{aligned} H_d &= -\frac{N^2}{2\beta^2}\sum_{\vec{x},\vec{y}} V^{-1}(\vec{x}-\vec{y})\vec{\eta}(\vec{x})\cdot\vec{\eta}(\vec{y}) \\ &\quad -\frac{1}{\beta}\sum_{\vec{x}} \ln\left(\frac{I_{n/2-1}(\sqrt{n}|N\vec{\eta}(\vec{x})+\beta\vec{h}(\vec{x})|)}{(\sqrt{n}|N\vec{\eta}(\vec{x})+\beta\vec{h}(\vec{x})|)^{n/2-1}}\right). \end{aligned} \tag{3.6}$$

Our interest is in the $h \to 0$ limit. The first term in Eq. (3.6) is the same for all n. This term dominates, at low β, over the (second) n dependent term. As we will see, this dominance will enable us to get universal results for all n. From Eq. (3.1), and the identity

$$\frac{d}{dx}\left[\frac{I_\nu(x)}{x^\nu}\right] = \frac{I_{\nu+1}(x)}{x^\nu},$$

we find that

$$\begin{aligned} G(\vec{x}-\vec{y}) = \delta_{\vec{x},\vec{y}} + (1-\delta_{\vec{x},\vec{y}})\Bigg\langle \frac{\vec{\eta}(\vec{x})\cdot\vec{\eta}(\vec{y})}{|\vec{\eta}(\vec{x})||\vec{\eta}(\vec{y})|} \times \\ \frac{I_{n/2}(N\sqrt{n}|\vec{\eta}(\vec{x})|)I_{n/2}(N\sqrt{n}|\vec{\eta}(\vec{y})|)}{I_{n/2-1}(N\sqrt{n}|\vec{\eta}(\vec{x})|)I_{n/2-1}(N\sqrt{n}|\vec{\eta}(\vec{y})|)}\Bigg\rangle_d, \end{aligned} \tag{3.7}$$

where the average $(\langle . \rangle_d)$ is performed with the weights $\exp(-\beta H_d)$. Now, here is a crucial idea regarding our exact dual forms. From Eq. (3.3), *at high temperature*, the variables $\eta_i(\vec{k})$ strictly have sharply peaked Gaussian distributions of variance,

$$\left\langle \left|\eta_i(\vec{k})\right|^2 \right\rangle_d \approx \frac{-\beta v(\vec{k})}{N} \text{ as } \beta \to 0. \tag{3.8}$$

Importantly, this variance tends to zero as $\beta \to 0$. By Parseval's theorem and trans-

lational invariance,

$$\begin{aligned}\left\langle (\eta_i(\vec{x}))^2 \right\rangle_d &= \frac{1}{N}\sum_{\vec{x}} \left\langle (\eta_i(\vec{x}))^2 \right\rangle_d \\ &= \frac{1}{N^2}\sum_{\vec{k}} \left\langle \left|\eta_i(\vec{k})\right|^2 \right\rangle_d \approx -\beta V(0)/N^2\end{aligned}$$

Thus, at high temperature, $\langle[\eta_i(\vec{x})]^2\rangle \ll 1$. It is therefore useful to perform a series expansion in the dual variables η and this will give rise to a high temperature series expansion in the correlation function. The Hamiltonian in dual space is given by

$$\begin{aligned}H_d &= -\frac{N^2}{2\beta^2}\sum_{\vec{x},\vec{y}} V^{-1}(\vec{x}-\vec{y})\vec{\eta}(\vec{x})\cdot\vec{\eta}(\vec{y}) - \frac{N^2}{2\beta}\sum_{\vec{x},i}\eta_i(\vec{x})^2, \\ &= -\frac{N}{2\beta^2}\sum_{\vec{k},i}\frac{1}{v(\vec{k})}\left|\eta_i(\vec{k})\right|^2 - \frac{N}{2\beta}\sum_{\vec{k},i}\left|\eta_i(\vec{k})\right|^2, \end{aligned} \tag{3.9}$$

with errors of $\mathcal{O}(1/T)$. Expanding Eq. (3.7) to $\mathcal{O}(1/T^2)$,

$$\boxed{G(\vec{k}) = \frac{k_B T}{v(\vec{k}) + k_B T} + \frac{1}{N}\sum_{\vec{k'}}\frac{v(\vec{k'})}{v(\vec{k'}) + k_B T}.} \tag{3.10}$$

Equation(3.10) leads to counter-intuitive consequences for systems with long-range interactions. The second term in Eq. (3.10) is independent of $\vec{k}$ and ensures that $G(\vec{x}) = 1$ for $\vec{x} = 0$. Inverting this result enables us to find the microscopic (spin exchange or other) interactions from the knowledge of the high temperature correlation function. We thus flesh out (and further generalize for multicomponent systems such as spins) the mathematical uniqueness theorem of Henderson for fluids [73] for which a known correlation function $G(\vec{x})$ leads to a known pair potential function $V(\vec{x})$ up to an innocuous constant. Equation(3.10) leads to a correlation function which is

independent of $V(0)$. Therefore, we can shift $v(\vec{k})$ for all $\vec{k}$'s by an arbitrary constant or equivalently set $V(0)$ to an arbitrary constant. To $\mathcal{O}(1/T)$, for $V(0) = 0$, we have,

$$v(\vec{k}) = \frac{k_B T}{G(\vec{k})} - \frac{1}{N} \sum_{\vec{k'}} \frac{k_B T}{G(\vec{k'})}. \tag{3.11}$$

The leading term of this expression for $v(\vec{k})$ does not scale with T. This is so as $[1 - G(\vec{k})] \propto 1/T$ at high temperatures. Correlation functions obtained from experimental data can be plugged into the right hand side to obtain the effective pair potentials. Alternatively, in real space, for $\vec{x} \neq 0$,

$$\boxed{V(\vec{x}) = -k_B T G(\vec{x}) + k_B T \sum_{\vec{x'} \neq 0, \vec{x}} G(\vec{x'}) G(\vec{x} - \vec{x'})} \tag{3.12}$$

Note that the two terms in Eq. (3.12) are $\mathcal{O}(1)$ and $\mathcal{O}(1/T)$ respectively, since $G(\vec{x})$ is proportional to $1/T$ at high temperature for $\vec{x} \neq 0$. Extension to higher orders may enable better comparison to experimental or numerical data. Our expansion is analytic in the high temperature phase (i.e., so long as no transitions are encountered as $1/T$ is increased from zero). The Gaussian form of Eq. (3.9) similarly leads to the free energy density,

$$F = \frac{k_B T}{2N} \sum_{\vec{k}} \ln \left| \frac{k_B T}{v(\vec{k})} + 1 \right| + \mathcal{O}(1/T). \tag{3.13}$$

Armed with Eqs. (3.9) and (3.10), we can compute any correlation function with the aid of Wick's theorem. For example, for unequal $\vec{k_i}$s, we have, $\langle (\vec{s}(k_1) \cdot \vec{s}(-k_1)) ... (\vec{s}(k_m) \cdot \vec{s}(-k_m)) \rangle = (Nn)^m \prod_{i=1}^{m} G(\vec{k_i})$.

It is straightforward to carry out a full high temperature series expansion of the correlation function to arbitrary order. This is outlined in Appendix A. For example, when $V(\vec{x}=0)=0$, the real space correlation function for separations $\vec{x}\neq 0$ is, to order $\mathcal{O}(1/T^3)$, given by

$$\begin{aligned} G(\vec{x}) &= -\frac{V(\vec{x})}{k_BT}+\frac{1}{(k_BT)^2}\sum_{\vec{z}}V(\vec{z})V(\vec{x}-\vec{z}) \\ &\quad -\frac{1}{(k_BT)^3}\left[\sum_{\vec{y},\vec{z}}V(\vec{y})V(\vec{z})V(\vec{x}-\vec{y}-\vec{z})\right. \\ &\quad \left.-2V(\vec{x})\sum_{\vec{z}}V(\vec{z})V(-\vec{z})+2\frac{(V(\vec{x}))^3}{n+2}\right]. \end{aligned} \tag{3.14}$$

3.3 High temperature correlation lengths

We now illustrate that **(i)** in systems with short (or finite range) interactions, the correlation length tends to zero in the high temperature limit and **(ii)** in systems with long range interactions [74] the high temperature correlation length tends to the screening length and diverges in the absence of screening.

3.3.1 Decaying lengthscales

We consider first the standard case of short range interactions. On a hyper-cubic lattice in d spatial dimensions, nearest neighbor interactions have the lattice Laplacian $\Delta(\vec{k})=2\sum_{l=1}^{d}(1-\cos k_l)$, with k_l the l-th Cartesian component of the wave-vector $\vec{k}$ as their Fourier transform. In the continuum (small k) limit, $\Delta\sim|\vec{k}|^2$. Gen-

erally, in the continuum, arbitrary finite range interactions of spatial range p have $v(\vec{k}) \sim |\vec{k}|^{2p}$ with $p > 0$ (and superpositions of such terms) as their Fourier transforms. In general finite range interactions, similar multi-nomials in $(1-\cos k_l)$ and in k_l^2 appear on the lattice and the continuum respectively. For simplicity, we consider $v(\vec{k}) \sim |\vec{k}|^{2p}$. Correlation lengths are determined by the reciprocal of the imaginary part of the poles of Eq. (3.10), $|\text{Im } \{k_*\}|^{-1}$. We then find that in the complex k plane, $(k_*)^{2p} \sim -k_B T$. Poles are given by $k_* \sim (k_B T)^{1/(2p)} \exp[(2m+1)\pi i/(2p)]$ with $m = 0, 1, ..., 2p-1$. Correlation lengths then tend to zero in the high temperature limit as $\xi \sim T^{-1/(2p)}/|\sin(2m+1)\pi/(2p)|$ – there are p such correlation lengths. Similarly, there are p periodic modulation lengths scaling as $L_D \sim 2\pi T^{-1/(2p)}/|\cos(2m+1)\pi/(2p)|$. The usual case of $p = 1$ corresponds to an infinite L_D [i.e., spatially uniform (non-periodic) correlations] and $\xi \sim T^{-1/2}$.

3.3.2 Diverging lengthscales

An unusual feature arises in the high temperature limit of systems with long range interactions where $v(\vec{k})$ diverges in the small k limit. Such a divergence enables the correlator of Eq. (3.10) to have a pole at low k and consequently, on Fourier transforming to real space, to have a divergent correlation length. In the presence of screening $v(\vec{k})$ diverges and $G(k)$ has a pole when the imaginary part of k is equal to the reciprocal of the screening length. The correlation length then tends to the screening length at high temperature. For concreteness, we consider generic screened

interactions where the Fourier transformed interaction kernel $v_L(k) \sim \frac{1}{(k^2+\lambda^{-2})^{p'}}$ with $p' > 0$ and λ the screening length. Perusing the poles of Eq. (3.10), we find that for all p', the correlation lengths tend to the screening length in the high temperature limit,

$$\boxed{\lim_{T\to\infty} \xi(T) = \lambda.} \tag{3.15}$$

From Eq. (3.15), when λ becomes arbitrarily large, the *correlation length diverges*. Physically, such correlations enable global "charge neutrality" [75] for the corresponding long range interactions (Coulomb or other). It is notable that in several systems, e.g., [76], neutrality or (Gauss-like) constraints between charges (or defects) lead to algebraic correlations. In the high temperature limit, the bare interactions are faint relative to the temperatures yet constraints of charge neutrality may lead to weak long range correlations. This general divergence of high temperature correlation lengths in systems with long range interactions is related to the effective range of the interactions. At high temperature, the correlation function matches the "direct" contribution, $e^{-\beta V_{eff}(\vec{r})} - 1 \sim -\beta V_{eff}(\vec{r})$. If the effective interactions between two fields have a range λ, then that is reflected in the correlation length. In Coulomb systems, the Debye length λ_D sets the range of the interactions (for large distances, the interactions are screened). As stated earlier, at high temperature, λ_D diverges. As we see by Fourier transforming Eq. (3.10), although the imaginary part of the poles tends to zero (and thus the correlation lengths diverge), the prefactor multi-

plying $e^{-|\vec{x}|/\xi}$ is a monotonically decaying function of T. Thus in the high temperature limit the real space correlator $G(\vec{x})$ monotonically decays with temperature (as it must). For instance, for $p' = 1$ in $d = 3$ dimensions, the pair correlator $G(x) \sim e^{-x/\lambda}/(Tx)$ tends, for any non-zero x, to zero as $T \to \infty$. That is, *the amplitude vanishes* in the high temperature limit as $(1/T)$. We find similar results when we have more than one interaction. For instance, in the presence of both a short and a long range interaction, (at least) two correlation lengths are found. One correlation length (or, generally, set of correlation lengths) tends to zero in the high temperature limit (as for systems with short range interactions) while the other correlation length (or such set) tends to the screening length (as we find for systems with long range interactions). An example of a system where this can be observed is the screened "Coulomb frustrated ferromagnet", [33, 34] given by the Hamiltonian $H = [-J \sum_{\langle \vec{x},\vec{y} \rangle} S(\vec{x})S(\vec{y}) + Q \sum_{\vec{x} \neq \vec{y}} V_L(|\vec{x} - \vec{y}|)S(\vec{x})S(\vec{y})]$, with $J, Q > 0$ and the long range interaction $V_L(x) = \frac{e^{-x/\lambda}}{x}$ in $d = 3$ dimensions and $V_L(x) = K_0(x/\lambda)$ in $d = 2$ with λ the screening length and K_0 a modified Bessel function of the second kind. Similar dipolar systems [16, 18, 19] have been considered. Apart from the usual correlation length that vanishes in the high temperature limit, we find an additional correlation length that tends to the screening length λ.

3.4 Generalized Debye length (and time) scales

We now introduce the notion of generalized Debye length (and time) scales that are applicable to general systems with effective or exact long range interactions. These extend the notion of a Debye length from Coulomb type system where it is was first found. If the Fourier space interaction kernel $v(k)$ in a system with long range interactions is such that $\frac{1}{v(k)}$ is analytic at $k = 0$, then the system has a diverging correlation length, ξ_{long} at high temperature. To get the characteristic diverging lengthscales, we consider the self-consistent small k solutions to $k_BT/v(k) = -1$ for high temperature (which gives the poles in the correlation function). Thus, as $T \to \infty$, ξ_{long} diverges as $\sqrt[p]{k_BT}$, where p is the order of the first non-zero term in the Taylor series expansion of $\frac{1}{v(k)}$ around $k = 0$. This divergent length-scale could be called the generalized Debye length. If the long-range interactions in the system are of Coulomb type, then this corresponds to the usual Debye length λ_D where $p = 2$. A more common way to obtain this result is as follows. Suppose we have our translationally invariant system which interacts via pairwise couplings as in Eq. (2.1). We can define a potential function for this system as,

$$\phi(\vec{x}) = \sum_{\vec{y},\vec{y}\neq\vec{x}} V(|\vec{x}-\vec{y}|)S(\vec{y}). \tag{3.16}$$

The "charge" $S(\vec{x})$ in the system is perturbed by an amount $\hat{S}(\vec{x})$ and we observe the response $\hat{\phi}(\vec{x})$ in the potential function $\phi(\vec{x})$ assuming that we stay within the regime of linear response. We assume that $S(\vec{x})$ follows a Boltzmann distribution,

i.e., $S(\vec{x}) = A\exp\left(-\beta C\phi(\vec{x})\right)$, where C is a constant depending on the system. It follows that $\hat{S}(\vec{x}) = -\beta C S(\vec{x})\hat{\phi}(\vec{x})$. At this point, we can ignore the fluctuations in $S(\vec{x})$ as they do not contribute to the leading order term. Thus, $\hat{S}(\vec{x}) = -\beta C S_0\hat{\phi}(\vec{x})$, where $S_0 = \langle S(\vec{x})\rangle$. In Fourier space, this leads to the relation,

$$\hat{\phi}(\vec{k}) = -\beta C S_0 v(\vec{k})\hat{\phi}(\vec{k}) \tag{3.17}$$

The modes with non-zero response are therefore given by,

$$\boxed{-v(\vec{k}) \propto k_B T.} \tag{3.18}$$

For a Coulomb system, these modes are given by $(-k^{-2}) \propto k_B T$, yielding a correlation length $\lambda_D \propto \sqrt{k_B T}$.

As a brief aside, we discuss what occurs when the above considerations (and also those to be detailed anew in Sec. 3.6.1) are applied to an imaginary time action of a complex field ψ that has the form,

$$S_{action} = \frac{1}{2}\int d\tau d\tau' d^d x d^d x' \Big[\psi(x,\tau) K(x-x',\tau-\tau')\psi(x',\tau')\Big] + ... \quad . \tag{3.19}$$

In the above, the imaginary time coordinates $0 \leq \tau, \tau' \leq \beta$ with a kernel K that is long range in space or imaginary time and the ellipsis denoting higher order terms (e.g., generic $|\psi|^4$ type terms) or imposing additional constraints on the fields ψ [such as normalization that we have applied thus far for $O(n)$ systems]. In such a case, the associated Debye length (or imaginary time) scale may diverge in the weak coupling

(i.e., $K \to aK$ with $a \to 0^+$) limit. In an analogous way, repeating all of the earlier calculations done thus far for spatial correlations, we find divergent correlation times in the low coupling limit for systems with a kernel K that is long range in $|\tau - \tau'|$. An action such as that of Eq. (3.19) may also describe a system at the zero temperature limit (whence $\beta \to \infty$) and the (imaginary) time scale is unbounded.

In Appendix B, we will relate the divergence of the *generalized Debye type length scales* in the high temperature limit to a similar divergence in the largest correlation length in systems with long range interactions.

Confining potentials

We discussed long range interactions (with, in general, a screening which may be set to be arbitrarily small) such as those that arise in plasma, dipolar systems, and other systems in condensed matter physics. In all of these systems, the long range potentials dropped monotonically with increasing distance. Formally, we may consider generalizations which further encompass confining potentials such as those that capture the effective confining potentials in between quarks in quantum chromodynamics (QCD) as well as those between charges in one dimensional Coulomb systems (where the effective potentials associated with the electric flux tubes in one dimension lead to linear potentials). The derivations that we carried through also hold in such cases. For instance, in a one-dimensional Coulomb system, the associated linear potential $V(x) \sim |x|$ leads to the usual Coulomb Fourier space kernel $v(k) \sim k^{-2}$. In general,

for a potential $V(x) \sim |\vec{x}|^{-a}$ in d spatial dimensions, the corresponding Fourier space kernel is, as in the earlier case, $v(k) \sim |\vec{k}|^{-p}$, where $p = d - a$. Following the earlier discussion, this leads, at asymptotically high temperatures (and for infinitesimal screening), to correlation lengths that scale as $\xi \sim \sqrt[p]{T}$. In the presence of screening, the correlation length at infinite temperature saturates and is equal to the screening length. Similarly, as seen by Eq. (3.18), the generalized Debye screening length scales in precisely the same manner. In Eq. (B-13), we comment on the relation between the two scales.

3.5 Generalizations

Here we illustrate how our results can be generalized to systems which do not fall into the class of systems introduced in Sec. 2.2.

3.5.1 Disorder

When Eq. (2.1) is replaced by a system with non-translationally invariant exchange couplings $V(\vec{x}, \vec{y}) \equiv \langle \vec{x}|V|\vec{y}\rangle$, then V will be diagonal in an orthonormal basis ($|\vec{u}\rangle$) different from the momentum space eigenstates, i.e., $V|\vec{u}\rangle = v(\vec{u})|\vec{u}\rangle$. Our derivation will be identical in the $|\vec{u}\rangle$ basis. In particular, Eq. (3.10) will be the same with $v(\vec{k})$ replaced by $v(\vec{u})$.

3.5.2 Fluids

Our results can be directly applied to fluids. In this case the spin at each site in Eq. (2.1) may be replaced by the local mass density. The pair structure factor $S(k)$ is the same as the Fourier space correlation function $G(k)$ [77]. For $r \neq 0$, the pair distribution function $g(r)$ is related to the correlation function $G(r)$ defined above as

$$g(r) = G(r) + 1. \tag{3.20}$$

For $r = 0$, $g(r) = 0$.

3.5.3 General multi-component interactions

In the case of systems with multiple interacting degrees of freedom at each lattice site, we have a similar result. We consider, for instance, the non-rotationally invariant $O(n)$ Hamiltonian,

$$H = \frac{1}{2} \sum_{\vec{x} \neq \vec{y}} \sum_{a,b} V_{ab}(\vec{x}, \vec{y}) S_a(\vec{x}) S_b(\vec{y}), \tag{3.21}$$

where the interactions $V_{ab}(\vec{x}, \vec{y})$ depend on the spin components $1 \leq a, b \leq n$ as well as the locations $\vec{x}$ and $\vec{y}$. By fiat, in Eq. (3.21), $V_{ab}(\vec{x} = \vec{y}) = 0$. Non-rotationally symmetric interactions such as those of Eq. (3.21) with a kernel V_{ab} which is not proportional to the identity matrix in the internal spin space $1 \leq a, b \leq n$ appear in, e.g., Dzyaloshinsky-Moriya interactions [78, 79], isotropic [80] and non-isotropic compasses [81], Kugel-Khomskii- [80, 82] and Kitaev-type [83] models. Such interactions also appear in continuous and discretized non-Abelian gauge backgrounds (and

scalar products associated with metrics of curved surfaces) used to describe metallic glasses and cholesteric systems. [43, 44, 84–92]. The lattice "soccer ball" spin model [43] is precisely of the form of Eq. (3.21). Replicating the calculations leading to Eq. (A-9), for $\vec{x} \neq \vec{y}$, to $\mathcal{O}(1/T^2)$, we find that

$$\begin{aligned} G_{ab}(\vec{x},\vec{y}) &= \langle S_a(\vec{x}) S_b(\vec{y}) \rangle \\ &= -\frac{V_{ab}(\vec{x},\vec{y})}{k_B T} + \frac{1}{(k_B T)^2} \sum_{c,\vec{z}} V_{ac}(\vec{x},\vec{z}) V_{cb}(\vec{z},\vec{y}). \end{aligned} \tag{3.22}$$

Correspondingly, in Fourier space, this explicitly takes the form

$$G_{ab}(\vec{k}) = \delta_{ab} - \frac{v_{ab}(\vec{k})}{k_B T} + \frac{1}{(k_B T)^2} \sum_{c} v_{ac}(\vec{k}) v_{cb}(\vec{k}). \tag{3.23}$$

3.5.4 Bose/Fermi gases

Here we discuss Bose and Fermi systems to illustrate the generality of our result from Eq. (3.10). We consider the Hamiltonian given by

$$H = H_0 + H_I,$$

where

$$\begin{aligned} H_0 &= \sum_{\vec{x}} \hat{\psi}^\dagger(\vec{x}) \frac{\mathbf{p}^2}{2m} \hat{\psi}(\vec{x}), \\ H_I &= \frac{1}{2} \sum_{\vec{x},\vec{x}'} \hat{\rho}(\vec{x}) V(\vec{x}-\vec{x}') \hat{\rho}(\vec{x}'), \end{aligned} \tag{3.24}$$

with $\hat{\rho}(\vec{x}) = \hat{\psi}^\dagger(\vec{x})\hat{\psi}(\vec{x}) - \langle \hat{\psi}^\dagger \hat{\psi} \rangle_0$.

Here and throughout, $\langle \cdot \rangle_0$ denotes an average with respect to H_0 (the ideal gas Hamiltonian). The fields ψ obey appropriate statistics(Bose-Einstein or Fermi-Dirac)

depending on the system being studied. The standard partition function is

$$Z = Z_0 \int D\eta(\vec{x},\tau)\ e^{-\beta\Phi}. \tag{3.25}$$

Here, τ is the standard imaginary time coordinate ($0 \le \tau \le \beta$). Z_0 is the partition function of the non-interacting system described by H_0, and the η's are the dual fields after performing the HS transformation. We can express Φ as

$$\begin{aligned}\Phi = &-\frac{N^2}{2\beta^3}\int_0^\beta d\tau \sum_{\vec{x},\vec{x}'} \eta(\vec{x},\tau)V^{-1}(\vec{x}-\vec{x}')\eta(\vec{x}',\tau) \\ &-\frac{N}{\beta}\ln\left\langle T_\tau \exp\left(\frac{1}{\beta}\int_0^\beta d\tau \sum_{\vec{x}} \eta(\vec{x},\tau)\hat{\rho}(\vec{x},\tau)\right)\right\rangle_0 .\end{aligned} \tag{3.26}$$

where T_τ is the (imaginary) time-ordering operator. It is clear that the factor of the partition function which controls high temperature behavior comes from the first term in Φ. Thus, for small β (high temperature), Φ of Eq. (25) results in a distribution of the values of η which is sharply peaked around $\eta = 0$. Also, for small β, the integrands of Eq. (3.27) have little dependence on τ. Therefore, at high temperature,

$$\begin{aligned}\Phi = -\frac{N^2}{2\beta^2}\sum_{\vec{x},\vec{x}'} \eta(\vec{x}) \big[&V^{-1}(\vec{x}-\vec{x}') \\ &+\beta A(\vec{x}-\vec{x}')\big]\,\eta(\vec{x}'),\end{aligned} \tag{3.27}$$

where $A(\vec{x}-\vec{x}') = \langle\rho(\vec{x})\rho(\vec{x}')\rangle_0 = C\delta_{\vec{x},\vec{x}'}$, with $C = \rho_0^2$ being a constant. The correlation function for this system is defined as $G(\vec{x}-\vec{y}) = \langle\rho(\vec{x})\rho(\vec{y})\rangle$, It is easy to show that written in terms of the dual variables,

$$G(\vec{x}-\vec{y}) = \left\langle \frac{f'(N\eta(\vec{x}))}{f(N\eta(\vec{x}))}\frac{f'(N\eta(\vec{y}))}{f(N\eta(\vec{y}))}\right\rangle_d , \tag{3.28}$$

where $f(a) = \mathrm{Tr}_{\rho(\vec{x})}\ e^{a\rho(\vec{x})}$ and, as before, $\langle\cdot\rangle_d$ denotes the average with respect to the dual fields η. For small values of the η variables (high temperature), we have in general, $G(\vec{x}-\vec{y}) = C_0 + C_1\langle\eta(\vec{x})\eta(\vec{y})\rangle_d$, with C_0 chosen such that $G(\vec{x}) = C$ for $\vec{x} = 0$ and C_1 defined by the statistics of ρ and the form of the pair interaction V. Therefore, we have,

$$\begin{aligned} G(\vec{k}) &= C + \frac{C_1 k_B T}{C[Cv(\vec{k}) + k_B T]} \\ &\quad -\frac{1}{N}\sum_{\vec{k}} \frac{C_1 k_B T}{C[Cv(\vec{k}) + k_B T]}. \end{aligned} \tag{3.29}$$

This is similar to the classical $O(n)$ correlation function in Fourier space [Eq. (3.10)]. We can easily generalize Eq. (3.29) for multi-component or polyatomic systems as in Eq. (3.22). Applied to *scattering data* from such systems, our results may enable the determination of effective unknown microscopic interactions that underlie the system. Similarly, replication of the same derivation, *mutatis mutandis*, for quantum SU(2) spins $\vec{S} = (S_x, S_y, S_z)$ in the coherent spin representation leads to the high temperature result of three-component $[O(n = 3)]$ classical spins. This illustrates the well known maxim that at high temperature, details may become irrelevant and systems "become classical". In a similar manner, at high T, the details underlying the classical $O(n)$ model [the $O(n)$ normalization constraints concerning a fixed value of $|\vec{S}(\vec{x})|$ for n component vectors $\vec{S}(\vec{x})$ at all sites $\vec{x}$] effectively became irrelevant at high temperature – the behavior for all n was similar.

3.6 Approximate Methods

The exact high temperature results that we obtained for lattice spin systems and the generalizations that we discussed in Section 3.5 are, as we will show below, similar to those attained by several approximate methods. This coincidence of our exact results with the more standard and intuitive approximations enables a better understanding from different approaches. A corollary of what we discuss below is that the divergence of the correlation lengths in systems with long range interactions in the high temperature limit (as in Sec. 3.3) appears in all of these standard approximations. However, as we illustrated earlier in our work, and in Sec. 3.3 in particular, this divergence is not a consequence of a certain approximation but is an exact feature of all of these systems in their high temperature limit.

In what follows, we will specifically discuss **(i)** ϕ^4 field theories, **(ii)** the large n limit, and **(iii)** the OZ approach for fluids invoking the mean-spherical approximation (MSA) [93].

3.6.1 Ginzburg-Landau ϕ^4-type theories

In the canonical case, the free energy density of the ϕ^4 theory is given by

$$\mathcal{F} = \frac{1}{2}(\nabla\phi(\vec{x}))^2 + \frac{1}{2}r\phi^2(\vec{x}) + \frac{a}{4!}\phi^4(\vec{x}). \tag{3.30}$$

A finite value of a corresponds to the "soft-spin" approximation where the norm is not constrained, $\langle\phi^2(\vec{x})\rangle \neq 1$. Here, $r = c(T - T_0)$, with c a positive constant. The

partition function [94] is $Z = \int D\phi\ e^{-F}$ where $F = \int \mathcal{F}\ d^dx$ with d the spatial dimension. At high temperature, the correlator behaves in a standard way (the OZ form) $\left\langle |\phi(\vec{k})|^2 \right\rangle = \frac{1}{k^2+r}$. The irrelevance of the ϕ^4 term may, e.g., be seen by effectively setting $\phi^4(\vec{x}) \rightarrow 6\langle\phi^2(\vec{x})\rangle\phi^2(\vec{x})$ in the computation of the partition function. As $\langle\phi^2(\vec{x})\rangle$ is small [in fact, from Fourier transforming the above, $\langle\phi^2(\vec{x})\rangle = \mathcal{O}(1/T)$], the ϕ^4 term is smaller than the $(\nabla\phi)^2$ term in Eq. (3.30) by a factor of a/T and therefore can be neglected. When general two body interactions with an interaction kernel $v(\vec{k})$ are present, we similarly have $\langle|\phi(\vec{k})|^2\rangle = \frac{1}{v(\vec{k})+r}$. Our result of Eq. (3.10) for interactions of arbitrary spatial range illustrates that suggestive results for the correlation lengths attained by soft spin approximations are not far off the mark for general systems in the high temperature limit. As far as we are aware, the high temperature correlation length of general theories was not known to be similar to that suggested by various perturbative schemes (including the $1/n$ [95] and ϵ [96] expansions).

3.6.2 Correlation functions in the large-n limit

We now provide a derivation of Eq. (3.10) as it applies in the large n limit. Long ago, Stanley [62] demonstrated that the large n limit of the $O(n)$ spins is identical to the spherical model first introduced by Berlin and Kac [63].

The single component spherical model is given by the Hamiltonian,

$$H = \frac{1}{2}\sum_{\vec{x}\neq\vec{y}} V(|\vec{x}-\vec{y}|)S(\vec{x})S(\vec{y}). \tag{3.31}$$

The spins in Eq. (3.31) satisfy a single global ("spherical") constraint,

$$\sum_{\vec{x}} S^2(\vec{x}) = N, \tag{3.32}$$

enforced as an ensemble average [93] by a Lagrange multiplier μ. This leads to the functional $H' = H + \mu N$ which renders the model quadratic [as both Eqs. (3.31) and (4.16) are quadratic] and thus exactly solvable; see, e.g., Ref. [33].

From the equipartition theorem, in the higher temperature region of $T \geq T_c$ [when no order onsets and no Fourier mode is macroscopically occupied to form "a condensate" (i.e., $\langle|s(\vec{k})|^2\rangle/N^2 \to 0$ for all $\vec{k}$ in the thermodynamic ($N \to \infty$)) limit], the Fourier space correlator

$$G(\vec{k}) = \frac{1}{N}\langle|s(\vec{k})|^2\rangle = \frac{k_B T}{v(\vec{k})+\mu}. \tag{3.33}$$

The real space two point correlator is given by

$$G(\vec{x}) \equiv \langle S(0)S(\vec{x})\rangle = \frac{k_B T}{N}\sum_{\vec{k}} \frac{e^{i\vec{k}\cdot\vec{x}}}{v(\vec{k})+\mu}. \tag{3.34}$$

To complete the characterization of the correlation functions at different temperatures, we note that the Lagrange multiplier $\mu(T)$ is given by the implicit equation $1 = G(\vec{x}=0)$. Thus,

$$\frac{k_B T}{N}\sum_{\vec{k}} \frac{1}{v(\vec{k})+\mu} = 1. \tag{3.35}$$

This implies that the temperature T is a monotonically increasing function of μ. Equation (4.20) also implies that in the high temperature limit,

$$\mu = k_B T. \tag{3.36}$$

Taken together, Eqs. (4.18) and (3.36) yield Eq. (3.10) in the asymptotic high temperature limit. For completeness, we briefly note what happens at low T ($T < T_C$). In the spherical model, at the critical temperature (T_c), the Lagrange multiplier μ takes the value,

$$\mu_{min} = -\min_{\vec{k}}\{v(\vec{k})\}. \tag{3.37}$$

For $T < T_c$, (at least) one mode $\vec{q}$ is macroscopically occupied; the mode(s) $\vec{q}$ being occupied is one for which $v(\vec{k})$ is minimum. The "condensate fraction" $\langle|s(\vec{q})|^2\rangle/N^2 > 0$.

3.6.3 Ornstein-Zernike equation

As noted earlier, application of the MSA to the OZ equation for fluids reproduces similar results for the "total correlation function", $h(\vec{r})$. This is defined as $h(\vec{r}) = g(\vec{r}) - 1$, where $g(\vec{r})$ is the standard radial distribution function. The OZ equation for a fluid with particle density ρ is given by,

$$h(\vec{r}) = C(\vec{r}) + \rho \int dr' C(\vec{r} - \vec{r'}) h(\vec{r'}), \tag{3.38}$$

where $C(\vec{r})$ is the "direct correlation function". Using the MSA, $C(\vec{r}) = -\beta V(\vec{r})$ [93], we get in Fourier space,

$$S(\vec{k}) \;=\; \frac{k_B T}{\rho v(\vec{k}) + k_B T}. \tag{3.39}$$

This is similar to our result for $G(\vec{k})$. However, it is valid only for systems in which the MSA is a good approximation.

3.7 Conclusions

(i) We derived a universal form for high temperature correlators in general $O(n)$ theories as well as Bose and Fermi gases and quantum spin systems. This enables the *extraction of unknown microscopic interactions* from measurements of the high-temperature correlation functions. Similar considerations may also be enacted for general Potts and other systems.

(ii) We discovered *divergent* correlation lengths in systems with long range interactions in the high temperature limit. This divergence is replaced by a saturation when the long range interactions are screened.

(iii) We introduced *generalized Debye lengths (and times)* associated with such divergent correlation lengths (and decay times).

Chapter 4

Modulation and correlation lengths in systems with competing interactions

In this chapter, we investigate the general temperature dependence of the structural features that appear in such systems when competing interactions of short and long range are present.

The principal physics addressed in this work is that of rich nonuniform patterns and their evolution with temperature. We will examine these rather general classical systems by, predominantly, invoking large-n methods. Here, n is the number of components of the classical fields or spins that we consider. When competing interactions are present on different scales (including, notably, long range interactions), modula-

tion (or domain) lengths are seen to generally characterize oscillatory correlations. We find that *these modulation lengths often adhere to various scaling laws, sharp crossovers and divergences at various temperatures* (with no associated thermodynamic transition). We also find that in such systems, correlation lengths generically evolve into modulation lengths (and vice versa) at various temperatures. The behavior of correlation and modulation lengths as a function of temperature will afford us with certain selection rules on the possible underlying microscopic interactions. In their simplest incarnation, our central results are as follows:

1. In canonical systems harboring competing short (finite) and long range interactions modulated patterns appear. Depending on the type of the long range interaction, the modulation length either increases or decreases from its ground state value as the temperature is raised. We will relate this change, in lattice systems, to derivatives of the Fourier transforms of the interactions that are present.

2. There exist special crossover temperatures at which new correlation/modulation lengths come up or some cease to exist. The total number of characteristic length scales (correlation + modulation) remains conserved as temperature is varied, except at the crossover points.

3. The presence of the angular dependent dipolar interaction term that frustrates an otherwise unfrustrated ferromagnet vis a vis a simple scalar product be-

tween the dipoles adds new (dominant) length scales. The angular dependence significantly changes the system.

We will further investigate the ground state modulation lengths in general frustrated Ising systems and also point to discontinuous jumps in the modulation lengths that may appear in the large-n rendition of some systems.

Armed with these general results, we may discern the viable microscopic interactions (exact or effective) which underlie temperature dependent patterns that are triggered by two competing interactions. Our analysis suggests the effective microscopic interactions that may drive non-uniform patterns such as those underlying lattice analogs of the systems of Fig. 4.1.

The treatment that we present in this work applies to lattice systems and does not account for the curvature of bubbles and other continuum objects. These may be augmented by inspecting energy functionals (and their associated free-energy extrema) of various continuum field morphologies under the addition of detailed domain wall tension forms, e.g., explicit line integrals along the perimeter where surface tension exists, and the imposition of additional constraints via Lagrange multipliers, as in, e.g., Ref. [97]. We leave their analysis for future work. One of the central results of our work is the derivation of conditions relating to the increase/decrease of modulation lengths in lattice systems with changes in temperature. These conditions relate the change in the modulation length at low temperatures to the derivatives of the Fourier transforms of the interactions present.

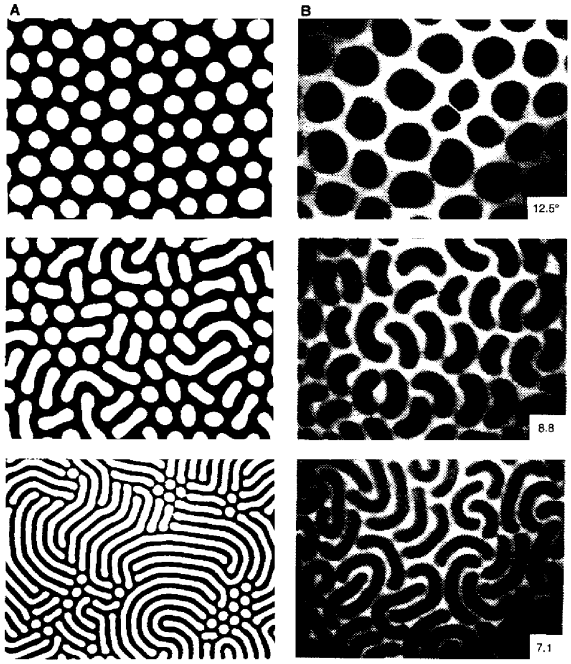

Figure 4.1: Reproduced with permission from Science, Ref.[2]. Reversible "strip-out" instability in magnetic and organic thin films. Period (L_D) reduction under the constraint of fixed overall composition and fixed number of domains leads to elongation of bubbles. Left panel (A) in magnetic garnet films, this is achieved by raising the temperature [labeled in (B) in degrees Celsius] along the symmetry axis, $H = 0$ (period in bottom panel, $\sim 10\mu m$) (see Fig. 5). Right panel (B) In Langmuir films composed of phospholipid dimyristolphosphatidic acid (DMPA) and cholesterol (98:2 molar ratio, pH 11), this is achieved by lowering the temperature at constant average molecular density [period in bottom panel, $\sim 20\mu m$]

.

In Sec. 4.1, we derive the scaling form for the Ising ground states for general frustrating long range interactions. Henceforth, we provide explicit expressions for the crossover temperatures and the correlations lengths in the large-n limit.

In Sec. 4.2, we introduce the two spin correlation function for a general system in this limit.

Based on the correlation function, we then present some general results for systems with competing nearest neighbor ferromagnetic interaction and an arbitrary long range interaction in Sec. 4.3. We start by deriving the equilibrium stripe width for a two-dimensional Ising system with nearest neighbor ferromagnetic interactions and competing long range interactions. We derive an expression for the change in modulation length with temperature for low temperatures for large-n systems. We illustrate how the crossover temperature, T^* arises in the large-n limit and show some general properties of the system associated with it.

We present some example systems in Sec. 4.4. We numerically calculate the correlation function for the screened Coulomb frustrated ferromagnet and the dipolar frustrated ferromagnet. We then study the screened Coulomb frustrated ferromagnet in more details. Next, we show some results for systems with higher dimensional spins. We study a system with the dipole-dipole interaction for three-dimensional spins, without ignoring the angular dependent term and show that this term changes the ground state length scales of the system considerably. We also present a system with the Dzyaloshinsky - Moriya interaction in addition to the ferromagnetic term

and a general frustrating long range term.

We give our concluding remarks in Sec. 4.5.

Throughout most of this work we will focus on systems with competing interactions having Hamiltonians of the following form.

$$H = -J \sum_{\langle \vec{x}, \vec{y} \rangle} S(\vec{x}) S(\vec{y}) + Q \sum_{\vec{x} \neq \vec{y}} V_L(|\vec{x} - \vec{y}|) S(\vec{x}) S(\vec{y}), \tag{4.1}$$

where the first term represents nearest neighbor ferromagnetic interaction for positive J and the second term represents some long range interaction that opposes the ferromagnetic interaction for positive Q. We will study properties of general systems of the form of Eq. (4.1). In order to flesh out the physical meaning of our results and illustrate their implications and meaning, we will further provide explicit expressions and numerical results for two particular examples. The Hamiltonian (4.1) represents a system that we christen to be the screened *Coulomb frustrated ferromagnet* when

$$\begin{aligned} V_L(r) &= \frac{e^{-\lambda r}}{4\pi r} \text{ in three dimensions, and} \\ V_L(r) &= K_0(\lambda r) \text{ in two dimensions,} \end{aligned} \tag{4.2}$$

where λ^{-1} represents the screening length and K_0 is a modified Bessel function,

$$K_0(x) = \int_0^\infty dt \frac{\cos xt}{\sqrt{1+t^2}}. \tag{4.3}$$

Throughout our work, we will discuss both the screened and unscreened renditions of the Coulomb frustrated ferromagnet. Equation (4.1) corresponds to a *dipolar*

frustrated ferromagnet when

$$\begin{aligned} V_L(r) &= \frac{1}{r^3} \\ &= \frac{1}{(r^2+\delta^2)^{3/2}} \text{ in the limit } \delta \to 0, \end{aligned} \tag{4.4}$$

on the lattices that we will consider. Later, we also consider a general direction dependent (relative to the location vectors) form of the dipolar interaction for three-dimensional spins; we will replace the scalar product form of the dipolar interactions in Eqs. (4.1) and (4.4) by the precise dipolar interactions between magnetic moments.

On a hypercubic lattice, the nearest neighbor interactions in real space of Eq. (4.1) have the lattice Laplacian

$$\Delta(\vec{k}) = 2\sum_{l=1}^{d}(1-\cos k_l), \tag{4.5}$$

as their Fourier transform. In the continuum (small k) limit, $\Delta(\vec{k}) = k^2$. The real lattice Laplacian

$$\langle \vec{x}|\Delta|\vec{y}\rangle = \begin{cases} 2d & \text{for } \vec{x}=\vec{y} \\ -1 & \text{for } |\vec{x}-\vec{y}|=1. \end{cases} \tag{4.6}$$

Notice that $\langle \vec{x}|\Delta^R|\vec{y}\rangle = 0$ for $|\vec{x}-\vec{y}| > R$, where R is the spatial range over which the interaction kernel is non-vanishing. The following corresponds to interactions of

Range=2 lattice constants,

$$\begin{aligned}\langle\vec{x}|\Delta^2|\vec{y}\rangle \;=\; & \quad 2d(2d+2) \text{ for } \vec{x}=\vec{y} \\ & -4d \text{ for } |\vec{x}-\vec{y}|=1 \\ & 2 \text{ for } (\vec{x}-\vec{y})=(\pm\hat{e}_\ell \pm \hat{e}_{\ell'}) \text{ where } \ell \neq \ell' \\ & 1 \text{ for a } \pm 2\hat{e}_\ell \text{ separation.}\end{aligned} \tag{4.7}$$

Correspondingly, in the continuum, the Lattice Laplacian and its powers attain simple forms and capture tendencies in numerous systems. Surface tension in many systems is captured by a $g(\nabla\phi)^2$ term where ϕ is a constant in a uniform domain. Upon Fourier transforming, such squared gradient terms lead to a k^2 dependence. The effects of curvature which are notable in many mixtures and membrane systems, can often be emulated by terms involving $(\nabla^2 h)$ with h being a variable parameterizing the profile; at times the interplay of such curvature terms with others leads, in the aftermath, to a simple short range k^4 term in the interaction kernel [the continuum version of the squared lattice Laplacian of Eq. (4.7)]. An excellent review of these issues is addressed in Ref. [2].

4.1 Ground-state stripe width for Ising systems: lattice versus continuum theory scaling

Next, we briefly discuss the ground state stripe width for systems where the long range interaction $V_L(|\vec{x}-\vec{y}|)$ in Eq. (4.1) has $v_L(k) = 1/k^p$ as its Fourier transform. Below, we discuss the Ising ground states. We will later on consider the spherical model that will enable us to compute the correlation functions at arbitrary temperatures. The upshot of the up and coming discussion is that in the long wavelength limit, the lattice and continuum results *differ* from one another due to the presence of the long range interaction and the ensuing non-trivial dependence of the modulation lengths on the lattice spacing.

We consider a system with Ising spins in d dimension and assume that the system forms a "striped" pattern (periodic pattern along one of the dimensions – stripes in two dimensions, parallel slices in three dimensions and so on) of spin-up and spin-down states of period l (the modulation length of the system at zero temperature, $L_D(T=0)$). We assume the "first" direction (i.e., that along $\hat{e}_1$) to be the direction along which we have the periodic pattern. We have $\left|s(\vec{k})\right| \neq 0$ only if $k_2 = k_3 = \ldots = k_d = 0$ and

$$\left|s(\vec{k})\right|^2 = \begin{cases} \frac{4}{\sin^2(k/2)}, & \text{when } k_1 \text{ is an odd multiple of } \frac{2\pi}{l}, \\ 0, & \text{when } k_1 \text{ is an even multiple of } \frac{2\pi}{l}. \end{cases} \tag{4.8}$$

For asymptotically small Q in Eq. (4.1), the ground state of the system will have

small wave-vectors $\vec{k}$. For small k's we have,

$$\left|s(\vec{k})\right|^2 \sim \frac{16}{k^2}, \text{ when } k_1 \text{ is an odd multiple of } \tfrac{2\pi}{l}. \tag{4.9}$$

We next compute the energy as a function of l and then minimize it with respect to l to get the equilibrium stripe width. For a general lattice constant a, we find that

$$l = \left[\frac{(2\pi)^{p+2} a^{3-d} J}{4Q(p+2-d)\left(1-\frac{1}{2^{p+2}}\right)\zeta(p+2)}\right]^{\frac{1}{p+3-d}}, \tag{4.10}$$

where $\zeta(t)$ is the Riemann zeta function,

$$\zeta(t) = \sum_{n=1}^{\infty} \frac{1}{n^t}. \tag{4.11}$$

Our lattice result of Eq. (4.10) may be contrasted with the continuum modulation period

$$l = 2\pi \left(\frac{2J}{pQ}\right)^{\frac{1}{p+2}} \tag{4.12}$$

obtained by finding the minimizing wave-vector q for the kernel $(J/k^2 + Q/k^p)$ [the Fourier transform of Eq. (4.1) and computing $(2\pi/q)$]. In the continuum, where no lattice length scale is present, Eq. (4.12) constitutes (up to an overall multiplicative numerical prefactor) the sole quantity that has the correct dimensions of length that can be built out of J and Q. The power law scaling of l on Q in the asymptotic small Q (or, equivalently, small k) limit is radically different between the cases of the lattice [Eq. (4.10)] and the continuum [Eq. (4.12)]. For the particular case the two-dimensional ($d = 2$) Coulomb frustrated ($p = 2$) ferromagnet, Eq. (4.10) states

that

$$l = 4\sqrt[3]{3Ja/Q}. \tag{4.13}$$

This result is in accord with the analysis of Refs. [42, 98]. For long range dipolar interactions ($p = 3$) in $d = 2$ dimensions, we find that

$$l = \delta\sqrt{\frac{3J}{Q}}. \tag{4.14}$$

4.2 Correlation Functions in the large-n limit: general considerations

The results reported henceforth were computed within the spherical or large-n limit [63]. It was found by Stanley long ago [62] that the large-n limit of the n component normalized spin systems [so called $O(n)$ spins] is identical to the spherical model first introduced by Berlin and Kac. [63]

The designation of "$O(n)$ spins" simply denotes real fields (spins) of unit length that have some arbitrary number (n) of components. For $n = 1$, the system is an Ising model: a single component real field having unit norm allows for only two scalars at any given site $\vec{x}$: $S(\vec{x}) = \pm 1$. The $n = 2$ system corresponds to a two component spin system in which the spins are free to rotate in a two-dimensional place – $S_1^2(\vec{x}) + S_2^2(\vec{x}) = 1$ (an XY spin system). The case of $n = 3$ corresponds to a

system of three component Heisenberg type spins, and so on. In general,

$$\sum_{a=1}^{n} S_a(\vec{x}) S_a(\vec{x}) = 1. \tag{4.15}$$

We now introduce the spherical model in its generality. The spins in Eq. (2.1) satisfy a single global ("spherical") constraint,

$$\sum_{\vec{x}} \langle S^2(\vec{x}) \rangle = N, \tag{4.16}$$

enforced by a Lagrange multiplier μ. This leads to the functional $H' = H + \mu N$, which renders the model quadratic [as both Eqs. (2.1) and (4.16) are quadratic] and thus exactly solvable, see, e.g., [33]. The continuum analogs of Eqs. (2.1, 4.16) read

$$H = \frac{1}{2} \int d^d x \; d^d y \; V(|\vec{x} - \vec{y}|) S(\vec{x}) S(\vec{y}),$$
$$\int d^d x \; \langle S^2(\vec{x}) \rangle = const. \tag{4.17}$$

The quadratic theory may be solved exactly. From the equipartition theorem, for $T \geq T_c$, the Fourier space correlator

$$G(k) = \langle |S^2(k)| \rangle = \frac{k_B T}{v(k) + \mu}. \tag{4.18}$$

The real space two point correlator is given by

$$G(\vec{x}) \equiv \langle S(0) S(\vec{x}) \rangle = k_B T \int_{BZ} \frac{d^d k}{(2\pi)^d} \frac{e^{i\vec{k} \cdot \vec{x}}}{v(k) + \mu}, \tag{4.19}$$

with d the spatial dimension and BZ denoting the integration over the first Brillouin zone. For a hypercubic lattice in d dimensions with a lattice constant that is set to

one, $-\pi < k_i \leq \pi$ for $i = 1, 2, ..., d$. Henceforth, to avoid cumbersome notation, we will generally drop the designation of BZ; this is to be understood on all momentum space integrals pertaining to the lattice systems that we examine. To complete the characterization of the correlation functions at different temperatures, we note that the Lagrange multiplier $\mu(T)$ is given by the implicit equation $1 = G(\vec{x} = 0)$. Thus,

$$1 = k_B T \int \frac{d^d k}{(2\pi)^d} \frac{1}{v(k) + \mu}. \tag{4.20}$$

This implies that the temperature T is a monotonic increasing function of μ. For a hypercubic lattice system, performing the momentum integration on a hypercube of side 2π in the reciprocal lattice, in the high temperature limit,

$$\mu = k_B T. \tag{4.21}$$

In continuum renditions of the large-n system, Eq. (4.20) also implies that in the high temperature limit,

$$\frac{\mu}{k_B T} = \frac{\pi^{d/2} \Lambda^d}{(2\pi)^d \Gamma(\frac{d}{2} + 1)} \tag{4.22}$$

$$\Longrightarrow \; T \propto \mu, \tag{4.23}$$

where Λ is the upper limit of the k integration, representing the ultra-violet cut-off. Furthermore, as the integration range in Eq. (4.20) is finite, we can prove that $\mu(T)$ is an analytic function of T (see Appendix F). This supports the assumption that $G^{-1}(T, k)$ is analytic in T and k at all points except $k = 0$ where $v(k)$ is usually singular.

We investigate the general character of the correlation functions given by Eq. (4.19) for rotationally invariant systems. If the minimum (minima) of $v(k)$ occur(s) at momenta q far from the Brillouin zone boundaries of the cubic lattice then we may set the range of integration in Eq. (4.19) to be unrestricted. The correlation function is then dominated by the location of the poles (and/or branch cuts) of $1/[v(k)+\mu]$. Thus, we look for solutions to the following equation.

$$v(k)+\mu=0. \tag{4.24}$$

The system is perfectly ordered in its ground state. From a temperature at which the system is not perfectly ordered, as we lower the temperature, the correlation length diverges at $T=T_c$. At $T=T_c$, μ takes the value,

$$\mu_{min}=-\min_{k\in BZ}[v(k)]. \tag{4.25}$$

As the temperature is increased, the disorder creeps in and in many systems, at a temperature T^*, the modulation length diverges.

The characteristic length scales of the system are governed by the poles of $[v(k)+\mu]^{-1}$.

$$J\Delta(\vec{k})+Qv_L(k)+\mu=0, \tag{4.26}$$

which in the continuum limit takes the form

$$Jk^2+Qv_L(k)+\mu=0. \tag{4.27}$$

Employing the above considerations, we will derive, in the next section, some general results for systems of the form (4.1).

Our work will focus on classical systems. The extension to the quantum arena [33] is straightforward. In, e.g., large-n bosonic renditions of our system, replicating the usual large-n analysis, we find [43] that the pair correlator

$$G_B(\vec{k}) = \frac{n_B\left(\sqrt{\frac{v(\vec{k})+\mu}{k_BT}}\right) + \frac{1}{2}}{\sqrt{\frac{v(\vec{k})+\mu}{k_BT}}}, \tag{4.28}$$

with the bosonic distribution function

$$n_B(x) = \frac{1}{e^x - 1}. \tag{4.29}$$

The correlator of Eq. (4.28) is of a similar nature as that of the classical correlator of Eq. (4.18) with branch cuts generally appearing in the quantum case. Our analysis below relies on the evolution of the poles of $v(k) + \mu$ as a function of temperature in classical systems.

In the quantum arena, we first choose the proper contour in the complex k-space (going around the branch cuts). Then, we argue that the only points that contribute to the integral are the points where the integrand is singular. This corresponds to $v(k) + \mu = 0$. Thus, the integral remains unchanged if we expand the integrand to lowest order in $v(k) + \mu$. Doing this, we get, to leading order,

$$G_B(k) = \frac{k_BT}{v(k) + \mu} \tag{4.30}$$

which is same as the classical expression of Eq. (4.18). The characteristic length scales of the system are therefore still determined by the zeros of $v(k) + \mu$ in the complex k plane in the exact same way.

For interactions that are not isotropic, for both classical and quantum cases, we need to consider the full six-dimensional space of the complex components of $\vec{k}$ along each of the three coordinate axes.

4.3 Large-n Results

In this section, we present some general results for systems of the form (4.1) in their large-n limit. First, we find the dependence of the modulation length on temperature, near T_c. Next, we will illustrate an analogy between the behavior of the correlation length near the critical temperature T_c and that of the modulation length near T^*. We will then discuss some aspects of the crossover points. We end this section with some results in the high temperature limit.

4.3.1 The low temperature limit: a criterion for determining an increase or decrease of the modulation length at low temperatures

In this section, we derive universal conditions for increasing or decreasing modulation lengths in general systems with pairwise interactions. Equations (4.41) and (4.43) show general conditions for the change in modulation length, L_D with temperature

for a general system of the form (4.1). The value, k_0 of k that satisfies Eq. (4.25),

$$v(k_0) = \min_{k \in BZ} v(\vec{k}) \tag{4.31}$$

determines the modulation length at $T = T_c$.

$$v(k_0) + \mu_{min} = 0, \tag{4.32}$$

$$v'(k_0) = 0. \tag{4.33}$$

As the temperature is raised, the new pole near k_0 will have an imaginary part corresponding to the finite correlation length. The real part will also change in general and this would induce a change in the modulation length. Let $\mu(T) = \mu_{min} + \delta\mu$ with $\delta\mu > 0$. Then we have,

$$\begin{aligned} k &= k_0 + \delta k, \\ \delta k &= \sum_{j=1}^{\infty} \delta k_j, \end{aligned} \tag{4.34}$$

where $\delta k_j \propto \delta\mu^{x_j}$, $x_{j+1} > x_j$. Our goal is to find the leading order real contribution to δk that would give us the change in modulation length with increasing μ and hence with increasing temperature.

$$\sum_{j=2}^{\infty} v^{(j)}(k_0) \frac{\delta k^j}{j!} + \delta\mu = 0. \tag{4.35}$$

Suppose $v^{(n)}(k_0) = 0$ for $2 < n < p$ and $v^{(p)}(k_0) \neq 0$. (Clearly, in most cases, the third derivative is not zero and $p = 3$.) We have,

$$\begin{aligned} &\frac{v^{(2)}(k_0)}{2!})(\delta k_1^2 + 2\delta k_1 \delta k_2 + ...) \\ +[&\frac{v^{(p)}(k_0)}{p!}(\delta k_1^p + p\delta k_1^{p-1}\delta k_2 + ...) + \frac{v^{(p+1)}(k_0)}{(p+1)!} \times \\ &(\delta k_1^{p+1} + (p+1)\delta k_1^p \delta k_2 + ...) + ...] + \delta\mu = 0. \end{aligned} \tag{4.36}$$

To leading order,

$$\begin{aligned} \frac{v^{(2)}(k_0)}{2!}\delta k_1^2 + \delta\mu = 0, \\ \delta k_1^2 = -\frac{2\delta\mu}{v^{(2)}(k_0)}. \end{aligned} \tag{4.37}$$

From this, we see that δk_1 is imaginary. This constitutes another verification of the well established result about the universality of the divergence of the correlation length, ξ at T_c with the mean-field type critical exponent $\nu = 1/2$ in the large-n limit.

$$\begin{aligned} \xi \propto (T - T_c)^{-\nu}, \\ \nu = \frac{1}{2}. \end{aligned} \tag{4.38}$$

The next, higher order, relations are obtained using the method of dominant balance.

$$\begin{aligned} v^{(2)}(k_0)(\delta k_1)(\delta k_2) + \frac{v^{(p)}(k_0)}{p!}(\delta k_1)^p = 0 \\ \delta k_2 = \frac{(-1)^{\frac{p+1}{2}} v^{(p)}(k_0)(\delta\mu)^{\frac{p-1}{2}}}{2p!(\frac{v^{(2)}(k_0)}{2!})^{\frac{p+1}{2}}}. \end{aligned} \tag{4.39}$$

Therefore, δk_2 is real if p is odd and imaginary if p is even. If,

$$L_D(T) = L_D(T_c) + \delta L_D, \tag{4.40}$$

then, for $p = 2n + 1$,

$$\delta L_D = \frac{2\pi}{k_0^2} \frac{(-1)^n v^{(2n+1)}(k_0) \delta\mu^n}{2(2n+1)!(\frac{v^{(2)}(k_0)}{2!})^{n+1}}. \tag{4.41}$$

Thus to get the leading order real contribution to δk for even $p[> 2]$, we have to go to higher order.

$$2(\frac{v^{(2)}(k_0)}{2!})\delta k_1 \delta k_3 + \frac{v^{(p+1)}(k_0)}{(p+1)!}\delta k_1^{p+1} = 0$$
$$\delta k_3 = \frac{(-1)^{1+p/2} v^{(p+1)}(k_0)(\delta\mu)^{p/2}}{2(p+1)!(\frac{v^{(2)}(k_0)}{2!})^{p/2+1}}. \tag{4.42}$$

For $p = 2n$,

$$\delta L_D = \frac{2\pi}{k_0^2} \frac{(-1)^n v^{(2n+1)}(k_0)(\delta\mu)^n}{2(2n+1)!(\frac{v^{(2)}(k_0)}{2!})^{n+1}}. \tag{4.43}$$

If, for $p = 2n$, $v^{(2n+1)}(k_0) = 0$, then we will need to continue this process until we get a real contribution to δk. In appendix D, we provide explicit forms for δL_D for different values of p.

In the most common case, where $v^{(3)}(k_0) \neq 0$, we have,

$$\delta L_D = -\frac{2\pi}{k_0^2} \frac{v^{(3)}(k_0)}{3[v^{(2)}(k_0)]^2} \delta\mu. \tag{4.44}$$

Also, applying this to a nearest neighbor system in the continuum frustrated by a general long range interaction given by $v_L(k)$ in Fourier space , we get,

$$\delta L_D = -\frac{2\pi}{k_0^2} \frac{Q v_L^{(3)}(k_0)}{3[v_L^{(2)}(k_0)]^2} \delta\mu. \tag{4.45}$$

This shows that it is the long range term that determines the sign of the change in modulation length with temperature as the system is heated from $T = T_C$. *The*

results derived above allow us to relate an increase/decrease in the modulation length at low temperatures to the sign of the first non-vanishing odd derivative (of an order larger than two) of the Fourier transform of the interactions that are present. It is important to emphasize that our results apply to any interaction. These may include screened or unscreened Coulomb and other long range interactions but may also include interactions that are strictly of finite range [e.g., next-nearest neighbor interactions on the lattice for which we have $v_L = -t\Delta^2$ (with a constant $t > 0$, see Eq. (4.7))].

The results from this section about modulation lengths just above T_C, can give us similar behavior of the correlation lengths at temperatures slightly below T^*.

4.3.2 A correspondence between the temperature T^* at which the modulation length diverges and the critical temperature T_c

The critical temperature T_c corresponds to the maximum value of μ for which Eq. (4.24) still attains a real solution. Thus,

$$\begin{aligned} v(k_0) + \mu_{min} &= 0, \\ v'(k_0) &= 0, \\ v''(k_0) &> 0. \end{aligned} \tag{4.46}$$

For systems in which the modulation length diverges at T^*, T^* corresponds to the minimum value of μ for which Eq. (4.24) has a purely imaginary solution. Thus, if $v(i\kappa) = \hat{v}(\kappa)$,

$$\begin{aligned} \hat{v}(\kappa_0) + \mu^* &= 0 \\ \hat{v}'(\kappa_0) &= 0 \\ \hat{v}''(\kappa_0) < 0 \implies v''(i\kappa_0) &> 0 \end{aligned} \tag{4.47}$$

Thus, we expect similar qualitative results for the correlation lengths at temperatures slightly above T_c as for modulation lengths slightly below T^* and vice-versa. [The relations for the derivatives of $\hat{v}(\kappa_0)$ in Eq. (4.47) are guaranteed to hold only if $T^* > T_c$.]

4.3.3 Crossover temperatures: emergent modulations

For systems with competing multiple range interactions, there may exist special temperatures at which the poles of the correlation function change character, thus changing modulation lengths to correlation lengths and vice-versa. In particular, for most systems we have a crossover temperature T^* above which the system does not have any modulation. Apart from this kind of phenomenon, there might also be finite discontinuous jumps in the modulation length. This is illustrated with an example in Sec. 4.3.4.

We start by defining the crossover temperature T^* for a ferromagnetic system

frustrated by a general long range interaction. Let $k = i\kappa$, $\kappa \in \mathbb{R}$ above T^* and $\kappa = \kappa_0$ at T^*. Let $v(k) = f(z)$, $z = k^2$. Above T^*, $\mu = \mu_{min} + \Delta\mu$ ($\Delta\mu > 0$). Using Eq. (4.25),

$$\begin{aligned} \mu = -f(-\kappa^2) &= -\min_{k\in\mathbb{R}} v(k) + \Delta\mu \\ &= \max_{k\in\mathbb{R}}[-v(k)] + \Delta\mu. \end{aligned} \tag{4.48}$$

T^* corresponds to the minimum value of $\Delta\mu$ for which we have at least one such solution (see Fig. 4.2). Thus,

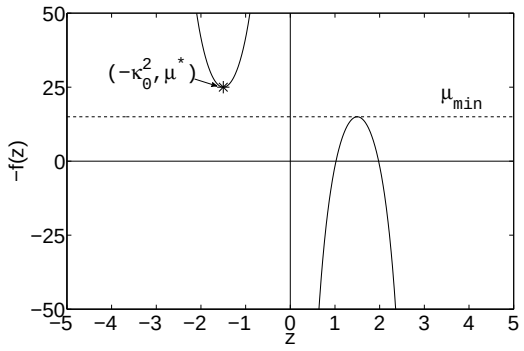

Figure 4.2: $-f(z) = -v(k) = \mu$ plotted against $z = k^2$ for purely real and purely imaginary k's ($T \to 0$ and $T \to \infty$ respectively). The negative z regime corresponds to temperatures (Lagrange multiplier, μ's) for which purely imaginary solutions exist. The maximum of the curve in the positive z regime corresponds to the modulations at $T = T_c$ [$\mu = \mu_{min}$], which is the maximum temperature at which pure modulations exist.

$$\begin{aligned} \mu^* &= \min_{\kappa \in \mathbb{R}} [-v(i\kappa)] \\ &\quad -v(i\kappa) \geq \mu_{min} \\ &= - \max_{\kappa \in \mathbb{R}} [v(i\kappa)]. \\ &\quad -v(i\kappa) \geq \mu_{min} \end{aligned} \tag{4.49}$$

Sometimes, the crossover point is slightly more difficult to visualize (see Fig. 4.3). In this case, the minimum upper branch of $-f(z)$ for $z < 0$ [equivalently the upper branches of $-v(i\kappa)$] gives us the value of μ^*. The branch chosen has to continue to $\mu = +\infty$ so that at least one term without modulation is always available as we increase the temperature, as required by the definition of T^*. The other branch provides such solutions only up to a certain temperature. Also, the part of it that is below μ_{min} is irrelevant.

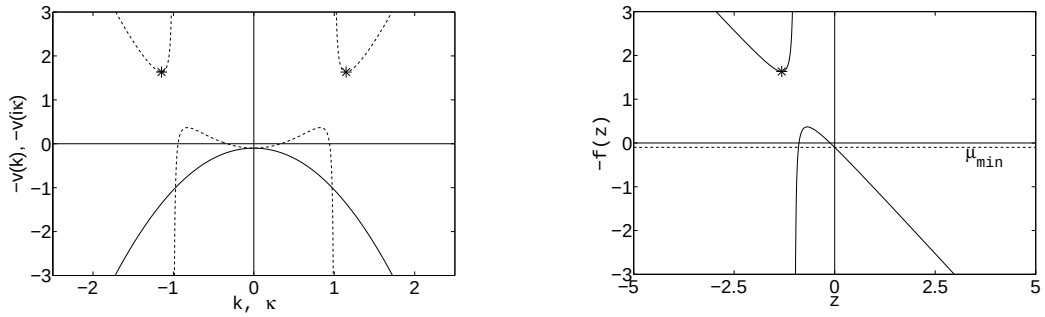

Figure 4.3: Left: *Solid line:* $-v(k)$ plotted against k; *Dashed line:* $-v(i\kappa)$ plotted against κ. Right: $-f(z)$ plotted against z.

If $f(z)$ is an odd function of z (e.g. the Coulomb frustrated ferromagnet), $\mu^* =$

$-\mu_{min}$ and the correlation length at T^* is the same as the modulation length at T_c.

Also, for the system in Eq. (4.1), if $\lim_{\kappa\to 0} v_L(i\kappa) = +\infty$, we have, $\mu^* = \mu_{min}$, and $T^* = T_c$.

$T^* = T_c$ if all the competing interactions are of finite range and crossover exists

For systems where all the competing interactions are of finite range, $T^* = T_c$. We prove this as follows. Since finite range interactions contribute to $v(k)$ as powers of $\Delta(\vec{k}) \to k^2$, for a system with only finite range interactions, $f(z)$ is analytic for all z. For a minimum of $-f(z)$ to exist in the $z < 0$ regime which is higher than the maximum in the $z > 0$ regime, we need $f(z)$ to be discontinuous at some point. Putting all of the pieces together, we find that there are no possibilities: (i) no crossover, i.e., $T^* = \infty$ or (ii) $\kappa_0 = 0$ and $\mu^* = \mu_{min}$ with $T^* = T_c$.

$T^* \to T_c$ as the strength of the long range interaction is turned off

The results from this section and the next hold for a general system, not just the frustrated ferromagnet.

The crossover temperature T^* tends to T_c for $Q = 0$ as $Q \to 0$. For a general system, let $G(T, k)$ denote the Fourier space correlation function at temperature T. By definition, at $T = T_c$ the correlation length is infinite. Thus, T_c is the solution to

$$G^{-1}(T, k) = 0, \tag{4.50}$$

such that $k \in BZ$ (or for continuum renditions, $k \in \mathbb{R}$).

T^* is the temperature at which the modulation length diverges for the frustrated ferromagnet, or becomes the same as the modulation length of the unfrustrated system at T_c for a general system. Thus, T^* is the solution to

$$G^{-1}(T, q + i\kappa) = 0, \tag{4.51}$$

with $\kappa \in \mathbb{R}$ ($q = 0$ for the case of the frustrated ferromagnet, $q = \pi$ for the frustrated anti-ferromagnet). At T_c, for $Q = 0$, we have,

$$G^{-1}(T_c, q) = 0. \tag{4.52}$$

This however also satisfies Eq. (4.51), with $\kappa = 0$. Therefore,

$$\lim_{Q \to 0} T^* = T_c. \tag{4.53}$$

We demonstrate this in the large-n limit (see Fig. 4.4). For $Q = 0$, we have $\mu_{min} = 0$ and $k_0 = 0$. Let $v_L(k)$ diverge as k^{-2p} near $k = 0$. For small Q, from Eq. (4.25), we have,

$$\begin{aligned} k_0 &= (\frac{pQ}{J})^{\frac{1}{2p+2}}, \\ \mu_{min} &= -\frac{p+1}{p^{\frac{p}{p+1}}} J^{\frac{p}{p+1}} Q^{\frac{1}{p+1}}. \end{aligned} \tag{4.54}$$

If p is odd,

$$\begin{aligned} \mu^* &= -\mu_{min}, \\ \kappa_0 &= k_0. \end{aligned} \tag{4.55}$$

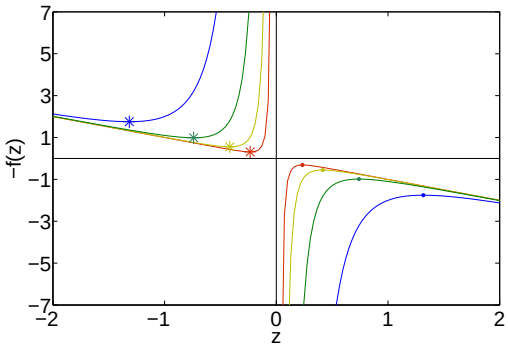

Figure 4.4: Illustration of the limit $T^* \to T_c$ as $Q \to 0$ with $v_L(k) = 1/k^3$. The plot shows $-f(z) = -v(k)$ vs $z = k^2$, for $v(k) = Jk^2 + Q/k^3$ with $J = 1$ and $Q = \{1-\text{Blue}, 0.1-\text{Green}, 0.01-\text{Yellow}, 0.001-\text{Red}\}$. '*' represents the value of μ^* and dot represents μ_{min}.

As $Q \to 0$, $\kappa_0 = k_0 = 0$ and $\mu^* = \mu_{min} = 0$, that is,

$$\lim_{Q\to 0} T^* = T_c(Q = 0). \tag{4.56}$$

Proof of the conservation of the total number of characteristic length scales

In this section we consider the general situation in which the Fourier transform of the interaction kernel, $v(k)$, is a rational function of $z = \Delta(k)$, ($z \to k^2$ in the continuum limit). That is, we consider situations for which

$$v(k) = f(z) = \frac{P(z)}{Q(z)}, \tag{4.57}$$

with P and Q polynomials (of degrees M_1 and M_2 respectively). We will now demonstrate that the combined sum of the number of correlation and the number of modulation lengths remains unchanged as the temperature is varied.

Before providing the proof of our assertion, we first re-iterate that the form of Eq. (4.57) is rather general. For a system with finite range interactions ($V(|\vec{x}-\vec{y}| > R) = 0$ with finite R) that is even under parity ($V(\vec{x}-\vec{y}) = V(\vec{y}-\vec{x})$), the Fourier transform of $V(\vec{x}-\vec{y})$ can be written as a finite order polynomial in $(1-\cos k_l)$ with the spatial direction index $1 \leq l \leq d$ where d is the dimensionality. In the small $|\vec{k}|$ (continuum limit), $(1-\cos k_l) \to k_l^2/2$. The particular case of a system with only finite range interactions that exist up to a specified range R on the lattice (the range being equal to a graph distance measuring the number of lattice steps beyond which the interactions vanish) of the form of Eq. (4.57) corresponds to $v(k) = P(z)$ with the order of the polynomial M_1 being equal to the interaction range, $R = M_1$. Our result below includes such systems as well as general systems with long range interactions. For long range interactions such as, e.g., the screened Coulomb frustrated ferromagnet, $f(z) = 1/(z+\lambda^2)$. The considerations given below apply to the correlations along any of the spatial directions l (and as a particular case, radially symmetric interactions for which the correlations along all directions attain the same form).

Returning to the form of Eq. (4.57), the Fourier space correlator of Eq. (4.18) is given by

$$G(\vec{k}) = k_B T \frac{Q(z)}{F(z)}; \quad F(z) = P(z) + \mu Q(z). \tag{4.58}$$

On Fourier transforming Eq. (4.58) to real space to obtain the correlation and modulation lengths, we see that the zeros of $F(z)$ determine these lengths. Expressed in

terms of its zeros, F can be written as

$$F(z) = A\prod_{j=1}^{M}(z - z_j), \tag{4.59}$$

where $M = \max[M_1, M_2]$. Perusing Eq. (4.58), we see that F is a polynomial in z with real coefficients. As $F^*(z) = F(z^*)$ it follows that all roots of F are either (a) real or (b) come in complex conjugate pairs ($z_j = z_i^* \neq z_i$). We now focus on the two cases separately.

(a) Real roots: If a particular root $z_j = a^2$, $a \in \mathbb{R}$ then on Fourier transforming Eq. (4.58) by the use of the residue theorem, we obtain a term with a modulation length, $L_D = 2\pi/a$. Conversely, if $z_j = -a^2$, we get a term with a correlation length, $\xi = 1/a$.

(b) Next we turn to the case of complex conjugate pairs of roots. If the pair of roots z_j, z_j^* is not real, that is, $z_j = |z_j|e^{i\theta}$, then on Fourier transforming, we obtain a term containing both a correlation length, $\xi = (\sqrt{|z_j|}|\sin\frac{\theta}{2}|)^{-1}$, and modulation length, $L_D = 2\pi(\sqrt{|z_j|}|\cos\frac{\theta}{2}|)^{-1}$.

Putting all of the pieces together see that as (a) each real root of $F(z)$ contributes to either a correlation length or a modulation length and (b) complex conjugate pairs of non-real roots contribute to one correlation length and one modulation length, *the total number of correlation and modulation lengths remains unchanged as the temperature (μ) is varied.* The total number of correlation + modulation lengths is given by the number of roots of $F(z)$ (that is, M). Thus, the system generally displays a net of M correlation and modulation lengths. This concludes our proof. At very

special temperatures, the Lagrange multiplier $\mu(T)$ may be such that several poles degenerate into one – thus lowering the number of correlation/modulation lengths at those special temperatures. Also, in case $M = M_2$, the total number of roots drops from M_2 to M_1 at $\mu = 0$. What underlies multiple length scales is the existence of terms of different ranges (different powers of z in the illustration above) – not frustration.

The same result can be proven using the transfer matrix method, for a one-dimensional system with Ising spins. This is outlined in appendix C. A trivial extension enables similar results for other discrete spin systems (e.g., Potts spins).

4.3.4 First order transitions in the modulation length

In this section, we show that there might be systems in which the modulation length makes finite discontinuous jumps. In these situations, the modulation length does not diverge at a temperature T^* (or set of such temperatures). The ground state modulation lengths (the reciprocals of Fourier modes $\{\vec{q}_i\}$ minimizing the interaction kernel) need not be continuous as a function of the parameters that define the interactions. As we will simply illustrate below, in a manner that is mathematically similar to that appearing in the Ginzburg-Landau constructs, a "first order transition" in the value of the ground state modulation lengths can arise. Such a possibility is quite obvious and need not be expanded upon in depth. As an illustrative example, let us consider

the Range=3 interaction kernel

$$v(k) = a[\Delta + \epsilon] + \frac{1}{2}b[\Delta + \epsilon]^2 + \frac{1}{3}c[\Delta + \epsilon]^3, \tag{4.60}$$

with $(0 < \epsilon \ll 1)$ and $c > 0$. If the parameters are such that $a > 0$ and $b < 0$, then $v(k)$ displays three minima, i.e. $[\Delta + \epsilon] = 0$ and $[\Delta + \epsilon] = \pm m_+^2$, where $m_+^2 = \frac{1}{2c}[-b + \sqrt{b^2 - 4ac}]$. the locus of points in the ab plane where the three minima are equal to one another is defined by $v(k) = 0$. This leads to the relation $m_+^2 = -\frac{4a}{b}$. Putting all of the pieces together, we see that $b = -4\sqrt{ca/3}$ constitutes a line of "first order transitions". On traversing this line of "first order transitions", the minimizing $[\Delta + \epsilon]$ (and thus the minimizing wavenumbers) changes discontinuously by $\Delta m = (-\frac{4a}{b})^{1/2} = (\frac{3a}{c})^{1/4}$.

4.4 Example systems

In this section, we will investigate in detail several frustrated systems. We will start our analysis by examining the screened Coulomb Frustrated Ferromagnet. A screened Coulomb interaction of screening length λ^{-1} has the continuum Fourier transformed interaction kernel $v(k) = [k^2 + \lambda^2]^{-1}$. The lowest order non-vanishing derivative of $v_L(k)$ of order higher than two is that of $p = 3$. Invoking Eq. (4.41), we find a modulation length that increases with increasing temperature as $T \to T_c^+$ (see also appendix D, Eq. (D-18) in particular) .

The dipolar interaction can be thought of as the $\delta \to 0$ limit of the interaction,

$$V_d = \frac{1}{[(\vec{x} - \vec{y})^2 + \delta^2]^{3/2}}. \tag{4.61}$$

This form has a simple Fourier transform. In two spatial dimensions,

$$v_d(k) = 2\pi\delta^{-1}e^{-k\delta}. \tag{4.62}$$

In three dimensions,

$$v_d(k) = 4\pi K_0(k\delta), \tag{4.63}$$

K_0 being a modified Bessel function (see Eq. (4.3)).

In this case, we similarly find that the first non-vanishing derivative of v_L is order of order $p = 3$ in the notation of Eq. (4.41). This, as well as the detailed form of Eq. (D-18) suggest an increasing modulation length with increasing temperature as $T \to T_c^+$.

4.4.1 Numerical evaluation of the Correlation function

In Figs.(4.5,4.6), we display a numerical evaluation of the correlation function for the Coulomb frustrated ferromagnet and the dipolar frustrated ferromagnet (see Eqs. (4.1, 4.2, 4.4)) on a two-dimensional lattice of size 100×100.

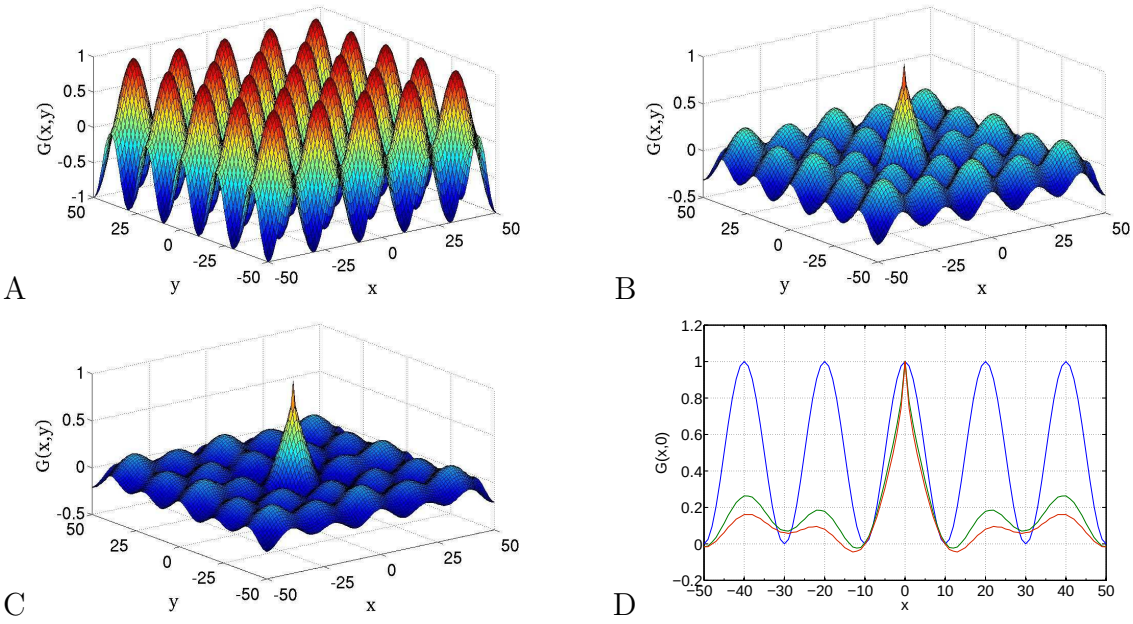

Figure 4.5: The correlator $G(x, y)$ for a two-dimensional screened Coulomb ferromagnet of size 100 by 100. $J = 1$, $Q = 0.0004$, screening length$= 100\sqrt{2}$. A: $\mu = \mu_{min} = -0.0874$, B: $\mu = \mu_{min} + 0.001$, C: $\mu = \mu_{min} + 0.003$, D: G(x,y) for $y = 0$ for A(blue)$[L_D = 20]$, B(green)$[L_D = 24]$ and C(red)$[L_D = 26]$.

4.4.2 Coexisting short range and screened Coulomb interactions

In this section, we study the screened Coulomb frustrated ferromagnet in more details. In the continuum limit, the Fourier transform of the interaction kernel of Eq. (4.1) with $V_L(x)$ given by Eq. (4.2) is

$$v(k) = Jk^2 + \frac{Q}{k^2 + \lambda^2}. \tag{4.64}$$

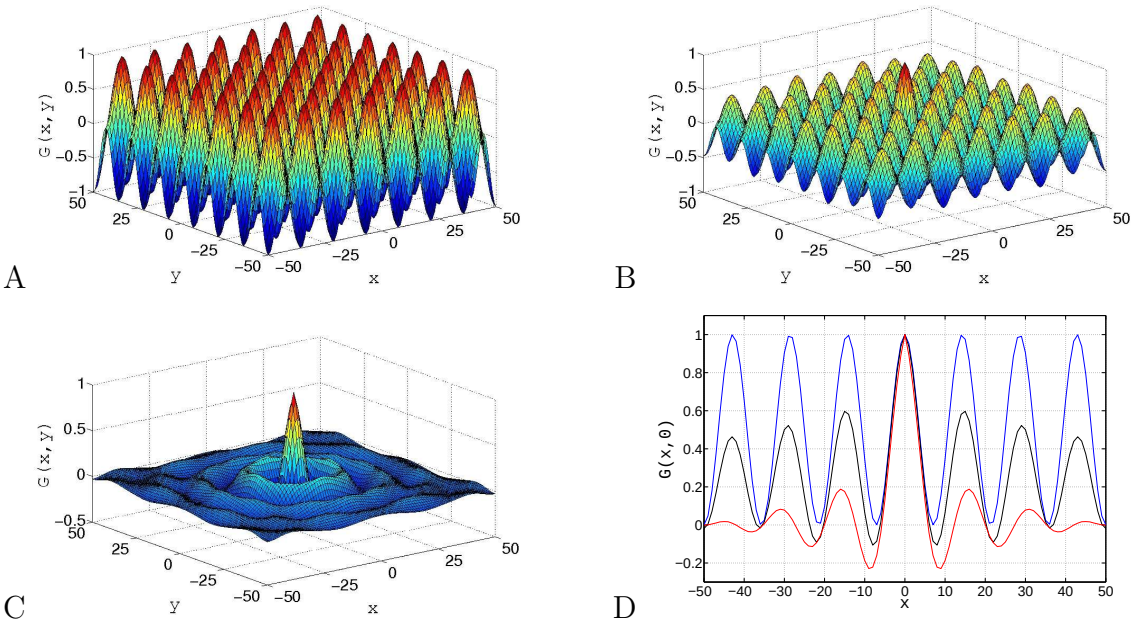

Figure 4.6: The correlator $G(x, y)$ for a two-dimensional dipolar ferromagnet of size 100 by 100. $J = 1$, $Q = 0.15$. A: $\mu = \mu_{min} = -1.1459$, B: $\mu = \mu_{min} + 4 \times 10^{-5}$, C: $\mu = \mu_{min} + 1 \times 10^{-3}$, D: G(x,y) for $y = 0$ for A(blue)[$L_D = 14$], B(green)[$L_D = 15$] and C(red)[$L_D = 16$].

In appendix E, we provide explicit expressions for the dependence of μ on the temperature T. This dependence delineates the different temperature regimes. For $T > T^*$ wherein the temperature T^* is set by

$$\mu(T^*) = J\lambda^2 + 2\sqrt{JQ}, \tag{4.65}$$

from Eq. (4.18), the pair correlator in $d = 3$ dimensions is given by

$$G(\vec{x}) = \frac{k_B T}{4\pi J|\vec{x}|} \frac{1}{\beta^2 - \alpha^2}$$
$$\times [e^{-\alpha|\vec{x}|}(\lambda^2 - \alpha^2) - e^{-\beta|\vec{x}|}(\lambda^2 - \beta^2)]. \tag{4.66}$$

Here,

$$\alpha^2, \beta^2 = \frac{\lambda^2 + \mu/J \mp \sqrt{(\lambda^2 - \mu/J)^2 - 4Q/J}}{2}. \tag{4.67}$$

By contrast, for temperatures $T < T^*$, we obtain an analytic continuation of Eq. (4.66) to complex α and β,

$$G(\vec{x}) = \frac{k_B T}{8\alpha_1\alpha_2\pi J|\vec{x}|} e^{-\alpha_1|\vec{x}|}$$
$$\times[(\lambda^2 - \alpha_1^2 + \alpha_2^2)\sin\alpha_2|\vec{x}| + 2\alpha_1\alpha_2\cos\alpha_2|\vec{x}|], \tag{4.68}$$

In Eq. (4.68), $\alpha = \alpha_1 + i\alpha_2 = \beta^*$. In a similar fashion, in $d = 2$ spatial dimensions, for $T > T^*$,

$$G(\vec{x}) = \frac{k_B T}{2\pi}\frac{1}{\beta^2 - \alpha^2}[(\lambda^2 - \alpha^2)K_0(\alpha|\vec{x}|)$$
$$+(\beta^2 - \lambda^2)K_0(\beta|\vec{x}|)]. \tag{4.69}$$

As in the three-dimensional case, the high temperature correlator of Eq. (4.69) may be analytically continued to lower temperatures, $T < T^*$, for which α and β become complex.

High temperature limit

In the high temperature limit, in two spatial dimensions, from Eq. (4.69), we have,

$$G(\vec{x}) = \frac{k_B T}{2\pi J} K_0\left(\sqrt{\frac{k_B T\Lambda^2}{4\pi J}}|\vec{x}|\right) - \frac{8\pi}{k_B T\Lambda^4} K_0\left(\lambda|\vec{x}|\right). \tag{4.70}$$

In three spatial dimensions, from Eq. (4.66), we have,

$$G(\vec{x}) = \frac{k_B T}{4\pi J|\vec{x}|} e^{-\sqrt{\frac{k_B T \Lambda^3}{6\pi^2 J}}|\vec{x}|} - \frac{9\pi^3 Q}{k_B T \Lambda^6 |\vec{x}|} e^{-\lambda|\vec{x}|}. \tag{4.71}$$

In the unscreened case, in two spatial dimensions,

$$\begin{aligned} G(\vec{x}) &= \frac{k_B T}{2\pi J} K_0 \left(\sqrt{\frac{k_B T \Lambda^2}{4\pi J}} |\vec{x}| \right) \\ &\quad - \frac{8\pi}{k_B T \Lambda^4} K_0 \left(\sqrt{\frac{4\pi Q}{k_B T \Lambda^2}} |\vec{x}| \right). \end{aligned} \tag{4.72}$$

In three spatial dimensions,

$$\begin{aligned} G(\vec{x}) &= \Big[\frac{k_B T}{4\pi J|\vec{x}|} e^{-\sqrt{\frac{k_B T \Lambda^3}{6\pi^2 J}}|\vec{x}|} \\ &\quad - \frac{9\pi^3 Q}{k_B T \Lambda^6 |\vec{x}|} e^{-\sqrt{\frac{6\pi^2 Q}{k_B T \Lambda^3}}|\vec{x}|} \Big]. \end{aligned} \tag{4.73}$$

From the above expressions, it is clear that the coefficients of the terms corresponding to the diverging correlation length goes to zero in the high temperature limit.

We note that two correlation lengths are manifest for all $(\mu - J\lambda^2)^2 > 4JQ$. This includes all unfrustrated screened attractive Coulomb ferromagnets (those with $Q < 0$)). The evolution of the correlation functions may be traced by examining the dynamics of the poles in the complex k plane as a function of temperature. At high temperatures, correlations are borne by poles that lie on the imaginary k axis.

Thermal evolution of modulation length at low temperatures

At $T = T^*$, the poles merge in pairs at $k = \pm i\sqrt{\lambda^2 + \sqrt{Q/J}}$. At lower temperatures, $T < T^*$, the poles move off the imaginary axis (leading in turn to oscillations in the

correlation functions). The norm of the poles, $|\alpha| = (Q/J + \lambda^2\mu(T)/J)^{1/4}$ tends to a constant in the limit of vanishing screening ($\lambda^{-1} = 0$) wherein the after merging at $T = T^*$, the poles slide along a circle (Fig. 4.7). In the low temperature limit of the unscreened Coulomb ferromagnet, the poles hit the real axis at finite k, reflecting oscillatory modulations in the ground state. In the presence of screening, the pole trajectories are slightly skewed (Fig. 4.8) yet for $Q/J > \lambda^4$, α tends to the ground state modulation wavenumber $\sqrt{\sqrt{Q/J} - \lambda^2}$. If the screening is sufficiently large, i.e., if the screening length is shorter than the natural period favored by a balance between the unscreened Coulomb interaction and the nearest neighbor attraction ($\lambda > (Q/J)^{1/4}$), then the correlation functions never exhibit oscillations. In such instances, the poles continuously stay on the imaginary axis and, at low temperatures, one pair of poles veers towards $k = 0$ reflecting the uniform ground state of the heavily screened system.

To summarize, at high temperatures the pair correlator $G(x)$ is a sum of two decaying exponentials (one of which has a correlation length which diverges in the high temperature limit). For $T < T^*$ in under-screened systems, one of the correlation lengths turns into a modulation length characterizing low temperature oscillations. At the cross-over temperature T^*, the modulation length is infinite. As the temperature is progressively lowered, the modulation length decreases in size – until it reaches its ground state value. The temperature $T^*(Q/J, \lambda)$ is a "disorder line" [99–102] like temperature (Fig 4.9). An analytical thermodynamic crossover does occur at $T = T^*$.

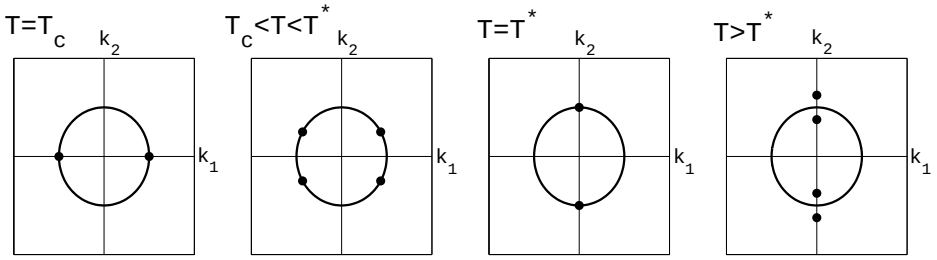

Figure 4.7: Location of the poles with increasing temperature (left to right) in the complex k-plane for the Coulomb frustrated ferromagnet. For temperatures below T_c, all the poles are real. Above T_c, the poles split in opposite directions of the real axis to give rise to two new complex poles. For $T_c < T < T^*$, we have complex poles. At T^*, pairs of such poles meet on the imaginary axis. Above T^*, the poles split along the imaginary axis. Thus, above T^*, the poles are purely imaginary.

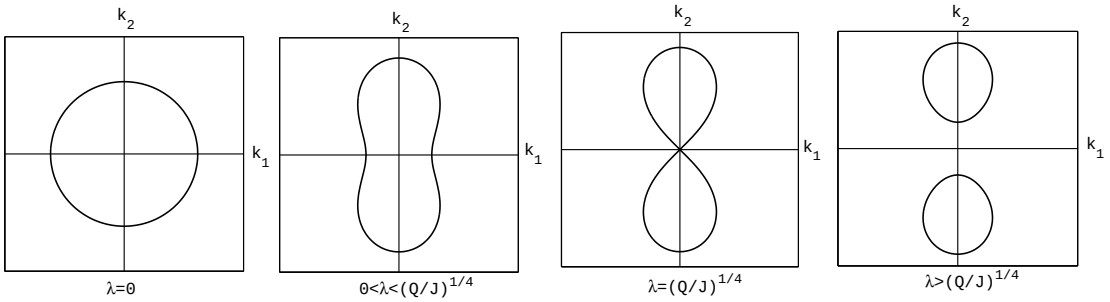

Figure 4.8: Trajectory of the poles in the complex k-plane for $T_c < T < T^*$ for the screened Coulomb ferromagnet. The screening length, λ^{-1} decreases from left to right. In the first figure $\lambda = 0$ and $\lambda > (Q/J)^{1/4}$ in the last figure.

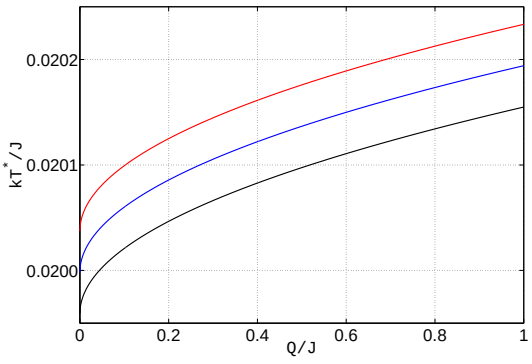

Figure 4.9: Temperature at which the modulation length diverges for a 100×100 Coulomb frustrated ferromagnet plotted versus the relative strength of the Coulomb interaction with respect to the ferromagnetic interaction. [Blue:$\lambda = \lambda_0 = 1/(100\sqrt{2})$; Red:$\lambda = 0.999\lambda_0$; Black:$\lambda = 1.001\lambda_0$]

A large-n calculation illustrates that the internal energy per particle

$$\frac{U}{N} = \frac{1}{2}(k_B T - \mu), \tag{4.74}$$

To detect a crossover in U and that in other thermodynamic functions, the forms of μ both above and below T^* may be derived from the spherical model normalization condition to find that the real valued functional form of $\mu(T)$ changes (See appendix E).

The system starts to exhibit order at the critical temperature $T = T_c$ given by

$$\frac{1}{k_B T_c} = \int \frac{d^d k}{(2\pi)^d} \frac{1}{v(\vec{k}) - v(\vec{q})}. \tag{4.75}$$

For $Q/J > \lambda^4$, the modulus of the minimizing (ground state) wavenumber ($|\vec{q}|$) is

given by

$$q = \frac{2\pi}{L_D^g} = \sqrt{\sqrt{Q/J} - \lambda^2}, \tag{4.76}$$

with L_D^g the ground state modulation length. Associated with this wavenumber is the kernel $v(\vec{q}) = 2\sqrt{JQ} - J\lambda^2$ to be inserted in Eq. (4.75) for an evaluation of the critical temperature T_c. Similarly, the ground state wavenumber $\vec{q} = 0$ whenever $Q/J < \lambda^4$. If $Q/J > \lambda^4$ and modulations transpire for temperatures $T < T^*$, the critical temperature at which the chemical potential of Eq. (4.19), $\mu(T_c) = J\lambda^2 - 2\sqrt{JQ}$, is lower than the crossover temperature T^* (given by Eq. (4.65)) at which modulations first start to appear. The Screened Coulomb Ferromagnet has $T_c(Q/J = \lambda^4) > 0$ in $d > 4$ dimensions and in any dimension $T_c(Q/J > \lambda^4) = 0$. For small finite n, a first order Brazovskii transition may replace the continuous transition occurring at T_c within the large-n limit [103]. Depending on parameter values such an equilibrium transition may or may not transpire before a possible glass transition may occur [41, 104].

Domain length scaling in the Coulomb Frustrated Ferromagnet

The characteristic length scales are governed by the position of the poles of $[v(k) + \mu]^{-1}$. See Fig. 4.7 for an illustration of the pole locations at low temperatures. For the frustrated Coulomb ferromagnet of Eq. (4.64) in the absence of screening ($\lambda^{-1} = 0$),

$$v(k) + \mu = \frac{J}{k^2}(k^4 + \frac{\mu}{J}k^2 + \frac{Q}{J}). \tag{4.77}$$

Eq. (4.77) enable us to determine, in our large-n analysis, the cross-over temperature T^* at which $\mu^* = \mu(T^*) = 2\sqrt{JQ}$. At $T = T^*$, the poles lie on the imaginary axis in k-plane. As the temperature is lowered below T^*, the two poles bifurcate. This bifurcation gives rise to finite size spatial modulations. At temperatures $T < T^*$, the four poles slide along a circle of fixed radius of size $(Q/J)^{1/4}$ (see Fig. 4.7). At zero temperature, these four poles merge in pairs to form two poles that lie on the real axis. The inverse modulation length is set by the absolute values of the real parts of the poles. We will set $\mu \equiv (2\sqrt{JQ} - \delta\mu)$. In the following, we will obtain the dependence of the real part of the poles on $\delta\mu$. The poles of $1/(v(k) + \mu)$ are determined by

$$k_{pole}^2 = -\frac{\mu}{2J} \pm i\sqrt{\frac{Q}{J} - \frac{\mu^2}{4J^2}} = \sqrt{\frac{Q}{J}}e^{\pm 2i\theta}. \tag{4.78}$$

At $\mu = \mu^*$, the angle $\theta = \pi/2$. This point corresponds to the transition between (i) the high temperature region ($T > T^*$) wherein the system does not exhibit any modulations and (ii) the low temperature region ($T < T^*$). (See Fig. 4.7.) Eq. (4.78) implies that $\cos 2\theta = [1 - \frac{\delta\mu}{\mu^*}]$ or

$$k_{pole,real} = \frac{\delta\mu^{1/2}}{2J^{1/2}}. \tag{4.79}$$

Thus, we get a crossover exponent of 1/2.

4.4.3 Full direction and location dependent dipole-dipole interactions

In this subsection and the next, we consider systems where the spins are three-dimensional and the interactions have the appropriate directional dependence. In this subsection, we will consider the effect of including the full dipolar interactions vis a vis the more commonly used scalar product form between two dipoles that is pertinent to two-dimensional realizations. The dipolar interaction is given by

$$H_{dip} = \sum_{\vec{x}\neq\vec{y}} \left[\frac{\vec{S}(\vec{x})\cdot\vec{S}(\vec{y})}{r^3} - \frac{3[\vec{S}(\vec{x})\cdot\vec{r}][\vec{S}(\vec{y})\cdot\vec{r}]}{r^5} \right]. \tag{4.80}$$

The two point correlator for a ferromagnetic system frustrated by this interaction is given, in the large-n approximation, by

$$G(\vec{x}) = k_B T \int \frac{d^d k}{(2\pi)^d} e^{i\vec{k}\cdot\vec{x}} \left[\frac{2}{J\Delta(\vec{k}) + Qv_d(k) + \mu} + \frac{1}{J\Delta(\vec{k}) - 2Qv_d(k) + \mu} \right], \tag{4.81}$$

where $v_d(k)$ is given by Eqs. (4.62,4.63). For temperatures $T \leq T_c$,

$$\mu_{min} = -\min_{k\in\mathbb{R}} \{ J\Delta(\vec{k}) + Qv_d(k), \; J\Delta(\vec{k}) - 2Qv_d(k) \}. \tag{4.82}$$

The Fourier transformed dipolar interaction kernel is positive definite, $v_d(k) > 0$. An unscreened dipolar interaction leads to a $v_d(k)$ that diverges (tends to negative infinity) at its minimum at $k = 0$. In the presence of both upper and lower distance

cutoffs (see, e.g., Eq. (4.4) for a lower cutoff) on the dipolar interaction, the minimum of $v_d(k)$ attains a finite value and the system has a finite critical temperature.

Examining Eq. (4.81), we see that the introduction of the angular dependence in the dipolar interaction changes the results that would be obtained if the angular dependence were not included in a dramatic way.

(i) New correlation and modulation lengths arise from the second term in Eq. (4.81).

(ii) At low temperatures, the second term in Eq. (4.81) becomes dominant as its poles have a smaller real part (and thus a larger correlation length) relative to the first term in Eq. (4.81) that appears for an isotropic dipole-dipole interactions.

4.4.4 Dzyaloshinsky- Moriya Interactions

As another example of a system with interactions having non-trivial directional dependence, we consider a system of three component spins with the Dzyaloshinsky-Moriya interaction [78, 79] present along with the ferromagnetic interaction and a long range interaction,

$$H = -J \sum_{\langle \vec{x},\vec{y} \rangle} \vec{S}(\vec{x}) \cdot \vec{S}(\vec{y}) + \sum_{\langle \vec{x},\vec{y} \rangle} \vec{D} \cdot [\vec{S}(\vec{x}) \times \vec{S}(\vec{y})] + Q \sum_{\vec{x} \neq \vec{y}} V_L(|\vec{x} - \vec{y}|) \vec{S}(\vec{x}) \cdot \vec{S}(\vec{y}). \tag{4.83}$$

We diagonalize this interaction kernel to obtain a Hamiltonian of the form,

$$H = \sum_{\vec{x},\vec{y}} \sum_{a} \hat{S}_a^*(\vec{x}) V_a(\vec{x},\vec{y}) \hat{S}_a(\vec{y}). \tag{4.84}$$

The $\hat{S}_a$'s are linear combinations of the components of $\vec{S}$. In a large-n approximation, the two point correlator is given by

$$G(\vec{x}) = k_B T \int \frac{d^d k}{(2\pi)^d} e^{i\vec{k}\cdot\vec{x}} \left[\frac{1}{J\Delta(\vec{k}) + Qv_L(k) + \mu} + \frac{2(J\Delta(\vec{k}) + Qv_L(k) + \mu)}{(J\Delta(\vec{k}) + Qv_L(k) + \mu)^2 + (D_1^2 + D_2^2 + D_3^2)[\Delta(\vec{k})]^2} \right]. \tag{4.85}$$

The presence of the Dzyaloshinsky-Moriya interaction does not alter the original poles and hence does not change the original length scales of the system. However, additional length scales arise due to the second term in Eq. (4.85).

A system of prominence where Dzyaloshinsky-Moriya interactions are important is MnSi [105]. The spiral order is naturally susceptible to glass like dynamics. [43, 105]

4.5 Conclusions

1. We studied the evolution of the ground state modulation lengths in frustrated Ising systems as the interaction parameters are varied.

2. We investigated, in large-n theories, the evolution of modulation and correlation lengths as a function of temperature in different classes of systems.

3. We proved that, in large-n theories, the combined sum of the number of correlation and the number of modulation lengths is conserved as the temperature is varied.

4. We studied three-dimensional dipolar systems. We found that the full dipolar interactions with angular dependence included, changes the ground state of the system and also adds new length scales.

Chapter 5

Universality of modulation length (and time) exponents

5.1 Introduction

In this chapter, we investigate the evolution of these length scales as a function of some parameter λ, such as the temperature T. We will largely focus on the temperature dependences of the correlation function to derive and discuss our results. We report on the temperature (or other parameter) dependence of emergent modulation lengths that govern the size of various domains present in some systems. Our central result is that if fixed wavelength modulations characterized by a particular *finite* length scale, L_*, appear beyond some temperature T_* then, the modulation length, L_D on

the other side of the crossover differs from L_* as

$$|L_D - L_*| \propto |T - T_*|^{\nu_L}. \tag{5.1}$$

When there are *no modulations* on one side of T_*, i.e., $L_* \to \infty$, we have near the crossover,

$$L_D \propto |T - T_*|^{-\nu_L}. \tag{5.2}$$

Apart from some special situations, we find that irrespective of the interaction, $\nu_L = 1/2$. We arrive at this rather universal result assuming that there is no phase transition at the crossover temperature T_*. Our result holds everywhere inside a given thermodynamic phase of a system.

Our considerations are not limited to continuous crossovers. A corollary of our analysis pertains to systems with discontinuous (*"first-order" like*) jumps in the correlation or modulation lengths.

We will further comment on situations in which a branch point appears at T_*. We will present examples where we obtain rational and irrational exponents and also the anomalous critical exponent η. Our analysis affords general connections to the critical scaling of correlation lengths in critical phenomena.

Our results for length scales can be extended to timescales. We will, amongst other notions, in employing a formal interchange of spatial with temporal coordinates, introduce the concept of a *Josephson timescale*.

Lastly, further deepening the analogy between results in the spatial and time

domain, we will comment on the presence of phases with aperiodic spatial "chaotic" modulations (characteristic of amorphous configurations) in systems governed by non-linear Euler-Lagrange equations. Aperiodic "chaotic" modulations may appear in strongly correlated electronic systems.

In Appendix G, we present applications to Fermi systems pertaining to metal–band insulator transition, change of Fermi surface topology, divergence of effective masses, Dirac systems and topological insulators.

5.2 A universal domain length exponent – Details of analysis

In this section, we derive (via various inter-related approaches), our central result – the existence of a new exponent for the domain length in rather general systems.

We will now consider the situation in which the system exhibits modulations at a fixed wave-vector q for a finite range of temperatures on one side of T_*, [viz., **(i)** $T > T_*$, or, **(ii)** $T < T_*$] and starts to exhibit variable wavelength modulations on the other side [**(iii)** $T < T_*$ for (i) and $T > T_*$ for (ii)]. A schematic illustrating this is shown in Fig. 5.1. In sub-section 5.2.1, we will assume that the pair correlation function is meromorphic (realized physically by *absence of phase transitions*) at the crossover point and illustrate how modulation length exponents may appear. In sub-section 5.2.2, we will comment on the situation where the crossover point may be a

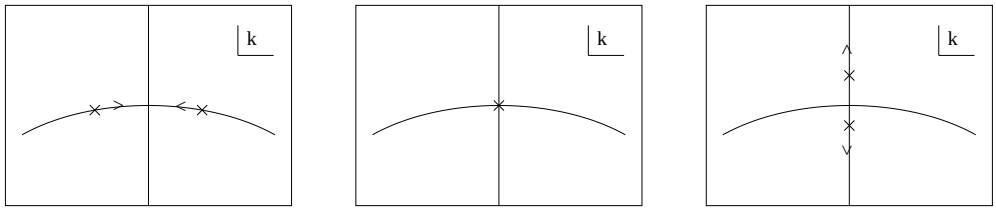

(a) Variable modulation length.

(b) The crossover point ($T = T_*$).

(c) Fixed modulation length.

Figure 5.1: Schematic showing the trajectories of the singularities of the correlation function near a fixed – variable modulation length crossover. Two poles of the correlation function merge at $k = k_*$ at $T = T_*$. On the fixed modulation length side of the crossover point, Re $k = q$.

branch point of the correlation function.

5.2.1 Crossovers at general points in the complex k-plane

In the up and coming, we will assume that the pair correlator, $G(T, k)$ is a meromorphic function of k and T near a crossover point. Our analysis below is exact as long as we do not cross any phase boundaries. Such a case is indeed materialized in the incommensurate-commensurate crossovers in the three-dimensional axial next-nearest-neighbor Ising (ANNNI) model [106, 107] (which is of type (ii) in the classification above). This phenomenon is also seen in the ground state phase diagram of Frenkel-Kontorova models [108] in which one of the coupling constants is tuned

instead of temperature.

In the following, we present two alternative derivations for the universal exponent characterizing this crossover.

First approach

In general, if the pair correlation function $G(T,k)$ is a meromorphic function of the temperature T and the wave-vector k near a crossover point (T_*k_*), then $G^{-1}(T,k)$ must have a Taylor series expansion about that point. We have,

$$G^{-1}(T,k) = \sum_{m_1,m_2=0}^{\infty} A_{m_1m_2}(T-T_*)^{m_1}(k-k_*)^{m_2}. \tag{5.3}$$

Since $G^{-1}(T_*,k_*)=0$, we have, $A_{00}=0$. Let us try to find the trajectory of the pole $K(T)$ (with $K(T_*)=k_*$) of $G(T,k)$ in the complex k-plane as the temperature is varied around T_*. Writing down the leading terms of $G^{-1}(T,k)$, we have, in general,

$$\begin{aligned} G^{-1}(T,k) \;\sim\; & \sum_{p=0}^{[m/a]} B_p(T-T_*)^{m-ap}(k-k_*)^{n+bp} + \\ & o((T-T_*)^m(k-k_*)^n), \end{aligned} \tag{5.4}$$

as $(T,k)\to(T_*,k_*)$ with m,n,a,b integers, $m,n\geq 0$, $a,b\geq 1$, and $B_p = A_{m-ap,\ n+bp}$ in Eq. (5.3). In the summand, $[x]$ represents the greatest integer less than or equal to x. Terms negligible compared to a quantity x are represented by $o(x)$. We have,

$$K(T) \sim k_* + C(T-T_*)^{a/b}, \tag{5.5}$$

where C is some constant, yielding $\nu_L = a/b$. By the very definition of T_*, on one side of T_* [(i) or (ii) above], there exists at least one root [say, $K(T)$] of G^{-1} satisfying

$K_R(T) = q$, where q is a constant. On the other side [(iii) above], $K_R(T) \neq q$. As such, the function $K(T)$ is non-analytic at T_*. The left hand side of Eq. (5.5) is therefore not analytic at $T = T_*$, implying that the right hand side cannot be analytic. This means that (a/b) cannot be an integer, which in turn implies that $b \geq 2$. Therefore, in the most common situations we might encounter,

$$G^{-1}(T,k) \sim A(T - T_*) + B(k - k_*)^2$$
$$\implies \quad a = 1 \text{ and } b = 2. \tag{5.6}$$

When Fourier transforming $G(T,k)$ by evaluating the integral in Eqs. (2.14, 2.15) using the technique of residues, the real part of the poles (i.e., K_R) gives rise to oscillatory modulations of length $L_D = 2\pi/K_R$. If the modulation length locks its value to $2\pi/q$ on one side of the crossover point, then, on the other side, near T_*, it must behave as

$$|2\pi/L_D - q| \propto |T - T_*|^{1/2}$$
$$\implies \boxed{\nu_L = 1/2.} \tag{5.7}$$

Second approach

We now turn to a related alternative approach that similarly highlights the universal character of the modulation length exponent. If the correlation function G is a meromorphic function of k, then, expanding about a zero $K_1(T)$ of G^{-1}, we have,

$$G^{-1}(T,k) = A(T)\,(k - K_1(T))^{m_1}\,G_1^{-1}(T,k), \tag{5.8}$$

where $G_1^{-1}(T,k)$ is an analytic function of k and $G_1^{-1}(T,K_1(T)) \neq 0$. We can do this again for the function $G_1^{-1}(T,k)$ choosing one of its zeros $K_2(T)$ and continue the process until the function left over does not have any more zeros. We have,

$$G^{-1}(T,k) = A(T)\prod_{a=1}^{p}(k-K_a(T))^{m_a}\,G_p^{-1}(T,k), \tag{5.9}$$

where the function $G_p^{-1}(T,k)$ is an analytic function with no zeros, m_as are integers and, in principle, p may be arbitrarily high. This factorization can be done in each phase where G is meromorphic. Let $K_1(T)$ be a non-analytic zero of G^{-1}, i.e., one for which Re $K_1(T) = q$ on one side of $T = T_*$. To ensure analyticity of G^{-1} in T in the vicinity of $T = T_*$, there must be at least one other root $K_2(T)$, such that as $T \to T_*$, both $K_1(T)$ and $K_2(T)$ veer towards k_*, where Re $k_* = q$ [e.g., see Fig. 5.2 which is of type (i) above, $k_* = \pm i$]. In other words, p in Eq. (5.9) cannot be smaller than two. The proof of this assertion is simple. If $p = 1$, then, according to Eq. (5.9), $G^{-1}(T,k) = A(k-K_1(T))G_1^{-1}(T,k)$. At $T = T_*$, however, $K_1(T)$ is not analytic, implying that $G^{-1}(T,k)$ can be analytic only if $p \geq 2$. For $p \geq 2$, at T_*, G^{-1} will, to leading order, vary quadratically in $(k-k_*)$ in the complex k plane near k_*. Thus,

$$\left.\frac{\partial G^{-1}}{\partial k}\right|_{(T_*,k_*)} = 0. \tag{5.10}$$

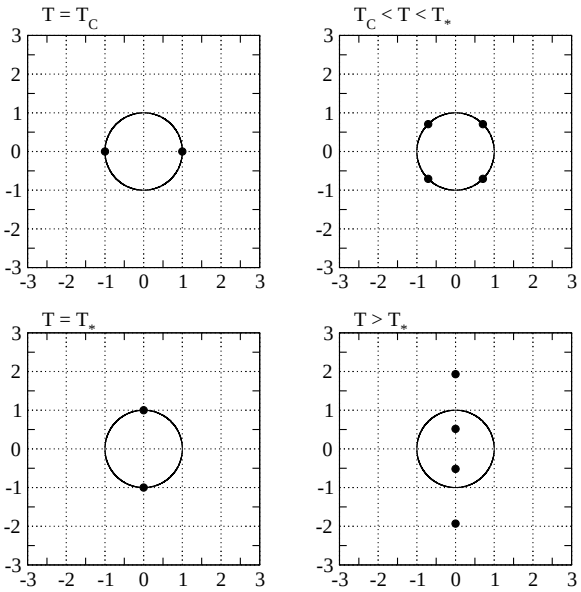

Figure 5.2: Location of the poles of the correlation function of the large-n Coulomb frustrated ferromagnet for $J = Q = 1$ in the complex k-plane. The circle and the Y-axis show the trajectory $K(T)$ of the poles as the temperature T is varied.

Now, if G^{-1} has a finite first partial derivative relative to the temperature T then, for a pole K near k_*, to leading order,

$$G^{-1}(T_*, k_*) + (T - T_*)\frac{\partial G^{-1}}{\partial T}\bigg|_{(T_*,k_*)} + \frac{(K - k_*)^2}{2!}\frac{\partial^2 G^{-1}}{\partial k^2}\bigg|_{(T_*,k_*)} = 0. \tag{5.11}$$

By its definition, k_* satisfies the equality $G^{-1}(T_*, k_*) = 0$. Therefore,

$$|K - k_*| = \sqrt{\frac{2(T_* - T)\ \frac{\partial G^{-1}}{\partial T}\big|_{(T_*,k_*)}}{\frac{\partial^2 G^{-1}}{\partial k^2}\big|_{(T_*,k_*)}}}. \tag{5.12}$$

Equation (5.7) is an exact equality. It demonstrates that the exponent $\nu_L = 1/2$

universally unless one of $\frac{\partial^2 G^{-1}}{\partial k^2}$ and $\frac{\partial G^{-1}}{\partial T}$ vanishes at (T_*, k_*).[109] Often, $G^{-1}(T,k)$ is a rational function of k, i.e.,

$$G^{-1}(T,k) = \frac{G_n^{-1}(T,k)}{G_d^{-1}(T,k)}, \tag{5.13}$$

where $G_n^{-1}(T,k)$ and $G_d^{-1}(T,k)$ are polynomial functions of k. In those instances, we get the same result as above by using $G_n^{-1}(T,k)$ in the above arguments. The value of the critical exponent is similar to that appearing for the correlation length exponent for mean-field or large-n theories. It should be stressed that our result of Eq. (5.7) is far more general.

Lock-in of the correlation length. Apart from the crossovers across which the modulation length locks in to a fixed value, we can also have situations where the correlation length becomes constant as a crossover temperature T_{**} is crossed. If this happens, our earlier analysis for the modulation length may be replicated anew for the correlation length. Therefore, if the correlation length has a fixed value ξ_0 on one side ($T < T_{**}$ or $T > T_{**}$) of the crossover point, then, on the other side ($T > T_{**}$ or $T < T_{**}$, respectively), near T_{**}, it must behave as,

$$|1/\xi - 1/\xi_0| \propto |T - T_{**}|^{\nu_c}, \tag{5.14}$$

where, like ν_L, $\nu_c = 1/2$ apart from special situations where it may take some other rational values. Here and throughout, we use ν_c to represent the usual correlation length exponent, ν to distinguish it from the modulation length exponent ν_L.

5.2.2 Branch points

A general treatment of a situation in which the crossover point is a branch point of the inverse correlation function in the complex k-plane is beyond the scope of this work. Branch points are ubiquitous in correlation functions in both classical as well as quantum systems.

For example, as in Chapter 4, in the large-n rendition of a bosonic system (with a Hamiltonian of Eq. (2.1) and $S(x)$ representing bosonic fields), the momentum space correlation function at temperature T is given by

$$G(\vec{k}) = \sqrt{\frac{\mu_1}{v(\vec{k})+\mu}}\left[n_B\left(\frac{\sqrt{\mu_1(v(\vec{k})+\mu)}}{k_BT}\right)+\frac{1}{2}\right], \tag{5.15}$$

where μ_1 is a constant having dimensions of energy, μ is the chemical potential, $n_B(x) = 1/(e^x-1)$ is the Bose distribution function and k_B is Boltzmann's constant.

Similar forms, also including spatial modulations in $G(r)$, may also appear. We briefly discuss examples where we have a branch cut in the complex k-plane.

The one-dimensional momentum space correlation function,

$$G(k) = \frac{1}{\sqrt{(k-q)^2+r}} + \frac{1}{\sqrt{(k+q)^2+r}}, \tag{5.16}$$

reflects a real space correlation function given by

$$G(x) = \frac{2\cos(qx)\mathrm{K}_0(x\sqrt{r})}{\pi}, \tag{5.17}$$

where $\mathrm{K}_0(\cdot)$ is a modified Bessel function. Thus, as is to be expected, we obtain length scales associated with the branch points $K = \pm q \pm i\sqrt{r}$.

Similarly, the three-dimensional real space correlation function corresponding to

$$G(k) = \frac{1}{\sqrt{(k-q)^2 + r}}, \tag{5.18}$$

exhibits the same correlation and modulation lengths along with an algebraically decaying term for large separations. Another related $G^{-1}(k)$ involving a function of $|\vec{k}|$ (i.e., not an analytic function of k^2) was investigated earlier.[110]

Throughout the bulk of our work, we consider simple exponents associated with analytic crossovers. In considering branch points, our analysis may be extended to critical points. As is well known, at critical points of d dimensional systems, the correlation function for large r, scales as

$$G(r) \propto \frac{1}{r^{d-2+\eta}}, \tag{5.19}$$

with η the *anomalous* exponent. Such a scaling implies, for non-integer η, the existence of a $k = 0$ branch point of $G(k)$.

If the leading order behavior of $1/G^{(m)}(T,k)$ is algebraic near a branch point (T_*, k_*), then we get an algebraic exponent characterizing a crossover at this point [m being the lowest order derivative of $G(k)$ which diverges at $k = k_*$ as in Eq. (2.17)]. That is, we have,

$$\begin{aligned} \frac{1}{G^{(m)}(T,k)} \quad &\sim \quad A(T-T_*)^{z_1} - B(k-k_*)^{z_2} \\ &\text{as } (T,k) \to (T_*, k_*). \end{aligned} \tag{5.20}$$

This implies that the branch points K deviate from k_* as

$$(K - k_*) \sim \left(\frac{A}{B}\right)^{1/z_2} (T - T_*)^{z_1/z_2}. \tag{5.21}$$

We therefore observe a length scale exponent $\nu = z_1/z_2$ at this crossover. This exponent may characterize a correlation lengths and/or a modulation lengths. The exponent z_1/z_2 may assume *irrational* values in many situations in which the function $G^{-1}(T, k)$ is not analytic near the crossover point. Such a situation could give rise to phenomena exhibiting anomalous exponents η. For example, if we have a diverging correlation length at a critical temperature T_c, for a system with a correlation function which behaves as in Eq. (5.19), then, we have in Eq. (5.20), $z_2 = 2 - \eta$. Thus, we have,

$$\begin{aligned} |L_D - L_{Dc}| &\propto |T - T_c|^{\frac{z_1}{2-\eta}}, \\ \implies & \boxed{\nu_L = \frac{z_1}{2-\eta}}, \end{aligned} \tag{5.22}$$

where $L_{Dc} = 2\pi/|\text{Re } k_*|$, and more importantly,

$$\begin{aligned} \xi &\propto |T - T_c|^{-\frac{z_1}{2-\eta}}, \\ \implies & \boxed{\nu_c = \frac{z_1}{2-\eta}}. \end{aligned} \tag{5.23}$$

Other critical exponents could also, in principle, be calculated using hyper-scaling relations.

If $G^{-1}(T, k)$ has a Puiseux representation about the crossover point, i.e.,

$$G^{-1}(T, k) = \sum_{m=m_0}^{\infty} \sum_{p=p_0}^{\infty} a_{mp} (k - k_*)^{m/a} (T - T_*)^{p/b}, \tag{5.24}$$

with $a_{m_0 p_0} = 0$, where $m_0,\ p_0,\ a$ and b are integers, then, the result we derived above applies to the relevant length scale and the crossover exponent $\nu = a/b$, is again a *rational number*.

Generalizing, if $G^{-1}(T, k)$ is the ratio of two Puiseux series, we use the numerator to obtain the leading order asymptotic behavior and hence obtain a rational exponent.

5.2.3 A corollary: Discontinuity in modulation lengths implies a thermodynamic phase transition

Non-analyticities in the correlation function $G(k)$ for real wave-vector k imply the existence of a phase transition. This leads to simple corollaries as we now briefly elaborate on. A sharp discontinuous jump in the value of the modulation lengths (and/or correlation lengths) implies that the zeros $\{K_a\}$ of $G^{-1}(k)$ in the complex k plane, exhibit discontinuous ("first order-like") jumps as a function of some parameter (such as the temperature T when $T = T_*$). When this occurs, as seen by, e.g., differentiating the reciprocal of the product of Eq. (5.9), the correlation function will, generally, not be analytic as a function of T at $T = T^*$. Putting all of the pieces together, we see that a discontinuous change in the modulation (or correlation) lengths impies the existence of a bona fide phase transition. Thus, all commensurate-commensurate crossovers must correspond to phase transitions. For example, see the ANNNI model.[102]

5.2.4 Diverging correlation length at a spinodal transition

Our analysis is valid for both annealed and quenched systems so long as translational symmetry is maintained (and thus, the correlation function is diagonal in k-space). In particular, whenever phase transitions are "avoided" the rational exponents of Eq. (5.5) will appear.[33, 34, 43]

In diverse arenas, we may come across situations in which there are no diverging correlation lengths even when the inverse correlation function has zeros corresponding to real values of the wave-vector. These are signatures of a first order phase transition, e.g., transition from a liquid to a crystal. If the first order phase transition is somehow avoided, then the system may enter a metastable phase and may further reach a point where the correlation length diverges, e.g., a spinodal point. If it is possible to reach this point and if the inverse correlation function is analytic there, then our analysis will be valid, thereby leading to rational exponents characterizing the divergence of the correlation length. There are existing works in the literature which seem to suggest that such a point may not be reachable. For example, in mode coupling theories of the glass transition, the system reaches the mode coupling transition temperature T_{MCT} at which the viscosity and relaxation times diverge and hence does not reach the point where the correlation length blows up.[111]

5.2.5 Conservation of characteristic length scales

In Ref. [59], it was mentioned that the total number of characteristic length scales in a large-n system remains constant in systems in which the Fourier space interaction kernel $v(\vec{k})$ is a rational function of k^2 and the real space kernel is rotationally invariant. (Similar results hold for systems with reflection point group symmetry.[112]) In this sub-section, we generalize that argument and say that whenever the Fourier space correlator $G(\vec{k})$ of a general rotationally invariant system is a rational function of k^2,i.e.,

$$G(\vec{k}) = \frac{P(k^2)}{Q(k^2)}, \tag{5.25}$$

the total number of correlation and modulation lengths remains constant apart from isolated points as a tuning parameter λ is smoothly varied. In Eq. 5.25, the functions $P(k^2)$ and $Q(k^2)$ are polynomial functions of k^2. Rotational invariance requires that $G(\vec{k})$ is real-valued for real wavevectors k. As argued in Ref. [59], all length scales in the such systems are associated with the poles of $G(k)$ in the complex k-plane and these remain constant for a given form of the function $G(k)$. Each real root of the function $Q(k^2)$ gives rise to a term in the real space correlation function which has one correlation or modulation length. Non-real roots (which necessarily come in complex conjugate pairs) give rise to a correlation and a modulation length. Thus, the total number of characteristic length scales in the system is equal to the order of the polynomial function $Q(k^2)$ which remains fixed.

5.3 $O(n)$ systems

The correlation function for $O(n)$ systems can be calculated exactly at both the low and the high temperature limits. At intermediate temperatures, various crossovers and phase transitions may appear. In this section, we discuss the low and high temperature behavior length scales characterizing $O(n)$ systems.

5.3.1 Low temperature configurations

It was earlier demonstrated [98] that for $O(n \geq 2)$, *all* ground states of a system have to be spirals (or poly-spirals) of characteristic wave-vectors $\vec{q}_\alpha$, given by

$$v(\vec{q}_\alpha) = -\min_{\vec{k}\in\mathbb{R}^d} v(\vec{k}), \tag{5.26}$$

where $\mathbb{R}^d$ represents the set of all d-dimensional real vectors. At $T = 0$, the modulation lengths in the system are given by

$$L_D^{i,\alpha}(T = 0) = 2\pi/q_{i,\alpha}, \tag{5.27}$$

where $i(1 \leq i \leq d)$ labels the Cartesian directions in d dimensions. This, together with Eq. (5.28) gives us the high and low temperature forms of the correlation function and its associated length scales.

5.3.2 High temperatures

As demonstrated in Chapter 3, diverse systems behave in the same way at high temperatures. For $O(n)$ systems,

$$G^{-1}(T,k) = 1 + v(k)/k_B T + \mathcal{O}(1/T^3). \tag{5.28}$$

The high temperature series may be extended and applied at the crossover temperature T_*, if there is no phase transition at temperatures above T_* and for all relevant real k's, $|v(k)| \ll k_B T_*$. [A detailed example will be studied in Sec. 5.3.5.] Generally, Eq. (5.28) may be analytically continued for complex k's and in the vicinity of T_*,

$$\delta k \sim \left[\frac{m!\; k_B(T_* - T)}{v^{(m)}(k_*)}\right]^{\frac{1}{m}}, \tag{5.29}$$

where k_* is a characteristic wave-vector at T_*. In the above, δk denotes the change in the location of the poles K of G^{-1} when the temperature is changed from T_* to T (i.e., $\delta k \equiv K - k_*$) and m is the order of the lowest non-vanishing derivative of $v(k)$ at k_*. As in previous analysis, $v'(k_*) = 0$ and $m \geq 2$. For general $v(k)$, typically $m = 2$ and $\nu_L = 1/2$ as before.

We now turn to examples which explicitly illustrate how our results are realized including exceptional systems with non-trivial exponents.

5.3.3 Large-n Coulomb frustrated ferromagnet – modulation length exponent at the crossover temperature T_*

In the current sub-section and the two that follow, we will discuss the large-n limit in $O(n)$ systems. The results in the previous two sections pertain to arbitrary n. We illustrate how our result applies to the large-n Coulomb frustrated ferromagnet. As mentioned in Chapter 4, in the large-n limit, $O(n)$ systems are exactly solvable and behaves as the spherical model. The correlation function in k-space is given by

$$G^{-1}(T,k) = [v(k) + \mu(T)]/k_B T, \tag{5.30}$$

where $v(k)$ is the Fourier space interaction kernel and $\mu(T)$ is a Lagrange multiplier, that enforces the spherical constraint. The paramagnetic transition temperature T_C is obtained from the relation, $\mu(T_C) = -\min_{k\in\mathbb{R}} v(k)$. Below T_C, the Lagrange multiplier $\mu(T) = \mu(T_C)$. Above T_C, $\mu(T)$ is determined by the global average constraint that $G(\vec{x}=0) = \frac{1}{N}\sum_{\vec{k}} G(\vec{k}) = 1$. This global constraint also implies that, above T_C, small changes in temperature result in proportional changes in $\mu(T)$ and at high temperatures, $\mu(T)$ is a monotonic increasing function of T. The Fourier space kernel $v(k)$ for the "Coulomb frustrated ferromagnet" (in which nearest neighbor ferromagnetic interactions of strength J compete with Coulomb effects of strength Q) is given by $v(k) = Jk^2 + Q/k^2$, where J and Q are positive constants. The critical temperature, T_C of this system is given by $\mu(T_C) = -2\sqrt{JQ}$. At T_C, the correlation length is infinity and the modulation length is $L_D = 2\pi\sqrt[4]{J/Q}$. As the temperature is in-

creased, the modulation length increases and the correlation length decreases. At T_*, given by $\mu(T_*) = 2\sqrt{JQ}$, the modulation length diverges and the correlation length becomes $\xi = \sqrt[4]{J/Q}$. At temperatures above T_*, the correlation function exhibits no modulations and there is one decreasing correlation length and one increasing correlation length. The term in the correlation function with the increasing correlation length becomes irrelevant at high temperatures because of an algebraically decaying prefactor. The divergence of the modulation length at T_* shows an exponent of $\nu_L = 1/2$.[59]

5.3.4 An example with $\nu_{\mathbf{L}} \neq \mathbf{1/2}$

In what follows, we demonstrate, as a matter of principle, that the exponent for the divergence of the modulation length (and also the correlation length) can be different from 1/2 in certain special cases. As an illustrative example, we consider a large-n (or spherical model) system for which in Eq. (2.6),

$$\begin{aligned} v(k) &= A(k^2 + l_s^{-2})^2 + 4B(k^2 + l_s^{-2}) \\ &\quad +4C/(k^2 + l_s^{-2}) + D/(k^2 + l_s^{-2})^2, \end{aligned} \tag{5.31}$$

where l_s is a screening length. If we set $A = B = C = D = 1$ then in the resultant system $\nu_L \neq 1/2$ at a crossover temperature. It has a critical temperature T_C, given by $\mu(T_C) = -10$. At T_C, the modulation length is $L_D = 2\pi/\sqrt{1 - 1/l_s^2}$ and the correlation length blows up (as required by definition). At the crossover temperature

T_* (for which $\mu(T_*) = 6$) the modulation length diverges and the correlation length scales as $\xi = 1/\sqrt{1 + 1/l_s^2}$. A temperatures just below T_*, the modulation length L_D diverges as $L_D \propto (T_* - T)^{-1/4}$ meaning that $\nu_L = 1/4$. This is because the first three derivatives of $v(k)$ vanish at $k = i$, which is the characteristic wave-vector at T_* (see Fig. 5.3).

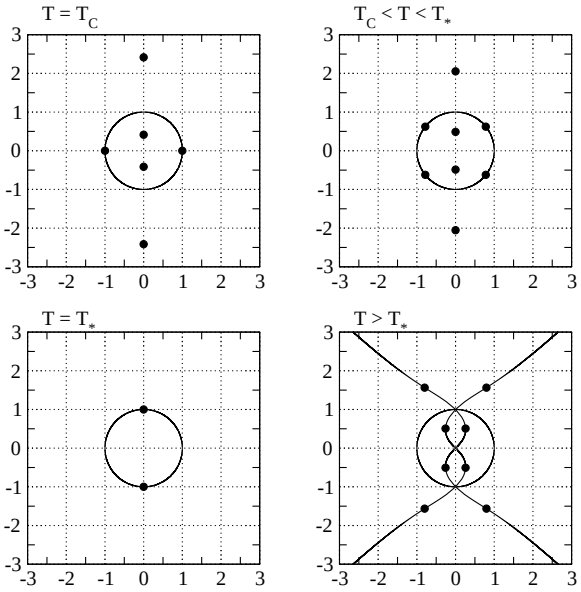

Figure 5.3: Location of the poles of the correlation function of the system in Eq. (5.31) for large l_s (small screening) in the complex k-plane.

5.3.5 An example in which T_* is a high temperature

We now provide an example in which the high temperature result of Sec. 5.3.2 (valid for any $O(n)$ system with arbitrary n) can be applied at a crossover point.

Consider the large-n system in Eq. (5.31) with $A = 1$, $B \gg 1$, $C = 1/4$, $D = 0$ and the screening length, $l_s \gg B$. The critical temperature of this system is given by $\mu(T_C) \sim -4\sqrt{B}$ where the modulation length is $L_D \sim 2\pi\sqrt[4]{4B}$. There is a crossover temperature T_* such that $\mu(T_*) \sim 4B^2$. One of the modulation lengths diverges at T_*. The corresponding correlation length is given by $\xi \sim 1/\sqrt{2B}$. This provides an example in which $|v(k)| \ll k_B T_*$ for all real k's satisfying $|k| \leq \pi$. The second derivative of $v(k)$ is non-zero at the crossover point, resulting in a crossover exponent $\nu_L = 1/2$.

5.4 Crossovers in the ANNNI model

We now comment on one of the oldest studied examples of a system with a crossover temperature. The following Hamiltonian represents the ANNNI model.[102, 106, 107]

$$H = -J_1 \sum_{\langle \vec{x},\vec{y} \rangle} S(\vec{x})S(\vec{y}) + J_2 \sum_{\langle\langle \vec{x},\vec{y} \rangle\rangle} S(\vec{x})S(\vec{y}), \tag{5.32}$$

where as throughout, $\vec{x}$ is a lattice site on a cubic lattice, and the spins $S(\vec{x}) = \pm 1$. The couplings, $J_1, J_2 > 0$. In the summand, $\langle\cdot\rangle$ represents nearest neighbors and $\langle\langle\cdot\rangle\rangle$ represents next nearest neighbors along one axis (say the Z-axis), see Fig. 5.4. Depending on the relative strengths of J_1 and J_2, the ground state may be either ferromagnetic or in the "$\langle 2 \rangle$ phase". The "$\langle 2 \rangle$ phase" is a periodic layered phase, in which there are layers of width two lattice constants of 'up" spins alternating with layers of "down" spins of the same width, along the Z-axis. As the temperature is

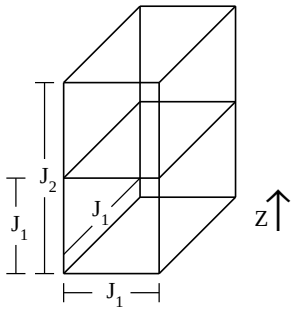

Figure 5.4: The coupling constants in the three-dimensional ANNNI model.

increased, the correlation function exhibits jumps in the modulation wave-vector at different temperatures. At these temperatures, the system undergoes first order transitions to different commensurate phases. The inverse correlation function $G^{-1}(T, k)$ is therefore not an analytic function of k and T at the transition points. The phase diagram for the ANNNI model, however, also has several crossovers where the system goes from a commensurate phase to an incommensurate phase with a continuously varying modulation length (see Fig. 5.5).[3, 4] At these crossover points, following our rigorous analysis, we expect a crossover exponent $\nu_L = 1/2$. Such a scaling of the modulation length has been estimated by several approximate techniques near the "Lifshitz point" P_L.[102, 113–118] The Lifshitz point is the point in the phase diagram of the ANNNI model at which the high temperature paramagnetic phase coexists with the ferromagnetic phase as well as a phase with continuously varying modulation lengths. It is marked as P_L in Fig. 5.5(b). Although the point P_L has a first order transition, it can be thought of as a limit in which the incommensurate and

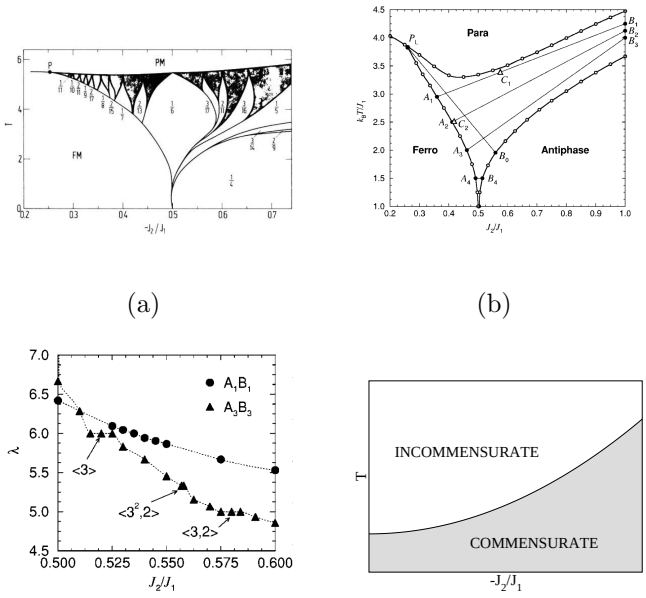

Figure 5.5: Existence of incommensurate phases between the commensurate regions in the phase diagram of the ANNNI model. **(a)** Mean field phase diagram of the ANNNI model in three dimensions. The shaded regions show higher order commensurate phases which have variable modulation length incommensurate phases in between (From Ref. [3]. Reprinted with permission from APS.) **(b)** Phase diagram for the three-dimensional ANNNI model using a modified tensor product variational approach (From Ref. [4]. Reprinted with permission from APS.) **(c)** Variation of wavelength along paths A_1B_1 and A_3B_3 of (b) showing a smooth variation of the wavelength near the paramagnetic transition line (From Ref. [4]. Reprinted with permission from APS.) **(d)** Cartoon of an incommensurate-commensurate crossover region from (a).

commensurate regions in Fig. 5.5(a) shrink and merge to a single point. We would also like to point out that it is known [119] that if the wave-vector takes all possible rational values ("complete devil's staircase"), we have no first order transitions. Additionally, non-analyticity of the correlation function does not prohibit other quantities from having continuous crossover behavior. For example, the correlation of the fluctuations, i.e., the connected correlation function may generally exhibit continuous variation from a fixed to a variable modulation length phase. If the inverse connected correlation function is analytic, our result can be applied to it resulting in a crossover exponent of 1/2.

5.5 Parameter extensions and generalizations

It is illuminating to consider simple generalizations of our result to other arenas. We may also replicate the above derivation for a system in which, instead of temperature, some applied other field λ is responsible for the changes in the correlation function of the system. Some examples could be pressure, applied magnetic field and so on. The complex wave-vector k could also be replaced by a frequency ω whose imaginary part would then correspond to some decay constant in the time domain.

More generally, we look for solutions to the equation

$$G^{-1}(\lambda, u) = 0, \tag{5.33}$$

with the variable u being a variable Cartesian component of the wave-vector, the

frequency, or any other momentum space coordinate appearing in the correlation function between two fields ($u = k_i, \omega$, and so on). Replicating our steps mutatis mutandis, we find that the zeros of Eq. (5.33) scale as $|u - u_0| \propto |\lambda - \lambda_*|^{1/2}$ whenever the real (or imaginary) part of some root becomes constant as λ crosses λ_*. Thus, our predicted exponent of $\nu_L = 1/2$ could be observed in a vast variety of systems in which a crossover occurs as the applied field crosses a particular value, in the complex wave-vector like variable.

Another generalization of our result proceeds as follows.[120] Suppose that we have a general *analytic* operator (including any inverse propagator) $G^{-1}(\lambda)$ that depends on a parameter λ. Let a_α be a particular eigenvalue,

$$G^{-1}(\lambda)\,|a_\alpha(\lambda)\rangle = a_\alpha(\lambda)\,|a_\alpha(\lambda)\rangle. \tag{5.34}$$

If $a_\alpha(\lambda)$ changes from being purely real to becoming complex as we change the parameter λ beyond a particular value λ_* (i.e., $a_\alpha(\lambda > \lambda_*)$ is real and $a_\alpha(\lambda < \lambda_*)$ is complex, or the vice versa), then the imaginary part of $a_\alpha(\lambda)$ will scale (for $\lambda < \lambda_*$ in the first case noted above and for $\lambda > \lambda_*$ in the second one) as $\mathrm{Im}\,\{a_\alpha(\lambda)\} \propto |\lambda - \lambda_*|^{1/2}$. A particular such realization is associated with the spectrum of a non-Hermitian Hamiltonian [playing the role of G^{-1} in Eq. (5.34)] which, albeit being non-Hermitian, may have real eigenvalues (as in $\mathcal{PT}$ symmetric Hamiltonians).[121] In this case, the crossover occurs when a system becomes $\mathcal{PT}$ symmetric as a parameter λ crosses a threshold λ_*.

Similarly, if $a_\alpha(\lambda)$ changes from being pure imaginary to complex at $\lambda = \lambda_*$, then the real part of the eigenvalue will scale in the same way. That is, in the latter instance, Re $\{a_\alpha(\lambda)\} \propto |\lambda - \lambda_*|^{1/2}$.

Our next brief remark pertains to some theories with multi-component fields, e.g. n component theories with Hamiltonians of the form,[43]

$$H = \frac{1}{2N} \sum_{\vec{k},i,j} v_{ij}(k) s_i(\vec{k}) s_j(\vec{k}), \tag{5.35}$$

in which, unlike Eq. (2.6) (as well as standard $O(n)$ theories), the interaction kernel v_{ij} might not be diagonal in the internal field indices $i, j = 1, 2, \ldots, n$. An example is afforded by a field theory in which n component fields are coupled minimally to a spatially uniform (and thus translationally invariant) non-Abelian gauge background which emulates a curved space metric.[43] In this case, the index α in Eq. (5.34) is a composite of an internal field component coordinate $w = 1, 2, \ldots, n$ and $\vec{k}$-space coordinates. For each of the n branches w, we may determine the associated $\vec{k}$-space zero eigenvalue of Eq. (5.34) which we label by K_w (i.e., $a_{w,k=K_w}(\lambda) = 0$). The largest correlation is length is associated with the eigenvector which exhibits the smallest value of |Im K_w|. As usual, as λ is varied, we may track for each of the n branches, the trajectories poles of G in the complex k-plane. Although the location of the multiple poles may vary continuously with the parameter λ, the dominant poles (those associated with the largest correlation length) might discontinuously change from one particular subset of eigenvectors to another (see Fig. 5.6). As such, the correlation

function of the system may show jumps in its dominant modulation length at large distances as λ crosses a threshold value λ_* even though no transitions (nor cross-overs similar to that of Fig. (5.1) which form the focus of this work) are occurring. Such

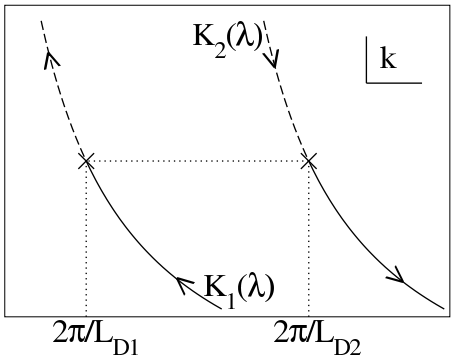

Figure 5.6: "Jumps" in the modulation length: The figure shows the evolution of the poles associated with two different eigenvectors with the parameter λ in the complex k-plane. The solid portion of the trajectories show which pole corresponds to the dominant term (larger correlation length) in the correlation function. The $\times$-s denote the poles at $\lambda = \lambda_*$ and the arrows denote the direction of increasing λ. It is evident, therefore, that the modulation length corresponding to the dominant term jumps from L_{D1} to L_{D2} as λ crosses the threshold value λ_*.

jumps in the large distance modulation lengths appear in $O(n)$ systems defined on a fixed, translationally invariant, non-Abelian background or metric as in Ref. [43].

In Appendix G, we discuss exponents associated with lock-ins of correlation and

modulation lengths in Fermi systems. When dealing with zero temperature behavior, we use the chemical potential μ as the control parameter λ. We discuss metal-insulator transition, exponents in Dirac systems and topological insulators. Additionally, we comment on crossovers related to changes in the Fermi surface topology as well as those related to situations with divergent effective mass.

5.6 Implications for the time domain: Josephson time scales

As we alluded to above, the results that we derived earlier that pertained to length scales can also be applied to time scales in which case we look at a temporal correlation function characterized by decay times (corresponding to correlation lengths) and oscillation periods (corresponding to modulation lengths). We may obtain decay time and oscillation period exponents whenever one of these time scales freezes to a constant value as some parameter λ crosses a threshold value λ_*.

Many other aspects associated with length scales have analogs in the temporal regime. Towards this end, in what follows, we advance the notion of a "Josephson time scale". We first very briefly review below the concept of a Josephson length scale. In many systems [with correlation functions similar to Eq. (5.19)], just below the critical temperature, the correlation function as a function of wave-vector, k

behaves as

$$G(k) \propto \begin{cases} k^{-2+\eta} & \text{for } k \gg 1/\xi_J, \\ k^{-2} & \text{for } k \ll 1/\xi_J, \end{cases} \tag{5.36}$$

thus defining the Josephson length scale, ξ_J.[122] Such an argument may be extended to a time scale, τ_J (real or imaginary) in systems with Lorentz invariant propagators. For a given wave-vector k, τ_J may be defined as,

$$G(k,\omega) \propto \begin{cases} \omega^{-2+\eta_t} & \text{for } \omega \gg 1/\tau_J, \\ \omega^{-2} & \text{for } \omega \ll 1/\tau_J, \end{cases} \tag{5.37}$$

where ω is the frequency conjugate to time while performing the Fourier transform and $\eta_t(\neq 0)$ is an anomalous exponent for the time variable.

5.7 Chaos and glassiness

Thus far, we have considered phases in which the modulation length is well defined. For completeness, in this section, we mention situations in which aperiodic phases may be observed. The general possibility of such phenomena in diverse arenas is well known.[119, 123] We focus here on translationally invariant systems of the form of Eqs. (2.1,2.12) with competing interactions on different scales that lead to kernels such as

$$v(k) = k^4 - c_1 k^2 + c_2, \tag{5.38}$$

where c_1 and c_2 are positive constants may give rise to glassy structures for non zero u. Such a dispersion may arise in the continuum (or small k) limit of hypercubic lattice systems with next nearest neighbor interactions (giving rise to the k^4 term) and nearest neighbor interactions (giving rise to the k^2 term). Within replica type approximations, such kernels that have a finite k minimum (i.e., ones with $c_1 > 0$) may lead to extensive configurational entropy that might enable extremely slow dynamics.[41, 43]

The simple key idea regarding "spatial chaos" is as follows. It is well known that nonlinear dynamical systems may have solutions that exhibit chaos. This has been extensively applied in the time domain yet, formally, the differential equations governing the system may determine not how the system evolves as a function of the time t but rather how fields change as a spatial coordinate (x) [replacing the time (t)]. Under such a simple swap of $t \leftrightarrow x$, we may observe spatial chaos as a function of the spatial coordinate x. In general, of course, more than one coordinate may be involved. The resultant spatial configurations may naturally correspond to amorphous systems and realize models of structural glasses. A related correspondence in disordered systems has been found in random Potts systems wherein spin glass transitions coincide with transitions from regular to chaotic phases in derived dynamical analogs.[124]

In the translationally invariant systems that form the focus of our study, an effec-

tive free energy of the form

$$\mathcal{F}[s] = \frac{1}{2}\int \frac{d^dk}{(2\pi)^d}(v(\vec{k})+\mu)|s(\vec{k})|^2 + \frac{u}{4}\int d^dx(S^2(\vec{x})-1)^2. \tag{5.39}$$

is generally associated with single component ($n = 1$) systems of the form of Eqs. (2.12). In Eq. (5.39), μ represents the deviation from the transition temperature in Ginzburg-Landau theories (or equivalently related to Eq. (5.30)).

Euler-Lagrange equations for the spins $S(\vec{x})$ are obtained by extremizing the free energy of Eq. (5.39). These equations are, generally, nonlinear differential equations (as discussed in Appendix H). As is well appreciated, however, nonlinear dynamical systems may exhibit chaotic behavior. In general, a dynamical system may, in the long time limit, either veer towards a fixed point, a limit cycle, or exhibit chaotic behavior. We should therefore expect to see such behavior in the spatial variables in systems which are governed by Euler-Lagrange equations with forms similar to nonlinear dynamical systems. Upon formally replacing the temporal coordinate by a spatial coordinate, chaotic dynamics in the temporal regime map onto to a spatial amorphous (glassy) structure.

In Fig. 5.7(a), we illustrate the spatial amorphous glass-like chaotic behavior that a one-dimensional rendition of the system of Eq. (5.38) exhibits. In Figs. 5.7(b)–5.7(g), we provide plots of the spatial derivatives of different order vs each other (and $S(x)$ itself).

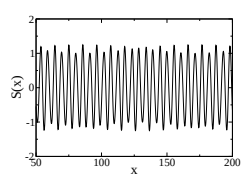

(a) $S(x)$ vs x

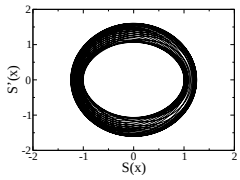

(b) $S(x)$ vs $S'(x)$

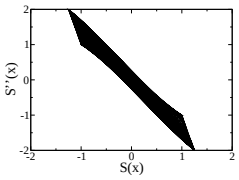

(c) $S(x)$ vs $S''(x)$

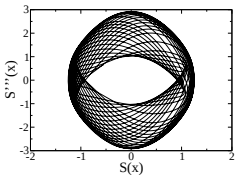

(d) $S(x)$ vs $S'''(x)$

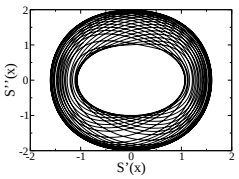

(e) $S'(x)$ vs $S''(x)$

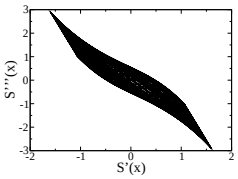

(f) $S'(x)$ vs $S'''(x)$

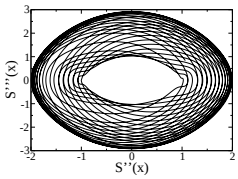

(g) $S''(x)$ vs $S'''(x)$

Figure 5.7: Glassiness in system with $v(k)$ as in Eq. (5.38) with $c_1 = 5$, $c_2 = 4$ and $u = 1$ and $\mu = 1$ in Eq. (5.39).

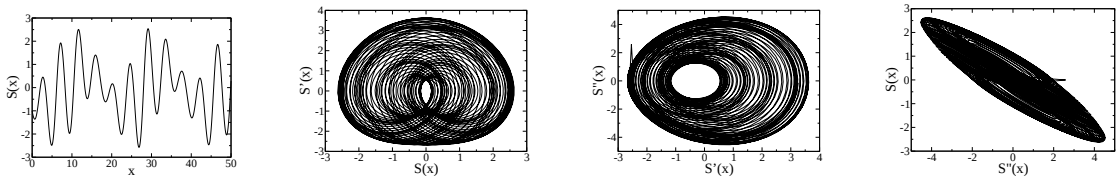

(a) $S(x)$ vs x (b) $S'(x)$ vs $S(x)$ (c) $S''(x)$ vs $S'(x)$ (d) $S(x)$ vs $S''(x)$

Figure 5.8: Example of aperiodic structure inspired by system with nonlinear jerks. Here $J(S(x), S'(x), S''(x)) = -2S'(x)+(|S(x)|-1)$ and initial conditions are $S(0) = -1$, $S'(0) = -1$, $S''(0) = 1$ (chosen from Ref. [5]).

Another example comes from the spatial analog of dynamical systems with non-linear "jerks". It is well known that systems with nonlinear "jerks" often give rise to chaos[5] "Jerk" here refers to the time derivative of a force, or, something which results in a change in the acceleration of a body. Translating this idea from the temporal regime to the spatial regime, one can expect to obtain a aperiodic/glassy structure in a system for which the Euler Lagrange equation, Eq. (H-50) may seem simple. For example, if we have the following, Euler Lagrange equation for a particular one-dimensional system,

$$S'''(x) = J(S(x), S'(x), S''(x)), \tag{5.40}$$

with a non-linear function $J(S(x), S'(x), S''(x))$ then the system may have aperiodic structure. An example is depicted in Fig. (5.8).

We now discuss $O(n)$ systems and illustrate the existence of periodic solutions (and absence of chaos) in a broad class of systems.

The Euler-Lagrange equations for the system in Eq. (5.39) [written longhand in Eqs. (H-50, H-56)] become linear in case of "hard" spins, i.e., when the $O(n)$ condition is strictly enforced, i.e., $u \to \infty$. In this limit, all configurations in the system can be described by a finite set of modulation wave-vectors (as was the case for the ground states in Sec. 5.3.1).

There are several ways to discern this result. First, it may be simply argued that since the Euler-Lagrange equations represent a *finite* set of coupled *linear* ordinary differential equations, chaotic solutions are not present. The configurations, therefore must be characterized by a finite number of modulation wave-vectors.

A second approach is more quantitative. The idea used here is the same as the one used in Ref. [98]. An identical construct can be applied to illustrate that spiral/poly-spiral states are the only possible states that satisfy the Euler-Lagrange equation if $n > 1$. With v being a functional of the lattice Laplacian of Eq. (2.7), the lattice rendition of the Euler-Lagrange equations in Fourier space reads

$$D(\Delta_{\vec{k}})s(\vec{k}) = 0. \tag{5.41}$$

In what follows we consider what transpires when the Euler-Lagrange equations have real wave-vectors $\mathcal{K} = \{\vec{q}_m\}$vas solutions.

$$D(\Delta_{\vec{k}})s(\vec{k})\Big|_{\vec{k}=\vec{q}_m} = 0. \tag{5.42}$$

To obtain a bound on the number of wave-vectors that can be used to describe a general configuration satisfying the Euler-Lagrange equations, we consider general situations wherein **(i)** $2(\vec{q}_m \pm \vec{q}_{m'}) \neq \vec{k}_{rec}$ for any $\vec{q}_m, \vec{q}_{m'} \in \mathcal{K}$, where $\vec{k}_{rec}$ represents a reciprocal lattice vector; and, **(ii)** $\vec{q}_m \pm \vec{q}_{m'} \neq \vec{q}_p \pm \vec{q}_{p'}$ for any $\vec{q}_m, \vec{q}_{m'}, \vec{q}_p, \vec{q}_{p'} \in \mathcal{K}$. Let a particular state be described as

$$\vec{S}_0(\vec{x}) = \sum_m \vec{a}_m e^{-i\vec{q}_m \cdot \vec{x}}, \tag{5.43}$$

where the vectors $\vec{a}_m$ have n components for $O(n)$ systems. As the states must have real components, the above equation must take the form,

$$\vec{S}_0(\vec{x}) = \sum_{m=1}^{N_q} \left(\vec{a}_m e^{-i\vec{q}_m \cdot \vec{x}} + \vec{a}_m^* e^{i\vec{q}_m \cdot \vec{x}} \right). \tag{5.44}$$

In the above, $\vec{a}_m^*$ denotes the vector whose components are complex conjugate those of the vector $\vec{a}_m$. In Eq. (5.44), we do not count terms involving the wave-vectors $\vec{q}_m$ and $-\vec{q}_m$ separately as such terms has been explicitly written in the sum.

We next define the complex vectors $\{\vec{U}_m\}$ and $\{\vec{V}_m\}$ as

$$\begin{aligned} \vec{U}_m &= \vec{a}_m e^{-i\vec{q}_m \cdot \vec{x}}, \\ \vec{V}_m &= \vec{a}_m e^{i\vec{q}_m \cdot \vec{x}}. \end{aligned} \tag{5.45}$$

The $O(n)$ normalization condition can then be expressed as,

$$\begin{aligned}
\sum_m |\vec{U}_m|^2 &= n, \\
\sum_m |\vec{V}_m|^2 &= n, \\
\sum_{\vec{q}_m - \vec{q}_{m'} = \vec{A}} \left(\vec{U}_m^* \cdot \vec{U}_{m'} \right. &+ \left. \vec{V}_{m'}^* \cdot \vec{V}_m \right) + \\
\sum_{\vec{q}_m + \vec{q}_{m'} = \vec{A}} \left(\vec{U}_m^* \cdot \vec{V}_{m'} \right. &+ \left. \vec{U}_{m'}^* \cdot \vec{V}_m \right) = 0.
\end{aligned} \tag{5.46}$$

Solutions to Eq. (5.46) are spanned by the set of mutually orthonormal basis vectors $\{\vec{U}_m\} \cup \{\vec{V}_m\}$. As these $2N_q$ basis vectors are described by n-components each, we must have,

$$N_q \leq n/2. \tag{5.47}$$

Therefore, such states satisfying the Euler-Lagrange equations for an $O(n \geq 2)$ system can at most be characterized by $n/2$ pairs of wave-vectors. These states can be described by N_q spirals (or "poly-spirals") each of which is described in a different orthogonal plane.

A few remarks are in order.

- When u in Eq. (5.39) is finite, i.e., in the soft spin regime, poly-spiral solutions could be present even though aperiodic solutions are also allowed.

- *Continuum limit:* In the hard-spin limit, i.e., $u \to \infty$ in Eq. (5.39), if the Fourier space Euler-Lagrange equation is satisfied by non-zero real wave-vectors,

we have poly-spiral solutions as in the lattice case. When u is finite, aperiodic solutions may also be present.

- If the Fourier space Euler-Lagrange equation does not have any real wave-vector solution, poly-spiral states are not observed.

In nonlinear dynamical systems, chaos is often observed via *intermittent phases*. As a tuning parameter λ is varied, the system enters a phase in which it jumps between periodic and aperiodic phases until the length of the aperiodic phase diverges. This divergence is characterized by an exponent $\nu = 1/2$ similar to ours.[125]

5.8 Conclusions

Most of the work concerning properties of the correlation functions in diverse arenas, has to date focused on the correlation lengths and their behavior. In this work, we examined the oscillatory character of the correlation functions when they appear.

We furthermore discussed when viable non-oscillatory spatially chaotic patterns may (or may not appear); in these, neither uniform nor oscillatory behavior is found. Our results are universal and may have many realizations. Below, we provide a brief synopsis of our central results.

1. We have shown the existence of a universal modulation length exponent $\nu_L = 1/2$ [Eq. (5.7)]. Here the scaling could be as a function of some general parame-

ter λ such as temperature. This is observed in systems with analytic crossovers including the commensurate-incommensurate crossover in the ANNNI model.

2. In certain situations the above exponent could take other rational values [Eq. 5.5].

3. This result also applies to situations where a correlation length may lock in to a constant value as the parameter λ is varied across a threshold value [as in Eq. (5.14)].

4. We extended our result to include situations in which the crossover might take place at a branch point. In this case irrational exponents could also be present. In Eqs. (5.22, 5.23), we provide universal scaling relations for correlation and modulation lengths.

5. We illustrate that discontinuous jumps in the modulation/correlation lengths mandate a thermodynamic phase transition.

6. We showed that in translationally invariant systems (with rotational and/or reflection symmetry), the total number of correlation and modulation lengths is generally conserved as the general parameter λ is varied.

7. Our results apply to both length scales as well as time scales. We further introduce the notion of a Josephson time scale.

8. We comment on the presence of aperiodic modulations/amorphous states in systems governed by nonlinear Euler-Lagrange equations. We illustrate that in a broad class of multi-component systems chaotic phases do not arise. Spiral/poly-spiral solutions appear instead.

9. Our results have numerous applications. We discussed several non-trivial consequences for classical system in the text. For completeness, in Appendix G, we discuss, rather simple applications of our results to non-interacting Fermi systems.

Chapter 6

A molecular dynamics study on the micro-structure of $Al_{88}Fe_5Y_7$

6.1 Introduction

The importance of metallic glasses has been acknowledged by materials scientists for more than half a century. Since then, there have been attempts at understanding their structure and properties. [53, 55, 126–129] More modern approaches are reported in [60, 130]. There is however very little knowledge about the physics that governs the microscopic structure and the properties of such systems. It is not known, for example, how the structure and composition of a system is correlated to its ease of vitrification. The influence of cooling rates on the resulting structures is also not clear.

Molecular dynamics (MD) simulations provide us with tools to study physical systems through controlled experiments on the computer. With the knowledge of the constituent elements first principles MD studies can be made on a variety of systems.

To perform such studies, however, in a feasible amount of time, it is necessary to keep the system small. Such problems are further magnified when studying systems without any long range order. It is not a problem when studying crystalline systems because of the periodicity.

Another way to hasten the simulation times or equivalently make the system size bigger is to make the theory simpler. This is done by replacing the ab-initio simulation by a classical MD simulation in which the system is made up of classical particles and we provide the inter-particle forces.

This work is an attempt to look at the local structure of a metallic system in the liquid and glassy phases through classical and ab-initio MD simulations. We studied the $Al_{88}Fe_5Y_7$ system using classical and ab-initio MD simulation techniques. In both cases we obtained a room temperature system configuration. We compared the pair structure factor calculated from the room temperature configurations obtained from the classical simulations with X-ray diffraction data taken on room quenched room temperature samples. Since the system size used for ab-initio simulations was not large enough, we compared the pair correlation functions obtained from ab-initio simulations to those obtained by Fourier transforming the experimental diffraction data. We also relaxed the room temperature structure to see the attributes which

the system preferred.

6.2 Results

There is increase in icosahedral order as the system is cooled. Both classical as well as ab-initio runs show this. This is manifested as an increase in the frequency distribution of W_6 near -0.169 (the value for the perfect icosahedron) [Figs. 6.1 to 6.3 and 6.4 to 6.6]. The Voronoi statistics corresponding to the perfect icosahedron,

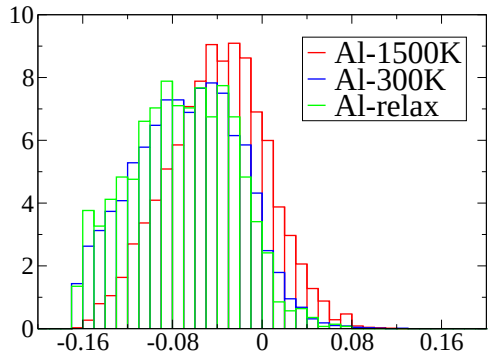

Figure 6.1: Distribution of W_6 for Al atoms obtained from classical simulation. The horizontal axis shows W_6 values and the vertical axis shows normalized frequency distribution.

(0,0,12) also increases as we cool the system. Relaxing further enhances icosahedral order showing that it is indeed preferred [Tables 6.1 and 6.2].

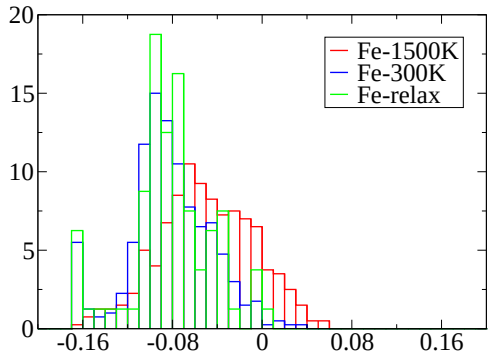

Figure 6.2: Distribution of W_6 for Fe atoms obtained from classical simulation.

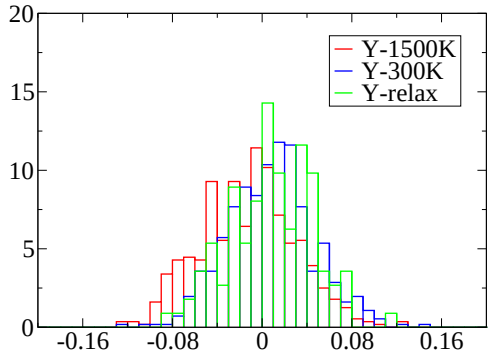

Figure 6.3: Distribution of W_6 for Y atoms obtained from classical simulation.

6.3 Methods

6.3.1 Classical molecular dynamics simulation

All of these simulations were done using a classical MD software developed by the Institute for Theoretical and Applied Physics (ITAP) called IMD [8, 131]

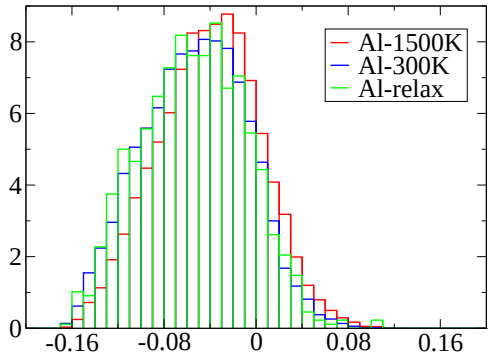

Figure 6.4: Distribution of W_6 for Al atoms for VASP run.

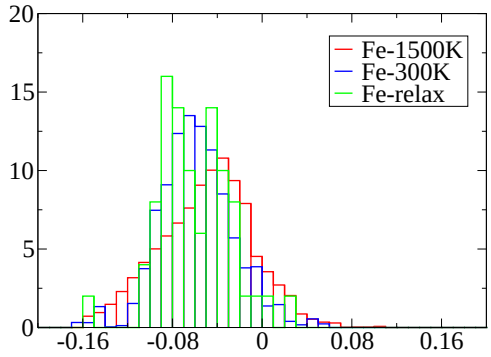

Figure 6.5: Distribution of W_6 for Fe atoms for VASP run.

Pair potentials

First, we developed the pair potentials that were used to perform the MD simulations. This was done by using data from ab-initio calculations on crystalline systems in which the same elements are in similar environment. The pair potentials for which the forces and energies were best fit were chosen for use in the IMD simulation. The fitted energies are shown in Fig. 6.7. The fitted forces are shown in Fig. 6.8. The

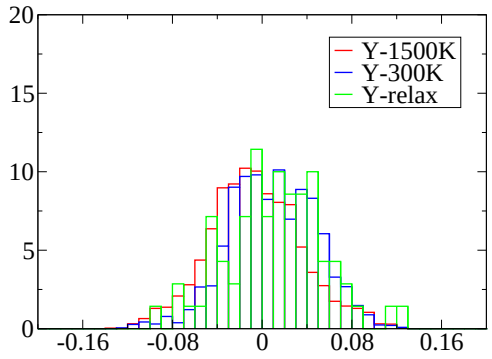

Figure 6.6: Distribution of W_6 for Y atoms for VASP run.

Voronoi	1500K			300K			Relax		
Types	Al	Fe	Y	Al	Fe	Y	Al	Fe	Y
(0,0,12)	0.28	0.00	0.00	3.55	3.75	0.00	3.98	3.75	0.00
(0,0,12,2)	0.00	0.00	0.00	0.21	0.00	0.00	0.21	0.00	0.00
(0,1,10,2)	0.28	0.00	0.00	1.78	0.00	0.00	2.63	0.00	0.00
(0,3,6,4)	0.65	0.00	0.00	1.35	0.00	0.00	1.42	0.00	0.00
(0,5,4,4)	0.36	0.00	0.00	0.64	0.00	0.00	0.28	0.00	0.00
(0,3,6)	0.00	8.75	0.00	0.00	7.50	0.00	0.00	10.00	0.00
(0,5,4)	0.21	6.25	0.00	0.00	17.50	0.00	0.00	15.00	0.00

Table 6.1: Voronoi statistics for IMD run. The figures show the proportion (percent) of the important different Voronoi polyhedra.

Voronoi	1500K			300K			Relax		
Types	Al	Fe	Y	Al	Fe	Y	Al	Fe	Y
(0,0,12)	0.23	0.00	0.00	0.80	2.00	0.00	1.02	2.00	0.00
(0,0,12,2)	0.11	0.00	0.00	0.00	0.00	0.00	0.00	0.00	0.00
(0,1,10,2)	0.11	0.00	0.00	0.91	0.00	0.00	1.59	0.00	0.00
(0,3,6,4)	0.23	0.00	0.00	0.57	0.00	0.00	1.14	0.00	0.00
(0,5,4,4)	0.91	0.00	0.00	0.23	0.00	0.00	0.45	0.00	0.00
(0,3,6)	0.11	10.00	0.00	0.00	14.00	0.00	0.23	6.00	0.00
(0,5,4)	0.00	12.00	0.00	0.00	22.00	0.00	0.00	20.00	0.00

Table 6.2: Voronoi statistics for VASP run. The figures show the proportion (percent) of the important different Voronoi polyhedra.

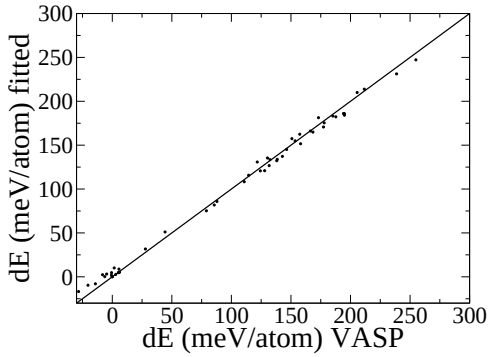

Figure 6.7: Energies fitted with first principles calculations.

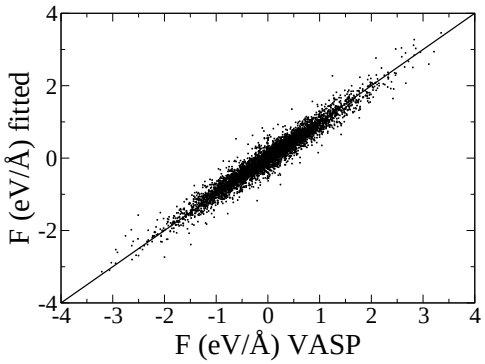

Figure 6.8: Forces fitted with first principles calculations.

pair potentials that were hence calculated are plotted in Fig. 6.9.

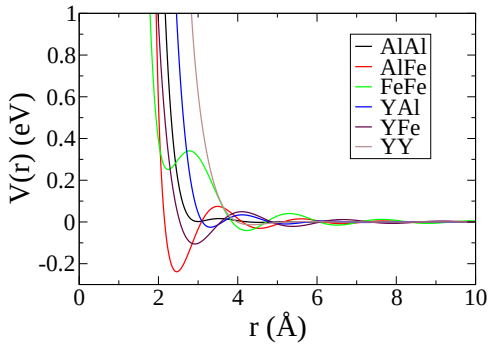

Figure 6.9: Pair potentials.

Some initial runs

We prepared a configuration with 200 atoms with the correct density and composition. We did different trial runs with IMD on this system. We also studied the diffusion rates at different temperatures and found out that 20 ps were long enough to obtain

configurations at 1500K which could be treated as independent.

Getting a large system configuration at room temperature

An initial large configuration at 1500K was created by doubling a smaller sized system (200 atoms) in all the Cartesian directions. The resulting system therefore had 1600 atoms. We then reduced the sizes of the basis vectors so that the volume matched the low-temperature volume. This system was then allowed to go to a physically preferred configuration by running it at that temperature for a long time (20.36 ps). Then, the system was cooled to 600K in 4.072 ps. It was then cooled to 500K in 20.36 ps. The final configuration was obtained by cooling the system to room temperature (300K) in 4.072 ps. The whole process was repeated 4 more times, each time starting with the final configuration at 1500K of the previous run and running it for 20.36 ps.

Relaxing the system

We relaxed the last room temperature configuration. The minimum energy configuration was obtained using the conjugate gradient method.

6.3.2 First principles molecular dynamics simulation

The first principles simulations that we performed were done using the Vienna ab-initio simulation package (VASP) [132–134].

Getting a room temperature sample

The initial configurations were obtained from IMD runs at 1500K on a systems having 200 atoms. These were allowed to run for 500 fs at 1500K. They were then cooled to 1000K in 500 fs. At this point, each of the simulation cell edge lengths were reduced by 1% to account for the volume change with temperature. The systems were again allowed to settle to the new volume for 500 fs. The systems were then cooled to 300K in 700 fs.

Relaxing the sample

We relaxed the room temperature configurations. The relaxation was done using VASP which also used the conjugate gradient algorithm.

6.3.3 Analysis

Pair correlation function and Structure factor

The pair correlation function is the normalized density of atoms around a particular atom. For atom types A and B, it is calculated by first forming a histogram of all B atoms at a distance between r and $r + \delta r$ from A atoms. This is then normalized by dividing by $4\pi r^2 \delta r$ and $n_A n_B$. The resulting function is then smeared with a Gaussian of standard deviation $0.025\mathring{A}$ to get the partial pair correlation function for pair A-B, $g_{AB}(r)$.

The partial structure factor $S_{AB}(q)$ for pair A-B is obtained from $g_{AB}(r)$ using

$$S_{AB}(q) = 1 + 4\pi\rho \int_0^\infty [g_{AB}(r) - 1] \frac{\sin(qr)}{qr} r^2 dr. \tag{6.1}$$

The total pair correlation function is obtained from the partials by normalized weighting in proportion to $n_A n_B Z_A Z_B$ where Z_A represents the atomic number of the A atoms and n_A the number of A atoms in the simulation cell. The total structure factor is also obtained in the same way.

Bond-orientational order parameter W_6

The bond-orientational order parameter, W_6 [55] helps us detect icosahedral order present in our system. The value of W_6 for an isolated icosahedral cluster is -0.169 which is very different from other clusters [bcc:+0.013; fcc:-0.013; hcp:-0.012]. Thus, distribution of W_6 values in a system can help us in quantifying the amount of icosahedral order.

For a given atom, W_6 is calculated as follows. Taking any reference frame, the orientational angles θ and ϕ are noted for all the bonds (line joining near neighbor atoms). The quantity $\bar{Q}_{6,m} = \langle Y_{6,m}(\theta, \phi) \rangle$ is then calculated for all m, $-6 \leq m \leq 6$, where the average is taken over all the bonds. From this, W_6 is calculated using the

following.

$$W_6 = (\sum_{m=-6}^{6} |\bar{Q}_{6,m}|^2)^{-3/2} \sum_{\substack{m_1, m_2, m_3, \\ m_1+m_2+m_3=0}} \begin{pmatrix} 6 & 6 & 6 \\ m_1 & m_2 & m_3 \end{pmatrix} \bar{Q}_{6,m_1}\bar{Q}_{6,m_2}\bar{Q}_{6,m_3} \quad (6.2)$$

where

$$\begin{pmatrix} 6 & 6 & 6 \\ m_1 & m_2 & m_3 \end{pmatrix}$$

represent the Wigner 3j symbols.

Voronoi analysis

Voronoi analysis helps us in visualizing the local environments around atoms. For this, first a Voronoi polyhedron is constructed around a chosen atom in the following way. Perpendicularly bisecting planes are drawn for all lines joining that atom to other atoms. The smallest closed polyhedron thus formed is the Voronoi polyhedron for this atom. It is then assigned a set of integers (F_3, F_4, F_5, ...) where F_i is the number of faces of the Voronoi polyhedron with i edges. For example, (0,0,12) represents the icosahedron, (0,12,0) represents the fcc and hcp, (0,6,0,8) represents the bcc, and so on. (0,0,12,x), $x = 2, 3, 4, ...$ represents icosahedral structures with disclinations.

Honeycutt-Anderson analysis

This is another method to characterize and quantify local order. Each bond between to atoms of types A and B is characterized by 3 integers $n_1n_2n_3$, where n_1 is 1 if the atoms are nearest neighbors, 2 if they are second neighbors and so on (We are not interested in $n_1 > 2$); n_2 is the number of common neighbors the two atoms have; and n_3 is the number of pairs of these common neighbors which are neighbors of each other. For example, 155 is characteristic of perfect icosahedra, 244 is present in bcc structures, 233 is present when an atom sits outside an icosahedron at second neighbor distance from the center atom, and so on. [Note: The distances corresponding to near neighbors, second neighbors, and so on, are obtained from the minima in the $g_{AB}(r)$ plot.]

6.4 Observations and inference

The total and partial pair correlation functions obtained from the classical molecular dynamics simulation has been plotted in Fig. (6.10). The structure factor was calculated from this and plotted in Fig. 6.11. A comparison with X-ray diffraction data has been shown in Fig. 6.12.

The pair correlation functions obtained from first principles MD simulation has been plotted in Fig. 6.13. The structure factors obtained from these has been shown in Fig. 6.14. It is to be noted, however, that due to the smallness of the system

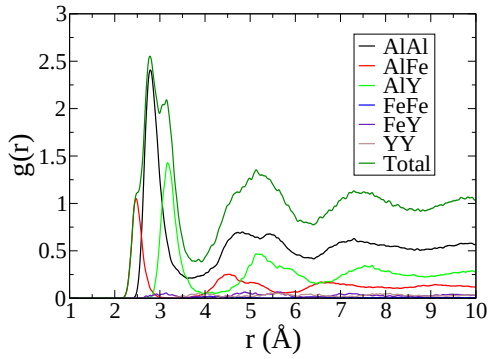

Figure 6.10: Total and partial pair correlation functions from the classical MD simulations.

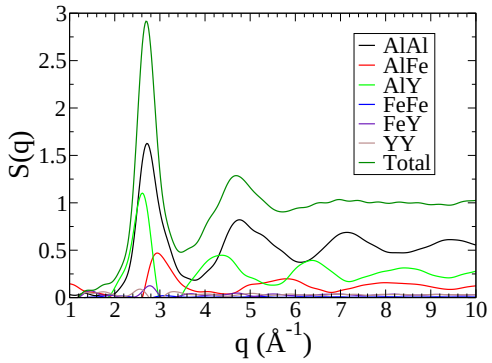

Figure 6.11: Total and partial structure factors obtained from classical simulation.

size, the total structure factor in Fig. 6.14 does not agree well with diffraction data. The range of wave-vectors for which diffraction data was available to us made us decide that it was more justified to compare the pair correlation functions obtained by Fourier transforming the diffraction data with those calculated using first principles simulation. Such a comparison is shown in Fig. 6.15.

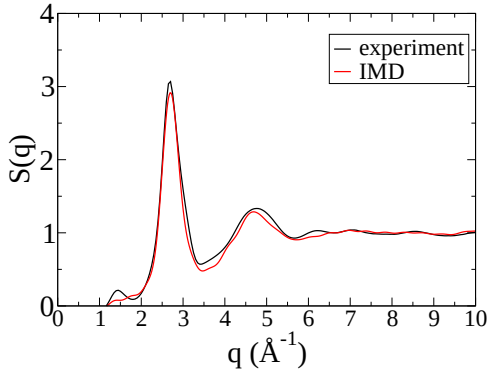

Figure 6.12: Comparison of total structure factors from experiment and classical MD simulation.

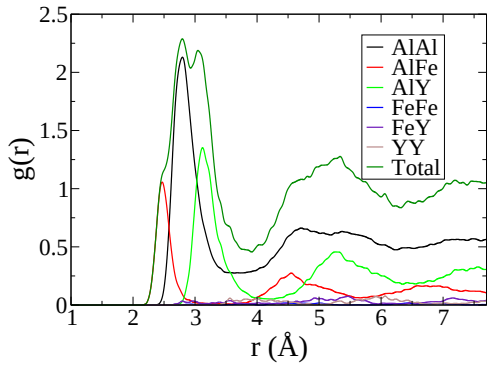

Figure 6.13: Total and partial pair correlation functions obtained from ab-initio simulation.

6.4.1 A look at the Al-Fe-Y phase diagram

The coexisting phases of Al-Fe-Y that may be present in our system are $Al_{10}Fe_2Y$.oC52, pure Al as Al.cF4 and an Al-Y binary as Al_3Y.hP8 [Fig. 6.16]. The Al8CeFe2.oP44

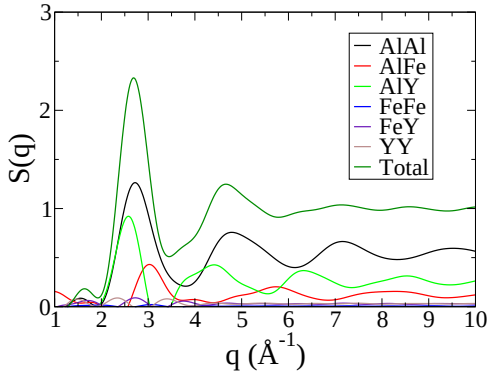

Figure 6.14: Total and partial structure factors obtained from ab-initio simulation.

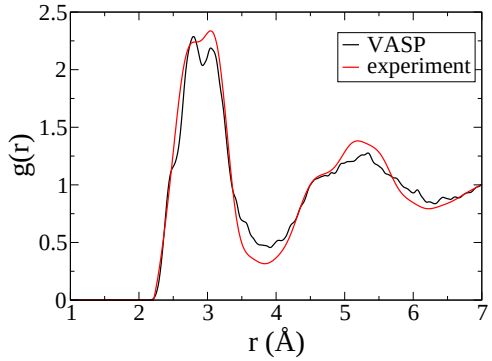

Figure 6.15: Comparison of pair correlation function from first principles simulation and Fourier transforming X-ray diffraction data.

and Al10Fe2Gd.oC52 [Gd can be replaced by Y] phases are theoretically predicted to be stable but are not yet experimentally verified.

We looked at the environments of Fe-Y and Y-Y in the $Al_{10}Fe_2Y$ crystal. In [Fig. 6.17], we see that Y-Y are second neighbors and there are 3 common Al neighbors which form a square (approximately). Presence of such a structure could be studied

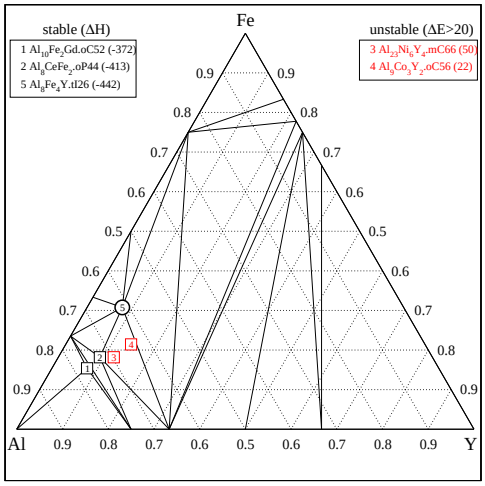

Figure 6.16: Al-Fe-Y phase diagram. Phases 2 and 3 are theoretically predicted to be stable but have not been found experimentally.

with Honecutt-Anderson (HA) analysis and looking for HA index 244 where the first 2 stands for second neighbors, the first 4 indicates 4 common neighbors and the last 4 shows the number of bonds between the common neighbors.

In [Fig. 6.18], we see that Fe-Y are second neighbors and there are 3 Al atoms which form an approximately equilateral triangle which are very close to being immediate neighbors for both Fe and Y. Such a structure would correspond to HA index of 233 if the Al atoms were indeed common neighbors. However, this structure could also be interpreted as an icosahedron with Fe as the centre atom and Al as the surrounding atoms and a Y atom outside this.

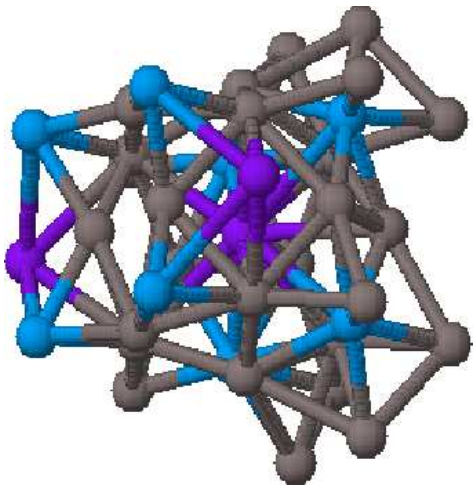

Figure 6.17: Y-Y environment in $Al_{10}Fe_2Y$. Grey atoms represent Al, blue represent Fe and purple represent Y.

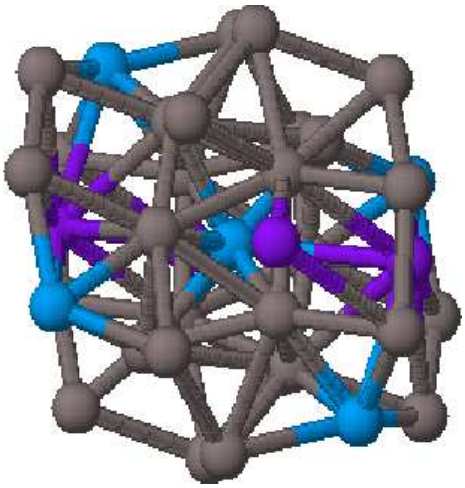

Figure 6.18: Y-Y environment in $Al_{10}Fe_2Y$. Grey atoms represent Al, blue represent Fe and purple represent Y.

6.4.2 Honeycutt-Anderson analysis

The distribution of the HA indices for the bonds in the configurations obtained from both classical and ab-initio simulations also show the increased icosahedral order in the cooled and relaxed configurations. These are plotted in Figs. 6.19–6.28.

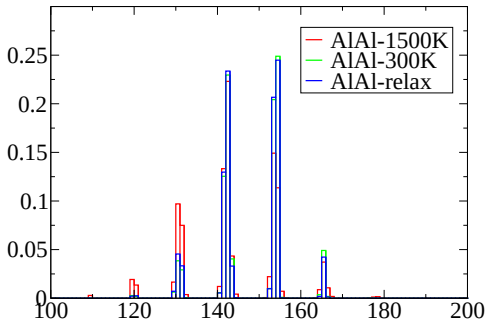

Figure 6.19: Statistics for nearest neighbor HA indices for Al-Al pairs obtained from classical simulation.

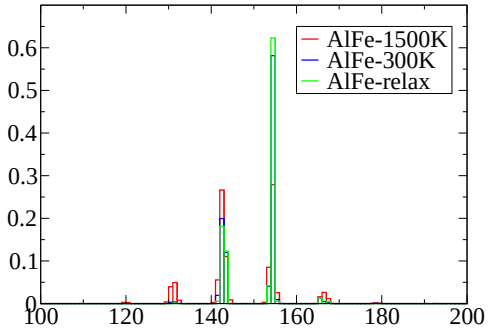

Figure 6.20: Statistics for nearest neighbor HA indices for Al-Fe pairs obtained from classical simulation.

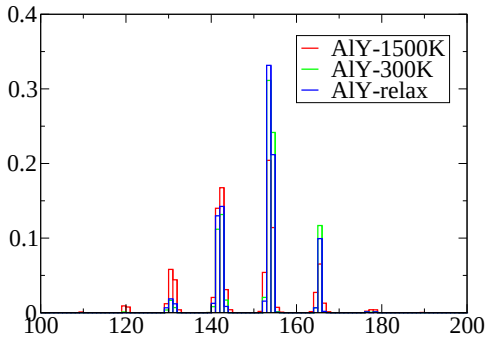

Figure 6.21: Statistics for nearest neighbor HA indices for Al-Y pairs obtained from classical simulation.

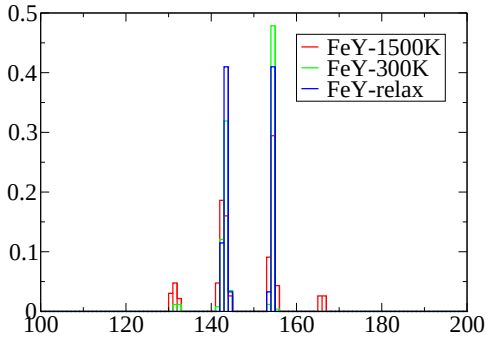

Figure 6.22: Statistics for nearest neighbor HA indices for Fe-Y pairs obtained from classical simulation.

Some second neighbor HA indices which we thought were interesting to look at were 244 for Y-Y pairs and 233 for Fe-Y pairs.

For the Y-Y pairs [Figs. 6.29 and 6.30], we see that 244 is preferred by the IMD configuration but not by the VASP configuration. Since 244 for Y-Y is a characteristic of the crystal structure, we conclude that the VASP run did a better job at going to

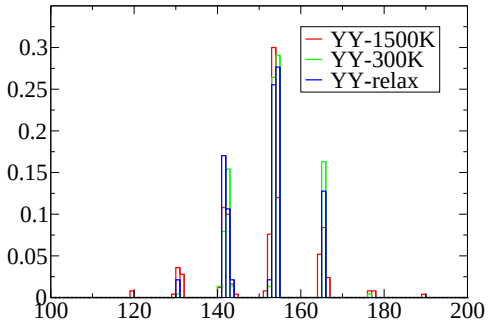

Figure 6.23: Statistics for nearest neighbor HA indices for Y-Y pairs obtained from classical simulation.

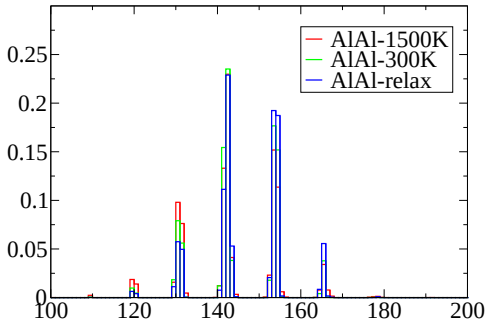

Figure 6.24: Statistics for nearest neighbor HA indices for Al-Al pairs obtained from first principles simulation.

the amorphous structure.

For the Fe-Y pairs [Figs. 6.31 and 6.32], we see that the 233 is preferred by VASP and not by IMD.

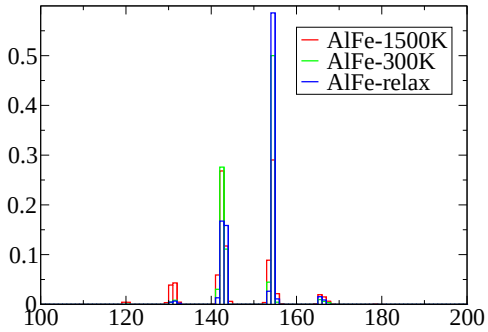

Figure 6.25: Statistics for nearest neighbor HA indices for Al-Fe pairs obtained from first principles simulation.

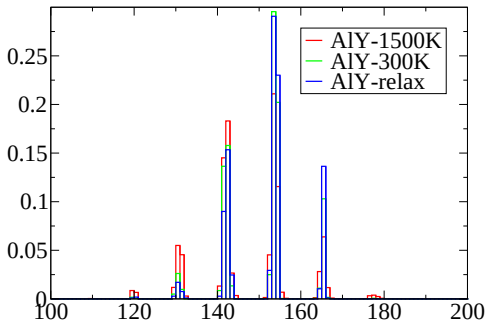

Figure 6.26: Statistics for nearest neighbor HA indices for Al-Y pairs obtained from first principles simulation.

6.4.3 Bond orientation

The distribution of W_6 values becomes more skewed on cooling and further on relaxing, towards the value for the perfect icosahedron (-0.169) for Al and Y centered analysis for both IMD and VASP runs. There is no such trend in the Y centered W_6 distribution.

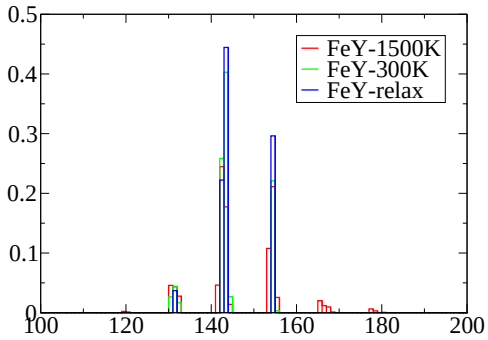

Figure 6.27: Statistics for nearest neighbor HA indices for Fe-Y pairs obtained from first principles simulation.

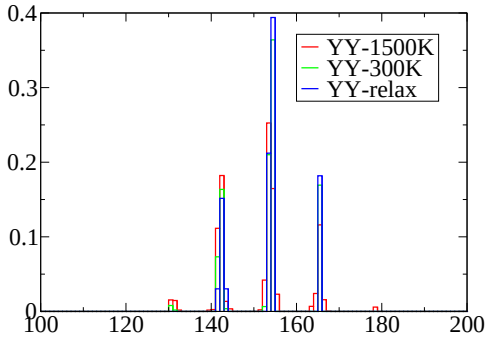

Figure 6.28: Statistics for nearest neighbor HA indices for Y-Y pairs obtained from first principles simulation.

6.4.4 Voronoi analysis

The Voronoi polyhedron representing the perfect icosahedron is $(0, 0, 12)$. For the IMD simulation (Table 6.1), Voronoi analysis indicated that the proportion of Al centered icosahedra increased on cooling, and increased further on relaxing. Fe cen-

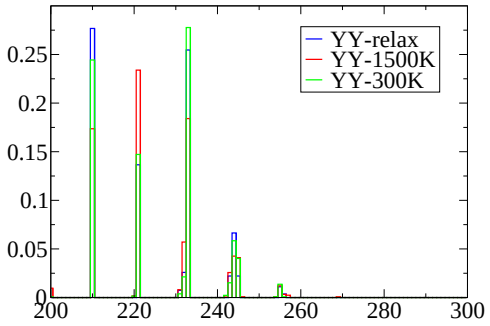

Figure 6.29: Statistics for second neighbor HA indices for Y-Y pairs obtained from classical simulation.

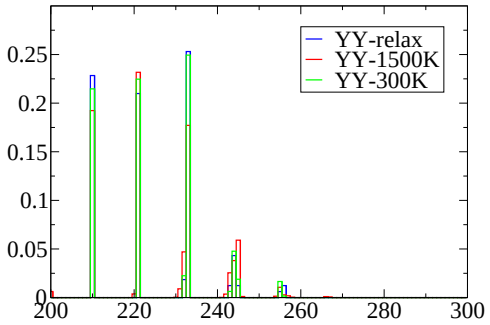

Figure 6.30: Statistics for second neighbor HA indices for Y-Y pairs obtained from ab-initio simulation.

tered icosahedra also increased in number on cooling but did not change on relaxing. An Y atom is too big to form an icosahedron with it at the center and Al atoms around.

For the VASP run (Table 6.2), the trends were exactly same as the IMD run. The numbers however, were much less in this case.

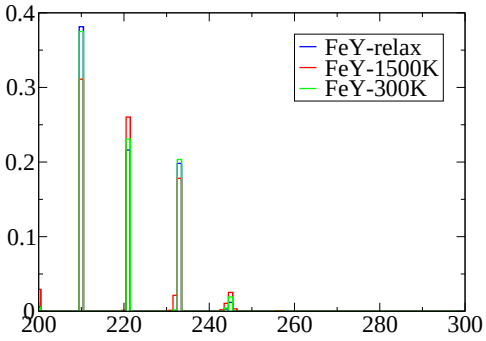

Figure 6.31: Statistics for second neighbor HA indices for Fe-Y pairs obtained from classical simulation.

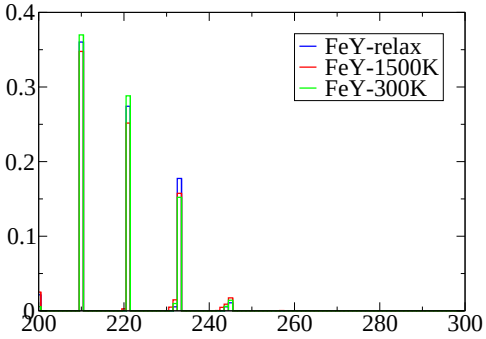

Figure 6.32: Statistics for second neighbor HA indices for Fe-Y pairs obtained from ab-initio simulation.

Chapter 7

Detecting hidden structures in metallic glasses by multiresolution network clustering

7.1 Introduction

This chapter introduces a new method of obtaining the essential structural features on all length scales in general complex systems with the knowledge of pairwise interaction strengths. We apply our methods to detect the natural scales and obtain the structures of metallic glasses. Complex systems and glasses are not easy to analyze with conventional theoretical tools.[135] In a gas, all interactions between the basic constituents are weak, so the system is easy to understand and analyze. At the other

extreme, the interactions in regular periodic solids are generally strong, and such solids may be characterized by their unit cells and related broken symmetries.

The situation is radically different for liquids and glasses. Liquids that are rapidly cooled ("supercooled") below their melting temperature cannot crystallize and instead, at sufficiently low temperatures, become "frozen" in an amorphous state (a "glass") on experimental time scales. On supercooling, liquids may veer towards local low energy structures,[130, 136] such as icosahedral structures observed in metallic glasses,[137, 138] before being quenched into the amorphous state. Lacking a simple crystalline reference, the general structure of glasses is notoriously difficult to quantify in a meaningful way beyond the smallest local scales. As such, it remains a paradigm for analyzing structure in complex materials.

Network analysis has been transformative in generating keen new insights in numerous areas such as sociology, homeland security, biology, and many other problems. Complex physical problems have not yet been examined before through this prism in this detail. We specifically introduce methods from the growing discipline of "community detection".[139] The key idea is that any complex physical system may be expressed as a network of nodes (e.g., atoms, electrons, etc.) and connecting links that quantify the relations (interactions/correlations) between the nodes. With this representation, we then apply *multiresolution* methods [6] from network theory to analyze the systems.

7.1.1 Partitions of large systems into weakly coupled elements

As depicted in Fig. 7.1, community detection describes the problem of finding clusters ("communities") of nodes with strong internal connections and weak connections between different clusters. The definitions of nodes and edges depend on the system being modeled. For the present system, between each pair of nodes i and j we have an edge weight V_{ij} which may emulate an interaction energy or measured correlation between sites i and j. The nodes may belong to any of q communities, $\{C_a\}_{a=1}^{q}$. In our particular realization, the nodes represent particles and edges model the pair-wise potential energy interactions.

7.1.2 Community detection method

Our (Potts type) Hamiltonian reads

$$H = \frac{1}{2}\sum_{a=1}^{q}\sum_{i,j\in C_a}(V_{ij}-v)[\theta(v-V_{ij})+\gamma\theta(V_{ij}-v)]. \tag{7.1}$$

In Eq. (7.1), the inner sum is over nodes i and j in the same community C_a, and the outer sum is performed over the q different communities. The number of communities q may be specified from the outset or left arbitrary (the usual case) allowing the algorithm to determine q based on the lowest energy solution(s).[6, 140]

Minimizing this Hamiltonian corresponds to identifying strongly connected clusters of nodes. The parameter $\gamma > 0$ tunes the relative weights of the connected and

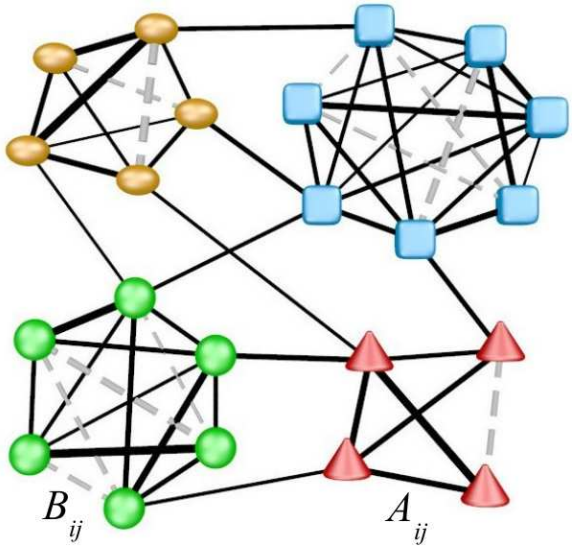

Figure 7.1: A weighted network with 4 natural (strongly connected) communities. The goal in community detection is to identify such strongly related clusters of nodes. Solid lines depict weighted links corresponding to complimentary or attractive relationships between nodes i and j (denoted by A_{ij}) $[(V_{ij} - v) < 0$ in Eq. (7.1)]. Gray dashed lines depict missing or repulsive edges (denoted by B_{ij}) $[(V_{ij} - v) > 0]$. In both cases, the relative link weight is indicated by the respective line thicknesses.

unconnected edges and allows us to vary the targeted scale of the community division (the "resolution"). The model for the current application could be further generalized by incorporating n-body interactions or correlation functions (such as three or four point correlation functions). Details concerning a greedy minimization of Eq. (7.1) appear in Refs. [6] and [140].

7.1.3 Multiresolution network analysis

We address multi-scale partitioning [6] by employing information-theory measures [141, 142] to examine contending partitions for each system scale. While decreasing γ, we minimize Eq. (7.1) resulting in partitions with progressively lower intra-community edge densities, effectively "zooming out" toward larger structures. A key construct in our approach is the application of *replicas* – independent solutions of the same problem. The number of replicas p may be set by the user where higher value of p leads to more accurate analysis.

In static systems replicas were formed by permuting the order of nodes in Ref. [6]. In this work, we take advantage of the dynamic system to implement a further generalization where replicas are defined at different times (see Fig. 7.2. We automatically determine the natural scales of a system by identifying the values of γ for which these replicas agree most strongly via information theory measures such as normalized mutual information NMI and variation of information VI.

The central result from Ref. [6], that we use in this work, is that *extrema* (including plateaux) of information theory overlaps (when averaged over all replica pairs) indicate the *"natural" network scales.*[6] That is, we find the values γ^* for which the average Q of information overlaps (over all replica pairs) is extremal, $(dQ/d\gamma)|_{\gamma=\gamma^*} = 0$. We then identify the parititions that correspond to these γ^*(s).

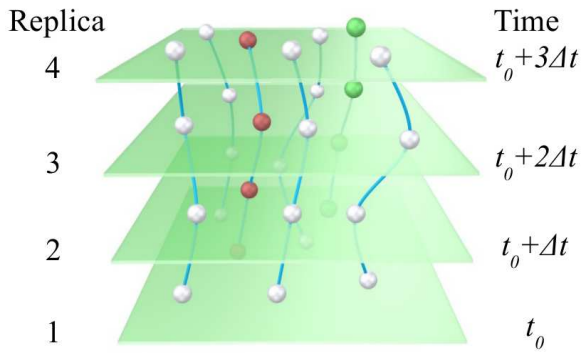

Figure 7.2: A set of replicas separated by a time Δt between successive replicas. We generate a model network for each replica using the potential energy between the atoms as the respective edge weights and then solve each replica independently by minimizing Eq. (7.1) over a range of γ values. We then use information measures [6] to evaluate how strongly pairs of replicas agree on the ground states of Eq. (7.1).

7.2 Systems studied

We examine a model glass former derived from the three-component AlYFe metallic glass of Chapter 6 which we designate as "A", "B", and "C" in mixture ratios of 88%, 7%, and 5%, respectively. We additionally test the ubiquitous Lennard-Jones potential using the Kob-Andersen (KA) 80:20 binary liquid [9] which lies in the glass-forming mixture region [143].

7.2.1 Ternary model glass former

In this section, we discuss our study on the ternary system mentioned above. As depicted in Fig. 7.4, we use classical molecular dynamics (MD) [8] to simulate the system dynamics.

	a_0	a_1	a_2	a_3	a_4	a_5
AA	*	*	*	*	*	*
AB	1.92	17.4	6.09	3.05	-4.68	3.48
AC	2.38	8.96	-14.9	3.11	-3.88	4.38
BB	*	*	*	*	*	*
BC	1.88	8.00	-3.42	2.53	-1.25	3.00
CC	*	*	*	*	*	*

Table 7.1: Fit parameters for Eq. (7.2) obtained from fitting configuration forces and energies to ab-initio data (as in Chapter 6). The units of the parameters are such that given r in $\mathring{A}$, $\phi(r)$ is in eV. (That is, the parameters a_1, a_4 and a_5 are dimensionless, a_0 is in $\mathring{A}$, a_2 is in $eV\mathring{A}^{a_5}$ and a_3 is in $\mathring{A}^{-1}$.) The same-species (*) data is replaced by a suggested potential derived from generalized pseudo-potential theory [7].

For this, as in Chapter 6, we need accurate effective pair potentials that portray the pairwise interactions between the atoms in the system. Our model potential

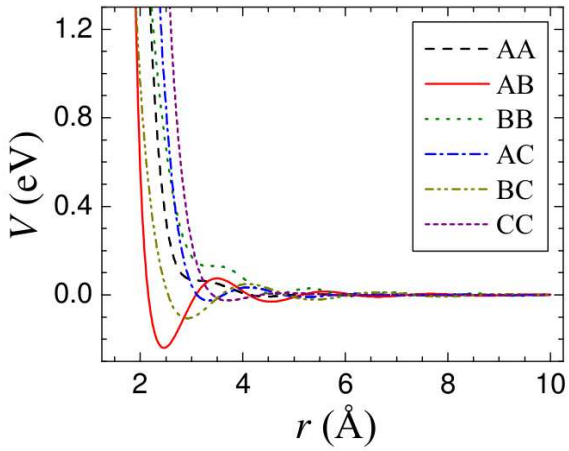

Figure 7.3: The pair potentials for our three-component model glass former (see Fig. 7.4). We indicate the atomic types by "A", "B", and "C" which are included with mixture ratios of 88%, 7%, and 5%, respectively. The units are given for a specific candidate atomic realization (AlYFe) discussed in the text. The same-species data uses a suggested potential derived from generalized pseudopotential theory [7].

energy function is,

$$\phi(r) = \left(\frac{a_0}{r}\right)^{a_1} + \frac{a_2}{r^{a_5}} \cos\left(a_3 r + a_4\right), \tag{7.2}$$

where r is the distance between the centers of two atoms. This potential form incorporates a realistic weak long range interaction. Table 7.1 summarizes the parameter values a_i which depend on the specific types for a pair of interacting atoms, and Fig. 7.3 shows the respective potential plots.

After the forces and energies were fit to first-principles data (as in Chapter 6, the same-species model interactions are finally replaced by that suggested by generalized

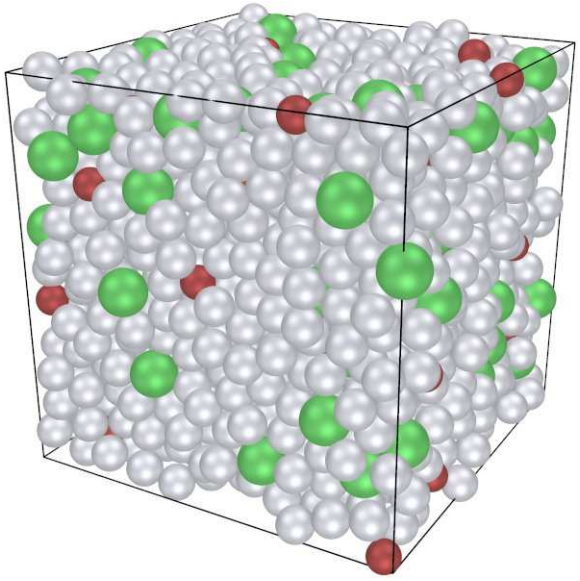

Figure 7.4: A depiction of our simulated model glass former with three components "A", "B", and "C" with mixture ratios of 88%, 7%, and 5%, respectively. The $N = 1600$ atoms are simulated via IMD [8] in cube of approximately 31 Å in size with periodic boundary conditions. The identities of the atoms are C (red), A (silver), B (green) in order of increasing diameters.

pseudo-potential theory (GPT).[7] As illustrated in Fig. 7.4, we simulate $N = 1600$ atoms in a cubic system approximately 31 Å in size using periodic boundary conditions. This width is approximately twice the size of any suspected MRO structures.

The system is initialized at a temperature of $T = 1500$ K and allowed to equilibrate for a long time using a constant number of atoms (N), a constant volume (V), and a constant energy (E). That is, we work within the NVE ensemble. After allowing for system equilibration, we save s high temperature configurations separated by a fixed

period of simulation time. (We fixed the value of s at 12 for all our simulations.) Prior to cooling, the length scales in the system are changed by 1% to account for the increase in density as a result of cooling since we choose to cool the system in an NVT ensemble to control the temperature. This was done to keep a realistic density difference between the high and low temperature configurations. It should not have any important physical consequences pertaining to local structure. The system is then rapidly quenched to a temperature of $T = 300$ K, and it is allowed to equilibrate (in a mostly frozen state) in an NVE ensemble. We again save s separate low temperature configurations separated by a long period of simulation time.

7.2.2 Lennard-Jones glass

Here we discuss the application of our methods to simulations of the Kob-Anderson mixture. The pair potentials are given by

$$\phi_{\alpha\beta}(r) = 4\epsilon_{\alpha\beta}\left[\left(\frac{\sigma_{\alpha\beta}}{r}\right)^{12} - \left(\frac{\sigma_{\alpha\beta}}{r}\right)^{6}\right] \tag{7.3}$$

where α or β designate one of two atomic types A and B. Specifically, in accord with KA we set the dimensionless units $\epsilon_{AA} = 1.0$, $\epsilon_{AB} = 1.5$, $\epsilon_{BB} = 0.5$, $\sigma_{AA} = 1.0$, $\sigma_{AB} = 0.80$, and $\sigma_{BB} = 0.88$.

As in the ternary glassy system above, we use MD [8] to simulate a LJ system of $N = 2000$ atoms. The system is initialized at a temperature of $T = 5$ (using energy units where the Boltzmann constant $k_B = 1$) and allowed to evolve for a long time.

We save s high temperature configurations separated by 10000 time steps. The time step size is $\Delta t = 0.0069$ in LJ time units. Then, the system is rapidly quenched to a temperature of $T = 0.01$ which is well below the glass transition temperature of the KA-LJ system. The system is evolved in this mostly frozen state, and we save s low temperature configurations separated by 10000 steps of simulation time.

7.3 Results

We assign edges between the nodes (atoms) with the respective weights based on the empirical pair-potentials given by Eqs. (7.2) and (7.3). Specifically, we calculate the potential energy ϕ_{ij} between each pair of nodes i and j in the system and then shift each value by a constant ϕ_0 to obtain $\phi'_{ij} = \phi_{ij} + \phi_0$ (assuming that $\phi_{ij} \to 0$ as the distance between particles i and j tends to infinity ($r \to \infty$)). The shift $\phi_0 > 0$ is necessary for the community detection algorithm to properly partition the network of atoms since it provides an objective definition of which interatomic spacings are preferable for a well-defined cluster and which are preferred to be excluded from a cluster.

In our particular application here, we calculate the average potential energy of the system and set $\phi_0 = -\phi_{\text{avg}}$. For use in Eq. (7.1), we define an edge with a weight $A_{ij} = -\phi'_{ij}$ between nodes i and j if $\phi'_{ij} < 0$, and we weight any missing links (or "repulsive edges") by $B_{ij} = \phi'_{ij}$ if $\phi'_{ij} \geq 0$. We then solve both model systems over a

large range of γ using $s = 12$ replicas and $t = 10$ optimization trials per replica.

While $\phi_0 = -\phi_{\text{avg}}$ is an intuitive shift that accomplishes the goal of an objective cluster definition here, it is not an appropriate shift for some problems. For example, using $\phi_0 = -\phi_{\text{avg}}$ turns out to be problematic in some cases for lattice models. In a general setting, we examine a continuum of potential shifts ϕ_0 and monitor extrema in the information theory measures as a function of both γ in Eq. (7.1) and ϕ_0.

In addition to the systems tested below, we applied the algorithm to various test cases including square, triangular, and cubic lattice structures. The algorithm is able to correctly identify the natural leading order scales (plaquettes and composites of plaquettes as "cascades" in the information theory correlations). Further testing involved two-dimensional defects (dislocations, interstitials, etc.) and domain walls in a lattice. Defects in triangular lattices occurred most frequently near cluster boundaries.

We also tested static configurations for the ternary model glass system where each replica is a model of the same configuration. There we detected structures in both low and high temperatures where the high temperature "structures" are more fragile (that is, harder to solve in the clustering problem). This corresponds to identifying relevant transient features in a dense liquid.

7.3.1 Ternary model glass results

In Figs. 7.5 and 7.6, panels (a) and (b) show the information theory based correlations (averaged over all replica pairs as in [6]) over a range of network resolutions.

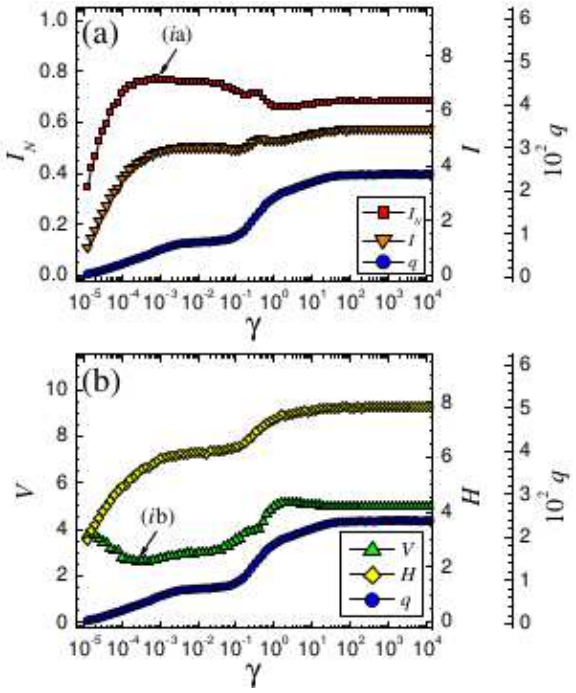

Figure 7.5: Panels (a) and (b) show the plots of information measures I_N, V, H, and I and the number of clusters q (right-offset axes) versus the Potts model weight γ in Eq. (7.1). The ternary model system contains 1600 atoms in a mixture of 88% type A, 7% of type B, and 5% of type C with a simulation temperature of $T = 300$ K which is well *below* the glass transition for this system. This system shows a strongly correlated set of replica partitions as evidenced by the information extrema at (i) in both panels. A set of sample clusters for the best resolution at $\gamma \simeq 0.001$ is depicted in Fig. 7.9.

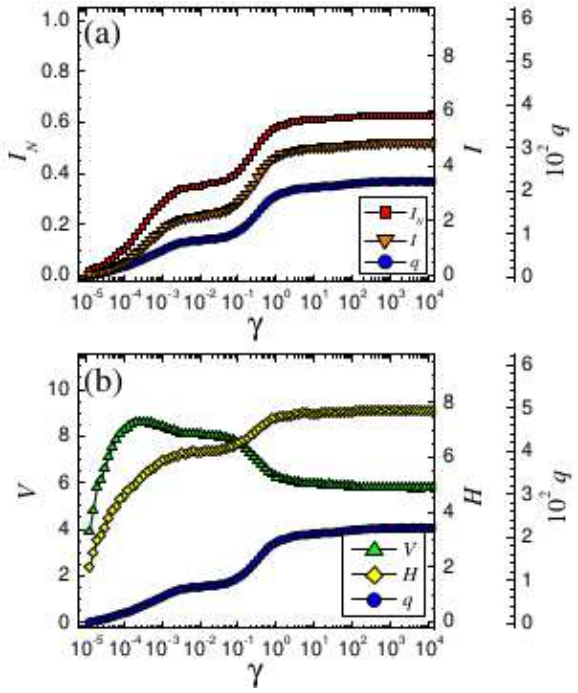

Figure 7.6: Panels (a) and (b) show the plots of information measures I_N, V, H, and I and the number of clusters q (right-offset axes) versus the Potts model weight γ in Eq. (7.1). The ternary model system contains 1600 atoms in a mixture of 88% type A, 7% of type B, and 5% of type C with a simulation temperature of $T = 1500$ K which is well *above* the glass transition for this system. At this temperature, there is no resolution where the replicas are strongly correlated. See Fig. 7.5 for the corresponding low temperature case where the replicas are much more highly correlated at $\gamma \simeq 0.001$.

The lower temperature system at $T = 300$ K in Fig. 7.5(a) shows a peak NMI at (ia) with a corresponding VI minimum at (ib). Fig. 7.7 depicts an example of the full system *partition*.

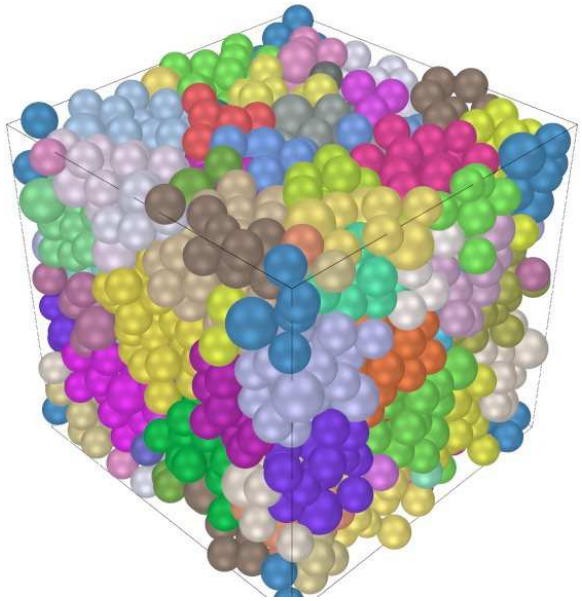

Figure 7.7: A depiction of the full *partitioned* system where unique cluster memberships are depicted as distinct colors (best viewed in color). The atomic identities are B, A, C in order of increasing diameters. Overlapping nodes (multiple memberships per node) are added to these communities to determine the best interlocking system clusters.

Fig. 7.8 shows some sample clusters within the simulation bounding box at resolution parameter value of $\gamma_{best} \simeq 0.001$ where we include overlapping node memberships (the replicas correlations are calculated on partitions), and Fig. 7.9 depicts additional samples of the best clusters.

The corresponding high temperature ($T = 1500$ K) solutions have a much lower NMI at $\gamma_{best} \simeq 0.001$ indicating significantly worse agreement among replicas. That is, one would expect that the high temperature system $T = 1500$ K is in a liquid state,

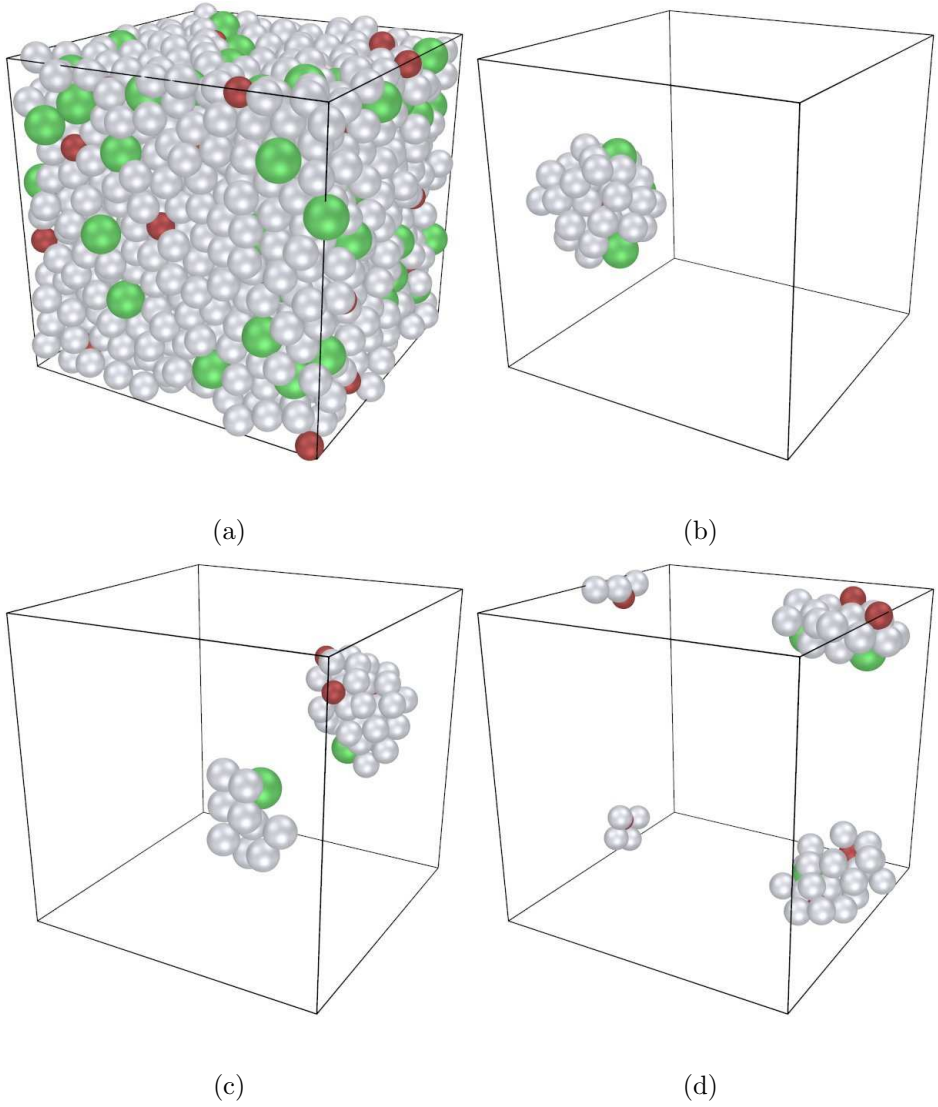

Figure 7.8: Panel (a) is the full system cube, and panels (b) – (d) show three sample clusters (one distinct cluster each using periodic boundary conditions) within the simulation box . Note that the algorithm can identify structures beyond immediate short range neighbors.

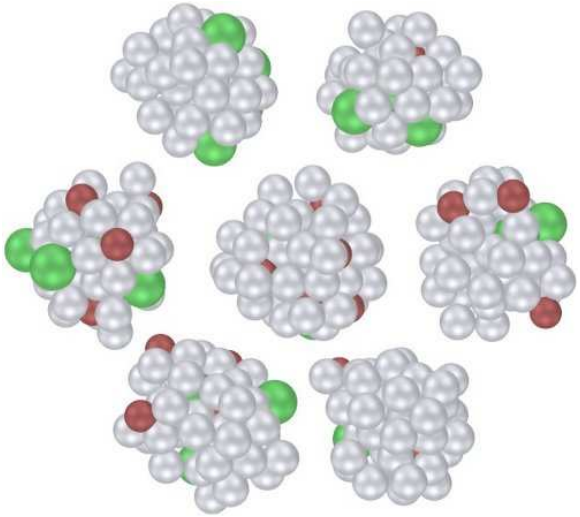

Figure 7.9: A depiction of some of the best clusters of the low temperature ($T = 300K$) ternary system at the peak replica correlation at feature (i) in Fig. 7.5. These clusters include overlapping node membership assignments where each node is required to have an overall negative binding energy to the other nodes in the cluster. The atomic identities are C (red), A (silver), B (green) in order of increasing diameters.

so any observed features are not dynamically stable across all replicas (snapshots of the system over time). At $T = 300$ K, the best structures have consistent cluster sizes that are exclusively MRO.

The plateau regions for $\gamma > 10$ are similar to the LJ plot in Fig. 7.10, but in this system the NMI plateau is lower. In the high temperature case in Fig. 7.6, there are additional "almost-plateaus" for the range $0.001 \lesssim \gamma \lesssim 0.1$. These plateaus represent a region of structural transition, but we are not concerned with them because the

replica correlations are very low.

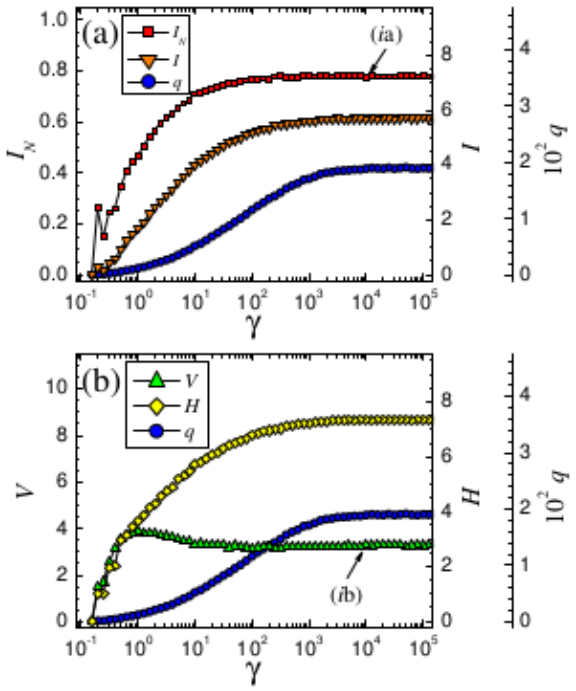

Figure 7.10: Panels (a) and (b) show the plots of information measures I_N, V, H, and I and the number of clusters q (right-offset axes) versus the Potts model weight γ in Eq. (7.1). The LJ system contains 2000 atoms in a mixture of 80% type A and 20% type B (Kob-Andersen binary LJ system [9]) with a simulation temperature of $T = 0.01$ (energy units) which is well *below* the glass transition of $T_c \simeq 0.5$ for this system. This system shows a somewhat strongly correlated set of replica partitions as evidenced by the information extrema at (*i*a,b) in panels (a) and (b). A set of sample clusters for the best resolution at $\gamma = 10^4$ is depicted in Fig. 7.11.

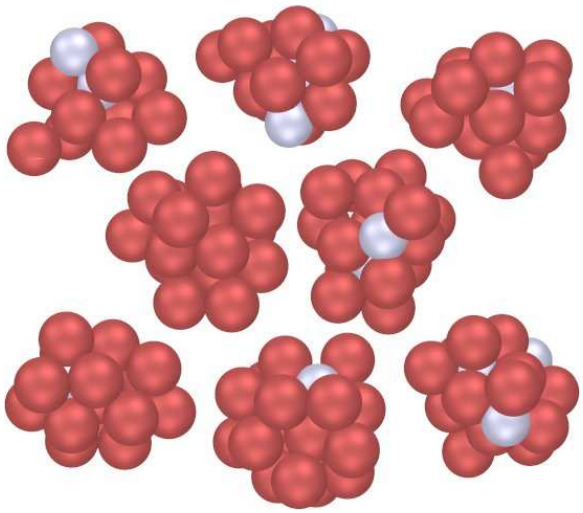

Figure 7.11: Several of the best clusters for the peak replica correlation at feature (i) in Fig. 7.10. These clusters include overlapping node membership assignments where each node is required to have a overall negative binding energy to the other nodes in the cluster. The atomic identities are B (silver) and A (red) in order of increasing diameters.

7.3.2 Binary Lennard-Jones glass results

In Figs. 7.10 and 7.12, panels (a) and (b) show the data for the replica information correlations over a range of network resolutions. The lower temperature system at a temperature of $T = 5$ (in units of $k_B = 1$) in Fig. 7.5(a) shows a plateau in NMI at (ia) with a corresponding VI plateau at (ib) which are the local extrema ($V = 0$ is a trivial solution with only one cluster in this problem). Fig. 7.11 depicts a sample of the best clusters, including overlapping node memberships, at resolution (i) for $\gamma_{best} \simeq 10^4$. The corresponding higher temperature solutions at $\gamma_{best} \simeq 10^4$

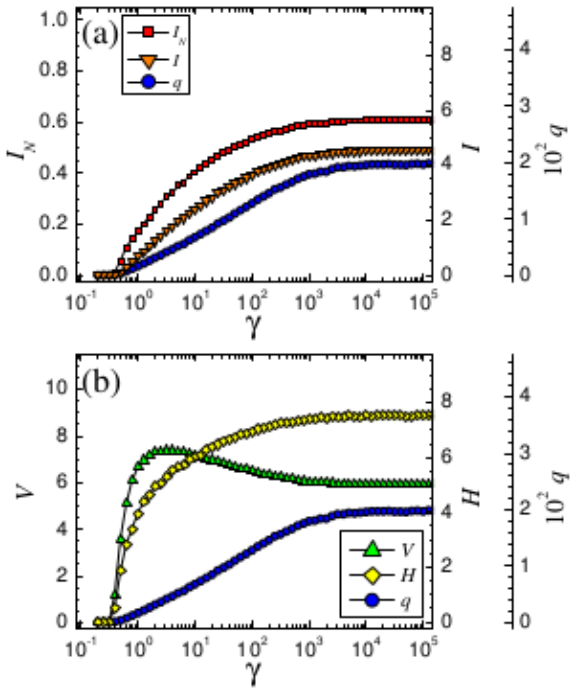

Figure 7.12: Panels (a) and (b) show the plots of information measures I_N, V, H, and I and the number of clusters q (right-offset axes) versus the Potts model weight γ in Eq. (7.1). The LJ system contains 2000 atoms in a mixture of 80% type A and 20% type B (Kob-Andersen binary LJ system [9]) with a simulation temperature of $T = 5$ (energy units) which is well *above* the glass transition of $T_c \simeq 0.5$ for this system. At this temperature, the replicas are significantly less correlated than the corresponding low temperature case in Fig. 7.10.

(see Figs. 7.12 and7.13) have a lower NMI (indicating a weak agreement among replicas). The dependence number of replicas (See Fig. 7.13) required to achieve high accuracy underscores the faint agreement between contending solutions and the

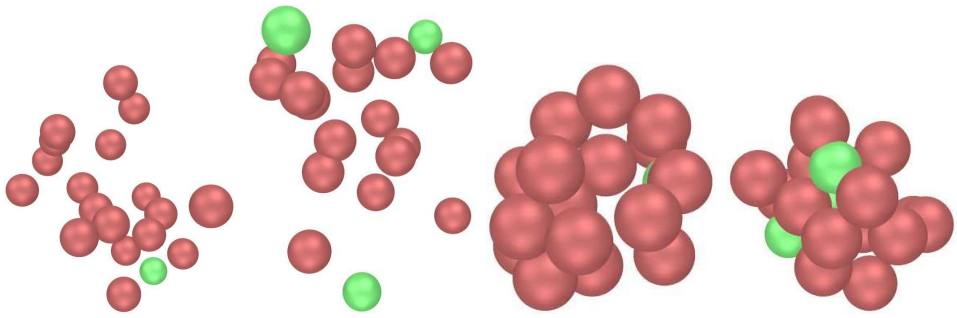

(a) (b) (c) (d)

Figure 7.13: A sample depiction of dispersed clusters for the LJ system Eq. (7.3) at a temperature of $T = 5$ (in units where $k_B = 1$). The shown clusters correspond to the multiresolution plot in Fig. 7.12 at value of the resolution parameter of $\gamma = 10^4$. These clusters are a sample of high temperature counterparts to the low temperature clusters in Figs. 7.10 and 7.11. Panels (a) and (b) show a more typical example of dispersed clusters at a number of replicas $s = 10$. In some cases, the identified high temperature clusters can be more compact, but not densely packed. Panels (c) and (d) provide sample solutions for $s = 20$ replicas.

high temperature complexity of the problem. Our identified structures for this LJ model system are consistent in terms of the cluster sizes and are almost exclusively SRO configurations with simple adjunct-type atoms extending into the low end of MRO size structures.

7.4 Conclusions

Our method is a new and very general approach to determine the natural multi-scale structures of complex physical systems. We do not bias the expected configurations in any way. The only required inputs are the pairwise interaction potentials between the atoms. In case information about such pairwise interactions are not easy to obtain, the algorithm can be used with the pair correlation functions used as weights. Information theory extrema (including plateaus) between contending solutions give the different pertinent structures on all important length scales (lattice scales and correlation lengths) of the system in an unbiased unified way.

Appendix

A High temperature series expansion of the correlation function

We now outline in detail how we may obtain a high temperature (T) series expansion of the correlation function to arbitrary order for a general system with translational invariance. The results we present below are valid in the high temperature phase of general lattice (spin or other) and continuum systems. However, these may hold at low temperatures, provided we can analytically continue to low temperatures from the high temperature phase, i.e., arrive at these without having a phase transition. We should emphasize that as we set the temperature to be arbitrarily high, the density does not have to be small as is assumed in methods derived from Mayer's cluster expansion for fluids. Our result is therefore valid for the high temperature phase of any system. Albeit trivial, we should remark that, formally, for any finite size system of N sites (or of finite volume for a continuum theory), no matter how large

yet still finite, there are no phase transitions [instead there might be progressively sharp (as N increases), yet analytic, crossovers]. Thus, in finite size systems, the radius of convergence of the high T expansion is infinite. In general, the long range character of the interactions will not enable us to invoke many of the simplifying elegant tricks presented elsewhere. For instance, the counting of connected contours and loops [144, 145] that appear in high temperature series expansions involving nearest neighbor interactions cannot be applied here.

We can perform the high temperature series expansion directly in the original spin space. However, we find it easier to make a transformation to a dual space where our Boltzmann weights become Gaussian in the high temperature limit.

The correlation function of the original theory can be expressed in terms of the correlation function (and higher moments) of the dual theory – we employ that in our calculation. The dual theory to a nearest neighbor ferromagnetic system is a Coulomb gas. A nearest neighbor ferromagnetic system in dimensions $d > 2$ at low T has an ordered phase and a small correlation length (the correlation length diverges at $T = T_c$). This does *not* imply that the Coulomb system has a small correlation length at high temperature. $O(n)$ constraints become faint at high T in the dual theory whereas in the exact Coulomb gas at high T, the $O(n)$ constraints are there. The same also applies for a soft spin realization of the Coulomb gas where $\exp[-\beta u(S^2-1)^2]$ which is zero as $\beta \to \infty$ (or $T \to 0$) unless $S^2 = 1$ everywhere. By contrast in the exact dual theory at high temperature, the relative strength of the $O(n)$

constraints becomes negligible relative to the "interaction" term containing $(\beta V)^{-1}$. Even though we can ignore β prefactors when $\beta = \mathcal{O}(1)$ and consider dual theories and soft spin realization we cannot ignore the T dependence at high T about the infinite T disordered limit. Otherwise we get a contradiction as our exact calculation with the exact dual theory (containing the T-dependent prefactors) shows.

We will keep things general and perform the simple series expansion of the dual Hamiltonian H_d in Eq. (3.6):

$$\begin{aligned} H_d &= -\frac{N^2}{2\beta^2}\sum_{\vec{x},\vec{y}} V^{-1}(\vec{x}-\vec{y})\vec{\eta}(\vec{x})\cdot\vec{\eta}(\vec{y}) \\ &\quad -\frac{1}{\beta}\sum_{\vec{x}} \ln\left(\frac{I_{n/2-1}(\sqrt{n}N|\vec{\eta}(\vec{x})|)}{(\sqrt{n}N|\vec{\eta}(\vec{x})|)^{n/2-1}}\right), \\ &= -\frac{N^2}{2\beta^2}\sum_{\vec{x},\vec{y}} V^{-1}(\vec{x}-\vec{y})\vec{\eta}(\vec{x})\cdot\vec{\eta}(\vec{y}) \\ &\quad -\frac{N^2}{2\beta}\sum_{\vec{x}} \vec{\eta}(\vec{x})\cdot\vec{\eta}(\vec{x}) \\ &\quad +\frac{N^4}{4(n+2)\beta}\sum_{\vec{x}} \left[\vec{\eta}(\vec{x})\cdot\vec{\eta}(\vec{x})\right]^2 + \ldots \quad . \end{aligned} \tag{A-4}$$

In Eq. (A-4), the interaction V should be thought of as a translationally invariant matrix. That is, in a Dirac type notation, $\langle\vec{x}|V|\vec{y}\rangle = V(\vec{x}-\vec{y})$. In Eq. (A-4), V^{-1} is the inverse Fourier transform of $1/v(\vec{k})$, where $v(\vec{k})$ is the Fourier transform of $V(\vec{x})$ [146].

Next, we separate H_d into a quadratic part H_{d0} and higher order (interaction

type) terms which we denote by ΔH. That is,

$$\begin{aligned} H_{d0} &= -\frac{N^2}{2\beta^2}\sum_{\vec{x},\vec{y}} V^{-1}(\vec{x}-\vec{y})\vec{\eta}(\vec{x})\cdot\vec{\eta}(\vec{y}) \\ &\quad -\frac{N^2}{2\beta}\sum_{\vec{x}}\vec{\eta}(\vec{x})\cdot\vec{\eta}(\vec{x}) \qquad \text{(A-5)} \\ \Delta H &= \frac{N^4}{4(n+2)\beta}\sum_{\vec{x}}\left[\vec{\eta}(\vec{x})\cdot\vec{\eta}(\vec{x})\right]^2 + \ldots\ . \qquad \text{(A-6)} \end{aligned}$$

The expectation value of any quantity X may be computed by

$$\begin{aligned} \langle X\rangle_d &= \frac{\langle X e^{-\beta\Delta H}\rangle_{d0}}{\langle e^{-\beta\Delta H}\rangle_{d0}}, \qquad \text{(A-7)} \\ &= \langle X\rangle_{d0} - \beta\left[\langle X\Delta H\rangle_{d0} - \langle X\rangle_{d0}\langle\Delta H\rangle_{d0}\right] \\ &\quad +\frac{\beta^2}{2!}\left[\langle X(\Delta H)^2\rangle_{d0} - 2\langle X\Delta H\rangle_{d0}\langle\Delta H\rangle_{d0}\right. \\ &\quad \left.+2\langle X\rangle_{d0}\langle\Delta H\rangle_{d0}^2 - \langle X\rangle_{d0}\langle(\Delta H)^2\rangle_{d0}\right] \\ &\quad +\ldots\ , \qquad \text{(A-8)} \end{aligned}$$

where $\langle\cdot\rangle_{d0}$ represents the expectation value calculated with the Boltzmann weight associated with the Hamiltonian H_{d0}. We may retain terms to arbitrary order in η^2 (or corresponding order in $1/T$). Equation (3.7) can be expanded to arbitrary order in η^2, where we rewrite all expectation values with respect to the Hamiltonian H_{d0}. The terms become expectation values of a product of an even number of η fields with respect to the quadratic Hamiltonian H_{d0}. We can then use Wick's theorem to compute the expectations with respect to H_{d0} to all orders. To order $1/T^3$ we obtain

for $\vec{x} \neq 0$,

$$
\begin{aligned}
& G(\vec{x}) = -\frac{V(\vec{x})}{k_B T} + \\
& \frac{1}{(k_B T)^2}\left[\sum_{\vec{z}} V(\vec{z})V(\vec{x}-\vec{z}) - 2V(0)V(\vec{x})\right] \\
+ \quad & \frac{1}{(k_B T)^3}\left[-\sum_{\vec{y},\vec{z}} V(\vec{y})V(\vec{z})V(\vec{x}-\vec{y}-\vec{z}) + \right. \\
& 2V(\vec{x})\sum_{\vec{z}} V(\vec{z})V(-\vec{z}) + 3V(0)\sum_{\vec{z}} V(\vec{z})V(\vec{x}-\vec{z}) \\
& \left. -5(V(0))^2 V(\vec{x}) - 2\frac{(V(\vec{x}))^3}{n+2}\right]. \qquad \text{(A-9)}
\end{aligned}
$$

As a brief aside, we note that from the fluctuation dissipation theorem the susceptibility $\chi = \beta \sum_{\vec{x}} G(\vec{x})$. At asymptotically high temperature, $G(\vec{x}) \simeq \delta_{\vec{x},0}$ giving rise to Curie's law, $\chi \propto 1/T$. The terms in Eq. (A-9) lead to higher order corrections. To next order, $\chi = \frac{1}{k_B(T-\theta_C)}$ with the Curie temperature $\theta_C = \sum_{\vec{x}\neq 0} V(\vec{x})$ in the weak coupling limit. Thus far, in the literature, the Curie-Weiss form has been invoked to ascertain whether a given system has dominantly ferromagnetic or anti-ferromagnetic interactions (by examining the sign of θ_C) and their strength ($|\theta_C|$). We see that by not focusing solely on $\chi = \beta G(\vec{k}=0)$ but rather on the scattering function $G(\vec{k})$ for all $\vec{k}$, we can in principle deduce the interaction $v(\vec{k})$ and hence $V(\vec{x})$. We further note, in passing, that for ferromagnetic systems (ones with $V(\vec{x}) \leq 0$), all terms in $G(\vec{x})$ are positive and the correlation functions are monotonically decreasing with T (or increasing with the inverse temperature β). This and similar relations are consequences of extensions of the standard Griffiths inequalities [147] to general $O(n)$

systems with arbitrary range (ferromagnetic) interactions. The extension of these relations to the $O(n)$ systems discussed here follows from, e.g., an explicit Feynman type diagrammatic expansion (e.g., [52]) that represents the high temperature series expansion and noting that each diagram is trivially positive. Replacing the sums for the clock model of Ref. [52], in e.g., $O(2)$ systems, all angular integrals reduce to products of the type $\int_0^{2\pi} d\theta \exp(in\theta) = 2\pi\delta_{n,0} \geq 0$.

In Fourier space, the real space convolutions become momentum space products and vice versa. Equation (A-9) then reads

$$\begin{aligned} G(\vec{k}) = 1 - \frac{v(\vec{k})}{k_B T} + \frac{1}{(k_B T)^2}\left[(v(\vec{k}))^2 - 2V(\vec{x}=0)v(\vec{k})\right] \\ + \frac{1}{(k_B T)^3}\Bigg[-(v(\vec{k}))^3 + \frac{2v(\vec{k})}{N}\sum_{\vec{k_1}}(v(\vec{k_1}))^2 \\ + 3V(\vec{x}=0)(v(\vec{k}))^2 - 5(V(\vec{x}=0))^2 v(\vec{k}) - \frac{2}{N^2(n+2)} \times \\ \sum_{\vec{k_1},\vec{k_2}} v(\vec{k_1})v(\vec{k_2})v(\vec{k}-\vec{k_1}-\vec{k_2})\Bigg] - G_1(0), \end{aligned} \tag{A-10}$$

where $G_1(0)$ is the value obtained by inserting $\vec{x} = 0$ in Eq. (A-9). It should be noted that the real space correlation function cannot change if we shift the on-site interaction $V(\vec{x} = 0)$ which is equivalent to a uniform shift to $v(\vec{k})$ for all k. This is because the $\mathcal{O}(n)$ spin is normalized – $|\vec{S}(\vec{x})|^2 = n$ at all sites $\vec{x}$. This invariance to a constant shift holds for all T and consequently to any order in $1/T$, the coefficients must be invariant to a global shift in $v(k)$. Among other things, we earlier invoked this invariance [72] to shift $v(\vec{k})$ to enable a HS transformation in the cases for which

initially $v(\vec{k}) > 0$ for some values of $\vec{k}$. We can, of course, invoke this invariance here also to obtain the above high temperature series expansion with a well-defined HS dual. The final results, as we re-iterated above are invariant under this shift as is also manifest in our series expansion in powers of $1/T$. Although obvious, we note that the expansion in Eq. (A-10) is performed in powers of $1/T$ involving $v(k)$ for real vectors $\vec{k}$. In examining the correlation lengths via contour integration in the complex k plane, the corresponding $v(k)$ may be extended for complex k.

We see from the expansion in Eq. (A-10) that already to $\mathcal{O}(1/T)$, it is also clear that the lengthscales of the system (which are determined by the poles of the Fourier space correlation function) are governed by the poles of $v(\vec{k})$ in the complex $\vec{k}$ space. Thus, if, e.g., $v(\vec{k}) = 1/(k^2 + \lambda^{-2})$, the correlation length tends to λ at high temperature. It therefore must diverge for a system with no screening.

In cases where the correlation function is known from some experimental technique or otherwise, the series expansion for the correlation function can be inverted to arbitrary order to obtain the pairwise interactions. To $\mathcal{O}(1/T^2)$, for non-zero separation $\vec{x}$, the potential function is given by,

$$\begin{aligned} V(\vec{x}) = -k_B T \Bigg[& G(\vec{x}) - {\sum_{\vec{z}}}' G(\vec{z}) G(\vec{x}-\vec{z}) \\ & + {\sum_{\vec{y},\vec{z}}}' G(\vec{y}) G(\vec{z}) G(\vec{x}-\vec{y}-\vec{z}) \\ & + 2G(\vec{x}) {\sum_{\vec{z}}}' G(\vec{z}) G(-\vec{z}) - \frac{2\left(G(\vec{x})\right)^3}{n+2} \Bigg]. \end{aligned} \tag{A-11}$$

The prime indicates that the sum excludes terms containing $G(0)$. As is evident from

our earlier results and discussion, in Eq. (A-11), each correlation function $G(\vec{x})$ is of order $(1/T)$.

We reiterate that, as in our discussion in Sec. 3.6, our results for lattice $O(n)$ spin models match with the leading order behavior at high temperature obtained from several standard approximate theories based on Mayer's cluster expansion derived for liquid systems, e.g., Born-Green theory [148] and OZ theory with the Percus-Yevick approximation [149] or MSA [93]. As implicit above, our $1/T$ expansion can indeed be extended to systems in which the liquid and the gas phase are not separated by a phase transition, e.g., for pressures larger than the pressure at the liquid-vapor critical point. As further noted in Sec. 3.6, various approximations also suggest that at high temperatures, the correlation length may match the length scale characterizing the interaction potential and, in particular, will diverge in systems having long range interactions (as we have established).

B Relation between the generalized Debye lengths and divergence of the high temperature correlation lengths

An intuitive approximate approach for the understanding of the rigorous yet seemingly paradoxical result that we report in this work – that of the divergence of the correlation lengths in the high temperature limit of systems with long range interactions – is afforded by the OZ framework. Specifically, in the language of OZ approximations, the "total" high temperature correlation function is the same as the "direct" correlation function [see, e.g., Ref. [77] (Sec. 2.6) for the definition of the "direct" OZ correlation functions] and behaves as

$$G(\vec{x}) \sim -\beta V(\vec{x}) \tag{B-12}$$

for $\vec{x} \neq 0$. Thus, if the potential is screened beyond a distance λ, the correlation length approaches λ at high temperature. That is, if we have an effective interaction resulting, e.g., from higher order effects in $1/T$, such as that leading to the Debye screening length (λ_D) in Coulomb systems [and generalizations introduced earlier in Eq. (3.18)], then at high temperature, the correlation length

$$\xi \xrightarrow[T\to\infty]{} \lambda_D. \tag{B-13}$$

This is a particular case of Eq. (3.15).

To $\mathcal{O}(1/T^2)$, Eq. (A-10) is identical to Eq. (3.10). The poles of G in the complex k plane can, of course, be computed by finding those of Eq. (3.10) or considering directly those of Eq. (A-10): both give rise to the same answer as they must.

C Transfer Matrix in the one-dimensional system with Ising spins

Thus far, we focused primarily on high dimensional continuous (large-n) spin systems. For completeness, we review and illustrate how some similar conclusions can be drawn for one-dimensional Ising systems with finite ranged interactions and briefly discuss trivial generalizations. In particular, we show how the sum of the number of modulation and number of correlation lengths does not change as the temperature is varied. In Sec. 4.3.3, we illustrated how this arises for general large-n systems.

For interactions of range R in a one-dimensional Ising spin chain, the transfer matrix, T is of dimension $M = \mathcal{O}(2^R)$. The correlation function for large system size, takes the form

$$G(x) = \sum_{k=1}^{2^R-1} A_k \left(\frac{\lambda_k}{\lambda_0}\right)^x, \tag{C-14}$$

where λ_is are the eigenvalues of the transfer matrix. Since the characteristic equation has real non-negative coefficients, from Perron-Frobenius theorem, λ_0 is real, positive and is non-degenerate. The secular equation, $\det(T - \lambda I) = 0$ is a polynomial in λ with real coefficients. Thus, two possibilities need to be examined: real roots, and,

complex conjugate pairs of roots. Real eigenvalues λ_p give terms with correlation length,

$$\xi = \ln\left(\frac{\lambda_0}{|\lambda_p|}\right). \tag{C-15}$$

Complex conjugate eigenvalues, λ_q and λ_q^* correspond to the same correlation length and modulation length, given by,

$$\xi = \ln\left(\frac{\lambda_0}{|\lambda_q|}\right), \tag{C-16}$$

$$L_D = \frac{2\pi}{\tan^{-1}\left(\frac{\mathrm{Im}\{\lambda_q\}}{\mathrm{Re}\{\lambda_q\}}\right)}. \tag{C-17}$$

Thus, the total number of correlation and modulation lengths is the order of the polynomial in λ in the secular equation, or simply the dimension of the transfer matrix – $\mathcal{O}(2^R)$. Similar to our conclusions for the high dimensional continuous spin systems, this number does not vary with temperature. For q state Potts type spins, replicating the above arguments mutatis mutandis, we find that the total number of correlation and modulation lengths is $\mathcal{O}(q^R)$. Similarly, for such a system placed on a d-dimensional slab of finite extent in, at least, $(d-1)$ directions along which it has a length of order $\mathcal{O}(l) > R$, there will be $\mathcal{O}(q^{l^{d-1}})$ transfer matrix eigenvalues and thus an identical number for the sum of the number of modulation lengths with the number of correlation lengths.

The eigenvalues change from being complex below certain crossover temperatures to being purely real above. These temperatures form the "disorder line".

D Detailed expressions for δL_D for different orders $p(\geq 3)$ at which the interaction kernel has its first non-vanishing derivative

If the lowest order (larger than $p = 2$) non-vanishing derivative of $v(k)$ at the minimizing wavenumber k_0 (see Eq. (4.31)) is of order $p = 3$ (the most common case) then, in the large-n limit, the change in the modulation length at temperatures $T > T_c$ ($\mu(T) = \mu_{min} + \delta\mu$)about its value at $T = T_c$ of Eq. (4.41) is given by

$$\delta L_D = -\frac{2\pi}{k_0^2}\frac{v^{(3)}(k_0)\delta\mu}{3(v^{(2)}(k_0))^2}. \tag{D-18}$$

We employ Eq. (D-18) in our analysis in Sec. 4.4. If the lowest order derivatives are of order $p = 4$ or 5 then,

$$\delta L_D = \frac{2\pi}{k_0^2}\frac{v^{(5)}(k_0)(\delta\mu)^2}{30(v^{(2)}(k_0))^3}. \tag{D-19}$$

Similarly, for $p = 6$ or 7,

$$\delta L_D = -\frac{2\pi}{k_0^2}\frac{v^{(7)}(k_0)(\delta\mu)^3}{630(v^{(2)}(k_0))^4}, \tag{D-20}$$

and so on.

E $\mu(T)$ for the screened Coulomb ferromagnet

We now briefly provide an explicit expression for the relation between the large-n Lagrange multiplier μ and the temperature T for the screened Coulomb ferromagnet.

In three dimensions, with Λ as an ultra-violet cutoff, at high temperatures [$T > T^*$], we get to the following implicit equation for $\mu(T)$ in the case of the screened Coulomb ferromagnet of Eq. (4.64),

$$\begin{aligned}\frac{1}{T} &= \frac{\Lambda}{2\pi^2} + \frac{\sqrt{2}}{4\pi^2 w} \\ &\times \Big(\frac{\lambda^2\mu - \mu^2 + \mu w - 2Q}{\sqrt{\lambda^2 + \mu + w}} \tan^{-1}\Big(\frac{\Lambda\sqrt{2}}{\sqrt{\lambda^2 + \mu + w}}\Big) \\ &- \frac{\lambda^2\mu - \mu^2 + \mu w + 2Q}{\sqrt{\lambda^2 + \mu - w}} \tan^{-1}\Big(\frac{\Lambda\sqrt{2}}{\sqrt{\lambda^2 + \mu - w}}\Big)\Big). \end{aligned} \tag{E-21}$$

In Eq. (E-21), we employed the shorthand $w \equiv \sqrt{(\mu - \lambda^2)^2 - 4Q}$. The parameter w vanishes at the crossover temperature T^* at which a divergent modulation length makes an appearance, $w(T = T^*) = 0$. At low temperatures, $T < T^*$, w becomes imaginary and an analytical crossover occurs to another real functional form.

F Proof that $\mu(T)$ is an analytic function of T

In this appendix, we illustrate that in the large-n limit, the thermodynamic functions are analytic for all temperatures $T > T_c$, including the discussed cross-over temperature $T = T^*$ (hence justifying the use of the term "cross-over") of, e.g, the Coulomb frustrated ferromagnet of Eqs. (2.1, 4.64).

From Eq. (4.20), using,

$$\mu > \mu_{\min} = -\min v(k), \tag{F-22}$$

it is clear that $\mu(T)$ is a continuous function of T. Differentiating,

$$\frac{d\mu}{d(k_BT)} = \left[(k_BT)^2 \int \frac{d^dk}{(v(k)+\mu)^2}\right]^{-1}, \tag{F-23}$$

and,

$$\frac{d^2\mu}{d(k_BT)^2} = -\frac{2}{k_BT}\frac{d\mu}{d(k_BT)} + 2(k_BT)^2\left(\frac{d\mu}{d(k_BT)}\right)^3 \int \frac{d^dk}{(v(k)+\mu)^3} \tag{F-24}$$

with the integrations performed over the first Brillouin zone on the lattice (or up to some ultra-violet cutoff Λ in the continuum). The first two derivatives are thus always finite so long as the integration range is finite. All higher order derivatives are sum of terms which are products of lower order derivatives, $(k_BT)^a$ and $\int \frac{d^dk}{(v(k)+\mu)^b}$, where a and b are integers, with $b > 0$. Thus, for finite integration range, $\mu(T)$ is an analytic function of T. In the large-n limit, the internal energy per site, $U/N = [k_BT - \mu(T)]/2$. Our result concerning the analyticity of $\mu(T)$ implies that the internal energy is analytic and thus all of its derivatives and all other thermodynamic potentials.

G Fermi systems

In this appendix, we discuss several examples of non-interacting fermionic systems where we observe a correlation or modulation length exponent. We will, in what follows, ignore spin degrees of freedom which lead to simple degeneracy factors for the systems that we analyze. In non-interacting Fermi systems, the mode occupancies

are given by the Fermi function. That is,

$$\langle n(\vec{k})\rangle = \langle c^{\dagger}(\vec{k})c(\vec{k})\rangle = \frac{1}{e^{\beta(\epsilon(\vec{k})-\mu)}+1}, \tag{G-25}$$

where $c(\vec{k})$ and $c^{\dagger}(\vec{k})$ are the annihilation and creation operators at momentum $\vec{k}$ and $\beta = 1/(k_B T)$ with T the temperature. The correlation function associated with the amplitude for hopping from the origin to lattice site $\vec{x}$ is given by

$$G(\vec{x}) = \langle C^{\dagger}(0)C(\vec{x})\rangle = \sum_{\vec{k}} \langle n(\vec{k})\rangle e^{-i\vec{k}\cdot\vec{x}}. \tag{G-26}$$

Thus far, in most explicit examples that we considered we discussed scaling with respect to a crossover temperature. In what follows, we will, on several occasions, further consider the scaling of correlation and modulation lengths with the chemical potential μ. We will use the letter υ to represent exponents corresponding to scaling with respect to μ and continue to use ν to represent scaling with respect to the temperature T.

The existence of modulated electronic phases is well known.[32, 150–164] In particular, the Fermi wave-vector dominated response of diverse modulated systems as evident in Lindhard functions, particular features of charge and spin density waves dominated by Fermi surface considerations in quasi- one dimensional and other systems have long been discussed and have numerous experimental realizations in diverse compounds.[163, 164] The exponents that we derived in this work appear for all electronic and other systems in which a crossover occurs in the form of the modulations seen in charge, spin, or other degrees of freedom. Our derived results concerning scal-

ing apply to general interacting systems. To highlight essential physics as it pertains to the change of modulations in systems of practical importance, we briefly review and further discuss free electron systems.

G.1 Zero temperature length scales – Scaling as a function of the chemical potential μ

We first consider a non-interacting fermionic system with a dispersion $\epsilon(\vec{k})$. At zero temperature, the number of particles occupying the Fourier mode $\vec{k}$ is given by

$$\langle n(\vec{k})\rangle = \begin{cases} 1 & \text{for } \epsilon(\vec{k}) < \mu \\ 0 & \text{for } \epsilon(\vec{k}) > \mu. \end{cases} \tag{G-27}$$

All correlation functions as all other zero temperature thermodynamic properties, are determined by the Fermi surface geometry. We now consider the correlation function of Eq. (G-26). This correlation function will generally exhibit both correlation and modulation lengths. To obtain the modulation lengths along a chosen direction (the direction of the displacement $\vec{x}$), a ray along that direction may be drawn. The intercept of this ray with the Fermi surface provides the pertinent modulation wave-vectors. As we vary μ we alter the density, ρ via

$$\rho = g_s \int_{\epsilon(\vec{k})<\mu} \frac{d^d k}{(2\pi)^d}, \tag{G-28}$$

g_s being the spin degeneracy ($g_s = 2$ for non-interacting spin-half particles such as electrons). As the *Fermi surface topology* is varied, the following effects may be

observed.

1. If two branches of the Fermi surface touch each other at $\mu = \mu_0$ and are disjoint for all other values of μ, then a smooth crossover will appear from one set of modulation lengths to another with $|L_D - L_{D0}| \propto |\mu - \mu_0|$ on both sides of the crossover. This crossover will be associated with an exponent $\upsilon_L = 1$ characterizing the scaling of the modulation lengths with deviations in the chemical potential. An example where a crossover of this kind is realized is the $\epsilon_g = 0$ case of the schematic shown in Fig. 7.14 in which the crossover occurs at $\mu = \mu_0$. Other examples of this occur at half filling of the square lattice

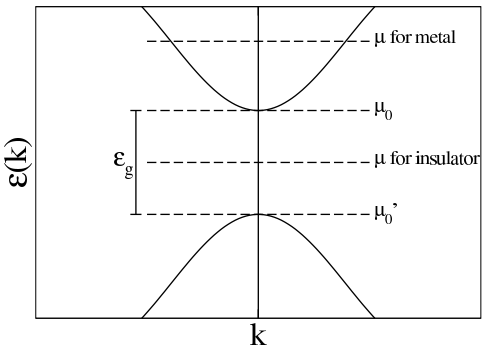

Figure 7.14: Transition from a metal to a band insulator. This figure is for illustration only.

tight binding model and at three-quarters filling of the triangular lattice tight binding model. These will be discussed later.

2. If on the other hand, one branch of the Fermi surface vanishes as we go past $\mu = \mu_0$, the crossover is not so smooth and we get some rational fraction υ_L (usually $\upsilon_L = 1/2$) as the crossover exponent: $|L_D - L_{D0}| \propto |\mu - \mu_0|^{\upsilon_L}$, on one side of the crossover. An example of this is shown in Fig. 7.15. Here,

$$|L_D - L_{D0}| = \frac{L_{D0}^2}{2\pi}\sqrt{\frac{2|\mu - \mu_0|}{|\epsilon''(2\pi/L_{D0})|}}, \tag{G-29}$$

where L_{D0} is the modulation length at the point where the $\mu = \mu_0$ line touches the $\epsilon(k)$ curve, such that $\epsilon'(2\pi/L_{D0}) = 0$ The hopping correlation function takes the form,

$$\begin{aligned} G(x) &= \frac{(ax)^{d/2}\mathrm{J}_{d/2}(ax)}{(2\pi)^{d/2}x^d} - \frac{(bx)^{d/2}\mathrm{J}_{d/2}(bx)}{(2\pi)^{d/2}x^d} \\ &\quad + \frac{(cx)^{d/2}\mathrm{J}_{d/2}(cx)}{(2\pi)^{d/2}x^d}, \end{aligned} \tag{G-30}$$

where $\mu_0' < \mu < \mu_0$ and a, b and c in Eq. (G-30) (corresponding to modulation lengths of $2\pi/a$, $2\pi/b$ and $2\pi/c$) are the values of k for which $\epsilon(k) = \mu$ (as shown in Fig. 7.15).

At arbitrarily small but finite temperatures, the correlation function exhibits modulations of all possible wavelengths. The prefactor multiplying a term with spatial modulations at wave-vector $\vec{k}$ is the exponential of $(-|\epsilon(\vec{k}) - \mu|)$. An illustrative example is provided in Fig. 7.16. Apart from the dominant zero temperature modulations, associated with the wave-vector k_2 in Fig. 7.16, at finite temperature, there are additional contributions from wave-vectors for which $|\epsilon(k) - \mu|$ is small relative

to k_BT. Near k_2, we can assume $\epsilon(k)$ is linear such that $\epsilon(k) \approx \mu + (k - k_2)\epsilon'(k_2)$. Similarly, near k_1, $\epsilon(k) - \mu \approx -\Delta - (k - k_1)^2\epsilon''(k_1)/2$, where $\Delta = \mu - \mu_0$ (see Fig. 7.16). For large β, both these contributions are highly localized around k_2 and k_1 respectively making the above approximations very good and the Fourier transforming integrals easy to evaluate ($\langle n(\vec{k})\rangle$ taking exponential and Gaussian forms). We have,

$$\begin{aligned} G(x) &= \frac{(k_2x)^{d/2}\mathrm{J}_{d/2}(k_2x)}{(2\pi)^{d/2}x^d} - \frac{2(k_2x)^{d/2}\mathrm{J}_{d/2-1}(k_2x)}{(2\pi)^{d/2}\beta\epsilon'(k_2)x^{d-1}} \\ &\quad + \frac{e^{-\beta\Delta}(k_1x)^{d/2}\mathrm{J}_{d/2-1}(k_1x)}{(2\pi)^{\frac{d-1}{2}}\sqrt{\beta\epsilon''(k_1)}x^{d-1}}, \end{aligned} \tag{G-31}$$

where $\beta \to \infty$ and $\Delta \to 0$, such that $\beta\Delta \to \infty$.

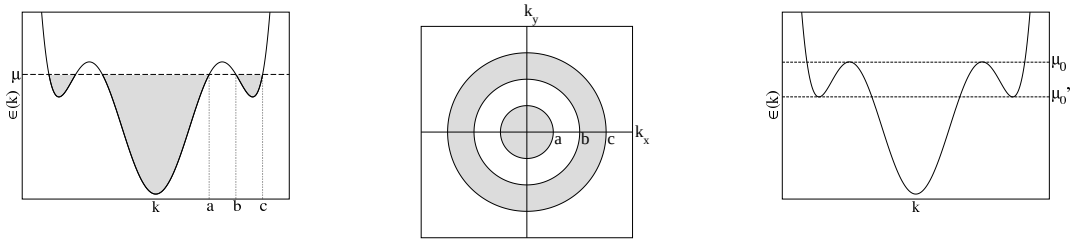

(a) (b) (c)

Figure 7.15: Example of a Fermi system where the modulation length exponent is 1/2. The gray region shows the filled states. When $\mu > \mu_0$, modulations corresponding to wave-vectors $k = a$ and $k = b$ cease to exist and we get an exponent of 1/2 at this crossover. Similarly, when $\mu < \mu_0'$, modulations corresponding to wave-vectors $k = b$ and $k = c$ die down.

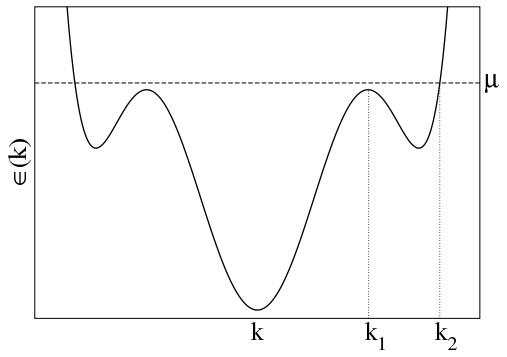

Figure 7.16: The same Fermi system as in Fig. 7.15, but now with a chemical potential $\mu = \mu_0 + \Delta$, slightly higher than μ_0. The temperature is small but finite.

Next, we will discuss scaling of the modulation length in with the chemical potential, μ in the familiar tight binding models on the square and triangular lattices at zero temperature.

Tight binding model on the square lattice

We consider a two-dimensional tight binding model of the square lattice. The dispersion in this model is given by

$$\epsilon(\vec{k}) = -2t\left(\cos k_x + \cos k_y\right). \tag{G-32}$$

The constant energy contours corresponding to Eq. (G-32) are drawn in Fig. 7.17. As is clear from Fig. 7.17, there are certain directions (e.g., along the X-axis) along which there is no $\vec{k}$ for $\epsilon(\vec{k}) > 0$. If we consider the same system at zero temperature,

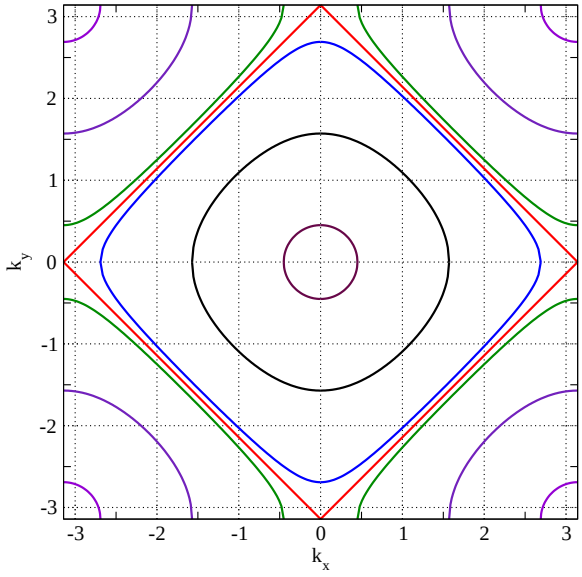

Figure 7.17: Constant energy contours for two-dimensional tight binding model on the square lattice in Eq. (G-32). The red square corresponds to the particle hole symmetric contour where $\epsilon(\vec{k}) = 0$. The contours inside it are for negative $\epsilon(\vec{k})$ and those outside are for positive $\epsilon(\vec{k})$.

the following three crossovers are observed.

(i) *Half filling:* The chemical potential μ is zero at the half filling state. The Fermi surface is given by $\pm k_x \pm k_y = \pi$. For small μ, we have,

$$\pm k_x \pm k_y = \pi + \frac{\mu}{2t \sin k_x}, \tag{G-33}$$

thus giving us an uninteresting modulation exponent, $\upsilon_L = 1$.

(ii) *Empty band:* When $\mu = -4t$, none of the states are occupied. As we increase μ by a tiny amount $\delta\mu$ above this value, we observe a non-zero modulation wave-vector,

$k = \sqrt{\delta\mu/t}$, thus showing a modulation exponent $\upsilon_L = 1/2$.

(iii) *Full inert bands:* When $\mu = +4t$, all the states are occupied. As we lower μ by a tiny amount $\delta\mu$ below this value, we observe a difference δk of the modulation vector from $\pm\hat{e}_x\pi \pm \hat{e}_y\pi$. We have, $\delta k = \sqrt{\delta\mu/t}$, thus showing a modulation exponent $\upsilon_L = 1/2$ again.

Tight binding model on the triangular lattice

The analysis of the triangular lattice within the tight binding approximation, is very similar to the square lattice discussed above. The dispersion $\epsilon(\vec{k})$ is given by

$$\epsilon(k) = -2t\cos k_x - 4t\cos\frac{k_x}{2}\cos\frac{k_y\sqrt{3}}{2}. \tag{G-34}$$

We have exponents similar to the square lattice.

(i) *Three-quarters filling:* The chemical potential $\mu = 2t$ corresponds to the three-quarters filling state. If we concentrate on the $\{k_x = \pi,\ k_y : -\pi/\sqrt{3} \rightarrow \pi/\sqrt{3}\}$ segment (same phenomenon is present at all the other segments of the quarter filling Fermi surface), we get,

$$\delta k_x \sim \frac{\delta\mu}{2\cos\left(\frac{k_y\sqrt{3}}{2}\right)}, \tag{G-35}$$

where $k_x = \pi + \delta k_x$ is obtained when $\mu = 2t + \delta\mu$. This leads to a modulation exponent of $\upsilon_L = 1$. The Fermi surfaces for chemical potentials μ close to three-quarters filling are schematically shown in Fig. 7.18.

(ii) *Empty band:* When $\mu = -6t$, none of the states is occupied. As we increase μ by

a tiny amount $\delta\mu$ above this value, we observe a non-zero modulation wave-vector, $k = \sqrt{2\delta\mu/3}$, thus showing a modulation exponent $\upsilon_L = 1/2$.

(iii) *Full inert bands:* When $\mu = 3t$, all of the states are occupied and close to this value the Fermi surface is composed of six small circles around $\vec{k} = \hat{x}\cos(n\pi/3) + \hat{y}\sin(n\pi/3)$, $n = \{0, 1, 2, 3, 4, 5\}$. If $\mu = 3t - \delta\mu$, we get, $|\delta\vec{k}| = 2\sqrt{\delta\mu/3}$, again giving us a modulation length exponent, $\upsilon_L = 1/2$.

Metal-Insulator transition

We discuss here the metal to band insulator transition at zero temperature. In a non-interacting system, this occurs when the Fermi energy is changed such that all occupied bands become completely full, as shown in Fig. 7.14. In the insulator, the Fermi energy lies in between two bands and thus the filled states are separated from the empty states by a finite energy gap. As the Fermi energy is tuned, the Fermi energy might touch one of the bands thereby rendering the system metallic. Close to this transition, the energy is quadratic in the momentum k, i.e., $|k| \propto |\delta\mu|^{1/2}$. This implies that,

$$|\delta k| \quad \propto \quad |\delta\mu|^{1/2}. \tag{G-36}$$

Following the scaling convention in Eq. (5.7), we adduce a similar exponent

$$\upsilon_L = 1/2 \tag{G-37}$$

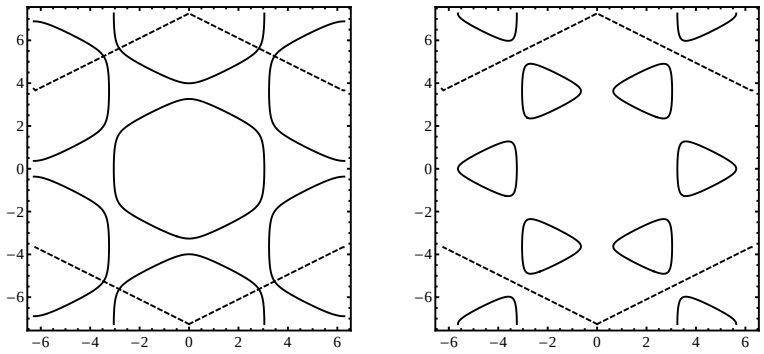

(a) $\mu = 1.8$ (b) $\mu = 2.2$

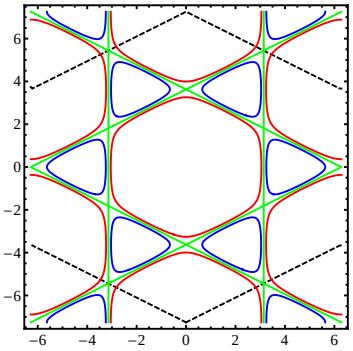

(c) $\mu = 2.2$(blue), $\mu = 2$(green) and $\mu = 1.8$(red)

Figure 7.18: Fermi surface for a triangular lattice with tight binding. The dashed lines are the Brillouin zone boundaries. This demonstrates a smooth crossover from one set of Fermi surface branches to another as μ is changed across $\mu = 2$. The points where the crossovers take place are $(0, \pm 2\pi/\sqrt{3})$, $(\pm\pi, \pm\pi/\sqrt{3})$. The modulation length exponent for this crossover is $\upsilon_L = 1$.

that governs the scaling of the modulation lengths with the shift $\delta\mu$ of the chemical potential (instead of temperature variations).

Dirac systems

The low energy physics of graphene and Dirac systems is characterized by the existence of Dirac points in momentum space where the density of states vanishes and the energy, $\epsilon(k)$ is proportional to the momentum k for small k. When we invoke and repeat our earlier analysis to these systems, we discern a trivial exponent

$$\begin{aligned} |\delta k| &\propto |\delta\mu| \\ \implies & \upsilon_{Dirac} = 1. \end{aligned} \tag{G-38}$$

This exponent may be contrasted with that derived from Eq. (G-37).

Topological Insulators – Multiple length scale exponents as a function of the chemical potential μ

The quintessential low energy physics of three-dimensional topological insulators can be gleaned from the following effective Hamiltonian[165] in momentum space,

$$\begin{aligned} H(\vec{k}) &= \epsilon_0(\vec{k}) I_{4\times 4} + \\ & \begin{pmatrix} \mathcal{M}(\vec{k}) & A_1 k_z & 0 & A_2 k_- \\ A_1 k_z & -\mathcal{M}(\vec{k}) & A_2 k_- & 0 \\ 0 & A_2 k_+ & \mathcal{M}(\vec{k}) & -A_1 k_z \\ A_2 k_+ & 0 & -A_1 k_z & -\mathcal{M}(\vec{k}) \end{pmatrix} \end{aligned} \tag{G-39}$$

where $\epsilon_0(\vec{k}) = C + D_1 k_z^2 + D_2 k_\perp^2$, $\mathcal{M}(\vec{k}) = M - B_1 k_z^2 - B_2 k_\perp^2$, with $k_\pm = k_x + i k_y$, $k_\perp = \sqrt{k_x^2 + k_y^2}$ and A_1, A_2, B_1, B_2, C, D_1 and D_2 constants for a given system. The

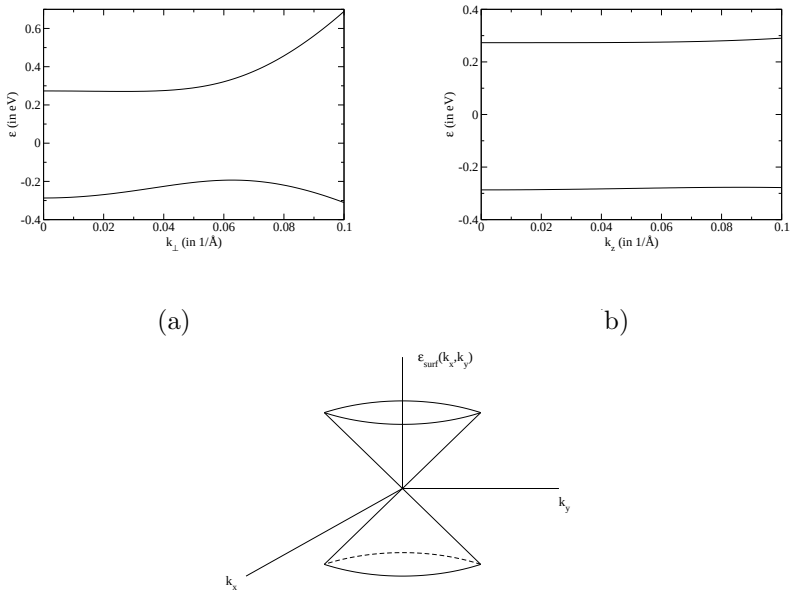

Figure 7.19: Energy levels of Bi_2Se_3 topological insulator.

7.19(a): $\epsilon(\vec{k})$ versus $k_\perp$ at $k_z = 0$; 7.19(b): $\epsilon(\vec{k})$ versus k_z at $k_\perp = 0$; 7.19(c): $\epsilon_{surf}(k_x, k_y)$ versus $\vec{k_\perp} \equiv (k_x, k_y)$.

energy bands are given by

$$\epsilon(\vec{k}) = \epsilon_0(\vec{k}) \pm \sqrt{\mathcal{M}(\vec{k})^2 + A_1 k_z^2 + A_2 k_\perp^2}. \tag{G-40}$$

These bands are plotted in Figs. 7.19(a) and 7.19(b). The finite gap between the two bands leads to an exponentially damped hopping amplitude, characterized by a finite correlation length when the Fermi energy lies within this gap. These energy bands

disperse quadratically for small k thus yielding

$$\begin{aligned} |\delta k| \quad &\propto \quad \sqrt{|\delta\mu|} \\ &\Longrightarrow \quad \upsilon_{bulk} = 1/2 \end{aligned} \tag{G-41}$$

whenever the correlation length diverges and a insulator to metal transition takes place in the bulk, thus allowing long range hopping. The same exponent is also expected whenever the modulation length becomes constant as μ crosses some threshold value.

The effective Hamiltonian for the surface states is given by

$$H_{surf} = \begin{pmatrix} 0 & A_2 k_- \\ A_2 k_+ & 0 \end{pmatrix}, \tag{G-42}$$

leading trivially to surface energies

$$\epsilon_{surf}(k_x, k_y) = \pm A_2 k_\perp. \tag{G-43}$$

Similar to the Dirac points in graphene (see Fig. 7.19(c)), we trivially find an exponent of

$$\upsilon_{surf} = 1. \tag{G-44}$$

An example of a zero temperature Fermi system in which υ_L is not half or one

Very large (or divergent) effective electronic masses m_{eff} can be found in heavy fermion systems (and at putative quantum critical points).[166, 167] If the electronic

dispersion $\epsilon(\vec{k})$ has a minimum at $\vec{k}_0$ then a Taylor expansion about that minimum trivially reads

$$\epsilon(\vec{k}) = \epsilon(\vec{k}_0) + \frac{\hbar^2}{2}\sum_{ij}\left(m_{eff}^{-1}\right)_{ij}(k_i - k_{0i})(k_j - k_{0j}) + \sum_{ijl} A_{ijl}(k_i - k_{0i})(k_j - k_{0j})(k_l - k_{0l}) + \ldots. \tag{G-45}$$

When present, parity relative to $\vec{k}_0$ or other considerations may limit this expansion to contain only even terms. As an example, we consider the dispersion

$$\epsilon(k) = c_1 - c_2(k^2 - k_0^2)^4, \tag{G-46}$$

where $c_2 > 0$. The hopping correlation function of such a system has a term which exhibits modulations at wave-vector $k = k_0$ at $\mu = \mu_* = c_1$. At higher values of the chemical potential, such a term ceases to exist. At lower values ($\mu = \mu_* - \delta\mu$), this term breaks up into two terms whose modulation wave-vectors are different from k_0 by,

$$\begin{aligned} k - k_0 \quad &\sim \quad \pm\frac{\delta\mu^{1/4}}{2k_0 c_2^{1/4}}, \\ &\Longrightarrow \quad \upsilon_L = 1/4. \end{aligned} \tag{G-47}$$

G.2 Finite temperature length scales – Scaling as a function of temperature

At finite temperatures, apart from the modulation lengths, there generally is a set of characteristic correlation lengths. From Eq. (G-26), these are obtained by finding

the poles (or other singularities) of the Fermi function. Along some direction $\hat{e}_0$, the wave-vector $\vec{k}_0 = \hat{e}_0 k_0$ is associated with a pole $k_0 = \pm 2\pi/L_0 \pm i/\xi_0$. At this wave-vector,

$$\epsilon(\vec{k_0}) = \mu + \frac{2n+1}{\beta} i, \tag{G-48}$$

where n is an integer. For a given μ, let us suppose that as we change the temperature, at $T = T_0$, we reach a saddle point of $\epsilon(\vec{k})$ in the complex plane of one of the Cartesian components of $\vec{k}$. Then, near this saddle point, the corresponding correlation and modulation lengths scale as,

$$\begin{aligned} |L_D - L_{D0}| &\propto |T - T_0|^{\nu_L}, \\ |\xi - \xi_0| &\propto |T - T_0|^{\nu_c}, \end{aligned} \tag{G-49}$$

where $\nu_L = \nu_c = 1/2$ in most cases (when the second derivative is not zero).

H Euler-Lagrange equations for scalar spin systems

We elaborate on the Euler-Lagrange equations associated with the free energy of Eq. (5.39) in Sec. 5.7. These assume the form,

$$\begin{aligned} \int d^d y \tilde{V}(\vec{x} - \vec{y}) S(\vec{y}) + \mu S(\vec{x}) \\ + u(S^2(\vec{x}) - 1) S(\vec{x}) = 0, \end{aligned} \tag{H-50}$$

where $\tilde{V}(\vec{x}) = [V(\vec{x}) + V(-\vec{x})]/2$. For example, if we consider the finite ranged system for which,

$$\begin{aligned} \int d^d y \tilde{V}(\vec{x}-\vec{y}) S(\vec{y}) &= a\nabla^2 S(\vec{x}) \\ &\quad + b\nabla^4 S(\vec{x}) + \ldots, \end{aligned} \tag{H-51}$$

then, we have,

$$\begin{aligned} a\nabla^2 S(\vec{x}) &+ b\nabla^4 S(\vec{x}) + \ldots + \mu S(\vec{x}) \\ &+ u(S^2(\vec{x}) - 1) S(\vec{x}) = 0. \end{aligned} \tag{H-52}$$

For lattice systems, the Euler Lagrange equation (H-50) reads

$$\begin{aligned} \sum_{\vec{y}} \tilde{V}(\vec{x}-\vec{y}) S(\vec{y}) &+ \mu S(\vec{x}) \\ &+ u(S^2(\vec{x}) - 1) S(\vec{x}) = 0. \end{aligned} \tag{H-53}$$

In general, it may be convenient to express the linear terms in the above equation in terms of the lattice Laplacian Δ. We write

$$D(\Delta) S(\vec{x}) \equiv \sum_{\vec{y}} \tilde{V}(\vec{x}-\vec{y}) S(\vec{y}) + \mu S(\vec{x}), \tag{H-54}$$

D being some operator which is a function of the lattice Laplacian Δ. The real-space lattice Laplacian Δ, given by the Fourier transform of Eq. (2.7), acts on a general field f as

$$\Delta f(\vec{x}) \equiv -\sum_{i=1}^{d} [f(\vec{x} + \hat{e}_i) + f(\vec{x} - \hat{e}_i) - 2f(\vec{x})]. \tag{H-55}$$

Here, $\{\hat{e}_i\}$ denote unit vectors along the Cartesian directions. (In the continuum limit, Δ can be replaced by $-\nabla^2$.) The Euler-Lagrange equation then, takes the form,

$$D(\Delta)S(\vec{x}) + u(S^2(\vec{x}) - 1)S(\vec{x}) = 0. \tag{H-56}$$

Equation H-51 corresponds, on the lattice, to

$$\begin{aligned} \sum_{\vec{y}} \tilde{V}(\vec{x} - \vec{y})S(\vec{y}) \quad &= \\ &-a\Delta S(\vec{x}) + b\Delta^2 S(\vec{x}) + \ldots. \end{aligned} \tag{H-57}$$

The Euler Lagrange equation for this finite ranged system reads

$$\begin{aligned} -a\Delta S(\vec{x}) \quad &+ \quad b\Delta^2 S(\vec{x}) + \ldots + \mu S(\vec{x}) \\ &+ \quad u(S^2(\vec{x}) - 1)S(\vec{x}) = 0. \end{aligned} \tag{H-58}$$

Bibliography

[1] A. Mesaros, K. Fujita, H. Eisaki, S. Uchida, J. C. Davis, S. Sachdev, J. Zaanen, M. J. Lawler, and Eun-Ah Kim. Topological defects coupling smectic modulations to intraunit-cell nematicity in cuprates. *Science*, 333(6041):426–430, 2011.

[2] Michael Seul and David Andelman. Domain shapes and patterns: The phenomenology of modulated phases. *Science*, 267(5197):476–483, 1995.

[3] Per Bak and J. von Boehm. Ising model with solitons, phasons, and "the devil's staircase". *Phys. Rev. B*, 21:5297–5308, Jun 1980.

[4] A. Gendiar and T. Nishino. Phase diagram of the three-dimensional axial next-nearest-neighbor Ising model. *Phys. Rev. B*, 71:024404, Jan 2005.

[5] J. C. Sprott. Simple chaotic systems and circuits. *American Journal of Physics*, 68(8):758–763, 2000.

[6] Peter Ronhovde and Zohar Nussinov. Multiresolution community detection for

megascale networks by information-based replica correlations. *Phys. Rev. E*, 80(1):016109, Jul 2009.

[7] J. A. Moriarty and M. Widom. First-principles interatomic potentials for transition-metal alumnides: Theory and trends across the 3d series. *Phys. Rev. B*, 56(13), Oct 1997.

[8] J. Stadler, R. Mikulla, and H. R. Trebin. IMD: A software package for molecular dynamics studies on parallel computers. *International Journal of Modern Physics C*, 8(5):1131–1140, Jun 1997.

[9] Walter Kob and Hans C. Andersen. Testing mode-coupling theory for a supercooled binary Lennard-Jones mixture I: The van Hove correlation function. *Phys. Rev. E*, 51(5):4626–4641, May 1995.

[10] S.K. Ma. *Modern Theory Of Critical Phenomena*. Advanced Book Classics. Perseus, 2000.

[11] Kenneth G. Wilson. Renormalization group and critical phenomena. I. renormalization group and the Kadanoff scaling picture. *Phys. Rev. B*, 4:3174–3183, Nov 1971.

[12] M E Fisher. The theory of equilibrium critical phenomena. *Reports on Progress in Physics*, 30(2):615, 1967.

[13] The approach of defining an order parameter does not work in many situations, e.g., gauge theories, classical XY models, one-dimensional quantum spin chains, etc. .

[14] Ernst Ising. Beitrag zur theorie des ferromagnetismus. *Zeitschrift für Physik A Hadrons and Nuclei*, 31:253–258, 1925.

[15] T. Dauxois, S. Ruffo, E. Arimondo, and M. Wilkens. *Dynamics and Thermodynamics of Systems With Long Range Interactions*. Lecture Notes in Physics. Springer, Berlin Heidelberg, 2010.

[16] Alessandro Giuliani, Joel L. Lebowitz, and Elliott H. Lieb. Striped phases in two-dimensional dipole systems. *Phys. Rev. B*, 76:184426, Nov 2007.

[17] Alessandro Giuliani, Joel L. Lebowitz, and Elliott H. Lieb. Ising models with long-range antiferromagnetic and short-range ferromagnetic interactions. *Phys. Rev. B*, 74:064420, Aug 2006.

[18] Alessandro Vindigni, Niculin Saratz, Oliver Portmann, Danilo Pescia, and Paolo Politi. Stripe width and nonlocal domain walls in the two-dimensional dipolar frustrated Ising ferromagnet. *Phys. Rev. B*, 77:092414, Mar 2008.

[19] C. Ortix, J. Lorenzana, and C. Di Castro. Frustrated phase separation in two-dimensional charged systems. *Phys. Rev. B*, 73:245117, Jun 2006.

[20] István Daruka and Zsolt Gulácsi. Correlation transitions in the Ising chain with competing short-range and long-range mirror interactions. *Phys. Rev. E*, 58:5403–5409, Nov 1998.

[21] Daniel G. Barci and Daniel A. Stariolo. Orientational order in two dimensions from competing interactions at different scales. *Phys. Rev. B*, 79:075437, Feb 2009.

[22] Michael Fogler. Stripe and bubble phases in quantum hall systems. In C. Berthier, L. Lévy, and G. Martinez, editors, *High Magnetic Fields*, volume 595 of *Lecture Notes in Physics*, pages 98–138. Springer, Berlin Heidelberg, 2002.

[23] Hyung-June Woo, Carlo Carraro, and David Chandler. Quantitative molecular interpretation of mesoscopic correlations in bicontinuous microemulsions. *Phys. Rev. E*, 52:6497–6507, Dec 1995.

[24] Frank H. Stillinger. Variational model for micelle structure. *The Journal of Chemical Physics*, 78(7):4654–4661, 1983.

[25] Ludwik Leibler. Theory of microphase separation in block copolymers. *Macromolecules*, 13(6):1602–1617, 1980.

[26] Takao Ohta and Kyozi Kawasaki. Equilibrium morphology of block copolymer melts. *Macromolecules*, 19(10):2621–2632, 1986.

[27] H. Kleinert. *Gauge fields in condensed matter*. Number v. 2 in Gauge Fields in Condensed Matter. World Scientific, 1989.

[28] Pierre-Henri Chavanis. Statistical mechanics of two-dimensional vortices and stellar systems. In Thierry Dauxois, Stefano Ruffo, Ennio Arimondo, and Martin Wilkens, editors, *Dynamics and Thermodynamics of Systems with Long-Range Interactions*, volume 602 of *Lecture Notes in Physics*, pages 208–289. Springer Berlin Heidelberg, 2002.

[29] H. Kleinert. *Gauge fields in condensed matter*. Number v. 1 in Gauge Fields in Condensed Matter. World Scientific, 1989.

[30] Yves Elskens. Kinetic theory for plasmas and wave-particle hamiltonian dynamics. In Thierry Dauxois, Stefano Ruffo, Ennio Arimondo, and Martin Wilkens, editors, *Dynamics and Thermodynamics of Systems with Long-Range Interactions*, volume 602 of *Lecture Notes in Physics*, pages 437–447. Springer Berlin Heidelberg, 2002.

[31] Y Elskens and D Escande. Microscopic dynamics of plasmas and chaos. *Plasma Physics and Controlled Fusion*, 45(4):521, 2003.

[32] V.J. Emery and S.A. Kivelson. Frustrated electronic phase separation and high-temperature superconductors. *Physica C: Superconductivity*, 209(4):597 – 621, 1993.

[33] L. Chayes, V.J. Emery, S.A. Kivelson, Z. Nussinov, and G. Tarjus. Avoided critical behavior in a uniformly frustrated system. *Physica A: Statistical Mechanics and its Applications*, 225(1):129 – 153, 1996.

[34] Zohar Nussinov, Joseph Rudnick, Steven A. Kivelson, and L. N. Chayes. Avoided critical behavior in $O(n)$ systems. *Phys. Rev. Lett.*, 83:472–475, Jul 1999.

[35] U. Löw, V. J. Emery, K. Fabricius, and S. A. Kivelson. Study of an Ising model with competing long- and short-range interactions. *Phys. Rev. Lett.*, 72(12):1918–1921, Mar 1994.

[36] E. W. Carlson, V. J. Emery, S. A. Kivelson, and D. Orgad. Concepts in high temperature superconductivity. In K. H. Bennemann and John B. Ketterson, editors, *Superconductivity*, chapter 21, pages 1225–1348. Springer Berlin Heidelberg, 2008. See also arXiv:cond-mat/0206217.

[37] V. B. Nascimento, Ang Li, Dilushan R. Jayasundara, Yi Xuan, Jared O'Neal, Shuheng Pan, T. Y. Chien, Biao Hu, X. B. He, Guorong Li, A. S. Sefat, M. A. McGuire, B. C. Sales, D. Mandrus, M. H. Pan, Jiandi Zhang, R. Jin, and E. W. Plummer. Surface geometric and electronic structures of $BaFe_2As_2(001)$. *Phys. Rev. Lett.*, 103:076104, Aug 2009.

[38] S-W. Cheong, G. Aeppli, T. E. Mason, H. Mook, S. M. Hayden, P. C. Can-

field, Z. Fisk, K. N. Clausen, and J. L. Martinez. Incommensurate magnetic fluctuations in $La_{2-x}Sr_xCuO_4$. *Phys. Rev. Lett.*, 67:1791–1794, Sep 1991.

[39] D. I. Golosov. Magnetic domain walls in single-phase and phase-separated double-exchange systems. *Phys. Rev. B*, 67:064404, Feb 2003.

[40] Daniel Kivelson, Steven A. Kivelson, Xiaolin Zhao, Zohar Nussinov, and Gilles Tarjus. A thermodynamic theory of supercooled liquids. *Physica A: Statistical and Theoretical Physics*, 219(1-2):27 – 38, 1995.

[41] Jörg Schmalian and Peter G. Wolynes. Stripe glasses: Self-generated randomness in a uniformly frustrated system. *Phys. Rev. Lett.*, 85:836–839, Jul 2000.

[42] M. Grousson, G. Tarjus, and P. Viot. Phase diagram of an Ising model with long-range frustrating interactions: A theoretical analysis. *Phys. Rev. E*, 62(6):7781–7792, Dec 2000.

[43] Zohar Nussinov. Avoided phase transitions and glassy dynamics in geometrically frustrated systems and non-abelian theories. *Phys. Rev. B*, 69:014208, 2004.

[44] G Tarjus, S A Kivelson, Z Nussinov, and P Viot. The frustration-based approach of supercooled liquids and the glass transition: a review and critical assessment. *Journal of Physics: Condensed Matter*, 17(50):R1143, 2005.

[45] B. V. Derjaguin and L. Landau, Acta Physiochim, URSS **14**, 633 (1941); E. J. Verwey and J. T. G. Overbeek *Theory of Stability of Lyophobic Colloids* (Elsevier, Amsterdam, 1948).

[46] C. Reichhardt and C. J. Olson. Novel colloidal crystalline states on two-dimensional periodic substrates. *Phys. Rev. Lett.*, 88:248301, May 2002.

[47] Julien Barré, David Mukamel, and Stefano Ruffo. Ensemble inequivalence in mean-field models of magnetism. In Thierry Dauxois, Stefano Ruffo, Ennio Arimondo, and Martin Wilkens, editors, *Dynamics and Thermodynamics of Systems with Long-Range Interactions*, volume 602 of *Lecture Notes in Physics*, pages 45–67. Springer Berlin Heidelberg, 2002.

[48] Mark Ya. Azbel'. Long-range interaction and heterogeneity yield a different kind of critical phenomenon. *Phys. Rev. E*, 68:050901, Nov 2003.

[49] S. Elitzur. Impossibility of spontaneously breaking local symmetries. *Phys. Rev. D*, 12:3978–3982, Dec 1975.

[50] John B. Kogut. An introduction to lattice gauge theory and spin systems. *Rev. Mod. Phys.*, 51:659–713, Oct 1979.

[51] X.G. Wen. *Quantum Field Theory of Many-Body Systems: From the Origin of Sound to an Origin of Light and Electrons*. Oxford graduate texts in mathematics. Oxford University Press, 2007.

[52] G. Ortiz, E. Cobanera, and Z. Nussinov. Dualities and the phase diagram of the p-clock model. *Nuclear Physics B*, 854(3):780 – 814, 2012.

[53] F. C. Frank. Supercooling of liquids. *Proceedings of the Royal Society of London. Series A. Mathematical and Physical Sciences*, 215(1120):43–46, 1952.

[54] C. Dasgupta, A. V. Indrani, Sriram Ramaswamy, and M. K. Phani. Is there a growing correlation length near the glass transition? *Europhysics Letters*, 15(3):307, 1991.

[55] Paul J. Steinhardt, David R. Nelson, and Marco Ronchetti. Bond-orientational order in liquids and glasses. *Phys. Rev. B*, 28(2):784–805, 1983.

[56] G. Voronoi. Nouvelles applications des paramètres continus à la théorie des formes quadratiques. Deuxième mémoire. Recherches sur les paralléllοèdres primitifs. *Journal für die reine und angewandte Mathematik*, 134:198–287, 1908.

[57] J. Dana Honeycutt and Hans C. Andersen. Molecular dynamics study of melting and freezing of small Lennard-Jones clusters. *J. Phys. Chem.*, 91(19):4950–4963, Sep 1987.

[58] Saurish Chakrabarty and Zohar Nussinov. High-temperature correlation functions: Universality, extraction of exchange interactions, divergent correlation lengths, and generalized Debye length scales. *Phys. Rev. B*, 84:064124, Aug 2011.

[59] Saurish Chakrabarty and Zohar Nussinov. Modulation and correlation lengths in systems with competing interactions. *Phys. Rev. B*, 84:144402, Oct 2011.

[60] P. Ronhovde, S. Chakrabarty, D. Hu, M. Sahu, K. Sahu, K. Kelton, N. Mauro, and Z. Nussinov. Detecting hidden spatial and spatio-temporal structures in glasses and complex physical systems by multiresolution network clustering. *Euro. Phys. J. E*, 34:1–24, 2011.

[61] P. Ronhovde, S. Chakrabarty, D. Hu, M. Sahu, K. K. Sahu, K. F. Kelton, N. A. Mauro, and Z. Nussinov. Detection of hidden structures for arbitrary scales in complex physical systems. *Sci. Rep.*, 2:329, 2012.

[62] H. E. Stanley. Spherical model as a limit of infinite spin dimensionality. *Phys. Rev.*, 176(2):718–722, 1968.

[63] T. H. Berlin and M. Kac. The spherical model of a ferromagnet. *Phys. Rev.*, 86:821–835, Jun 1952.

[64] P. Debye and E. Hückel. Debye-Hückel theory of electrolytes. *Phys. Z*, 24:185, 1923.

[65] G.S. Rushbrooke and P.J. Wood. On the Curie points and high temperature susceptibilities of Heisenberg model ferromagnetics. *Molecular Physics*, 1(3):257–283, 1958.

[66] H. E. Stanley and T. A. Kaplan. High-temperature expansions-the classical Heisenberg model. *Phys. Rev. Lett.*, 16:981–983, May 1966.

[67] K. Huang. *Statistical mechanics*. Wiley, 1987.

[68] J. Horbach, W. Kob, and K. Binder. Molecular dynamics simulation of the dynamics of supercooled silica. *Philosophical Magazine Part B*, 77(2):297–303, 1998.

[69] R. L. Stratonovich. On a method of calculating quantum distribution functions. *Soviet Physics Doklady*, 2:416, 1958.

[70] J. Hubbard. Calculation of partition functions. *Phys. Rev. Lett.*, 3:77–78, Jul 1959.

[71] Y.M. Ivanchenko and A.A. Lisyansky. *Physics of Critical Fluctuations*. Graduate Texts in Contemporary Physics. Springer-Verlag, 1995.

[72] The integrals in Eq.(3.3) converge if $v(\vec{k})$ is negative for all real $\vec{k}$. This can be achieved for all systems with finite range or screened interactions (with an arbitrarily large screening length) when $v(\vec{k})$ is bounded from above. As $(\vec{S}(\vec{x}))^2 = n$ for all $\vec{x}$, the kernel $v(\vec{k})$ for all $\vec{k}$ can be trivially made negative before performing the HS transformation by $V(\vec{x}) \to V(\vec{x}) + a\delta_{\vec{x},0}$ which merely shifts the energy by an additive constant, $H \to H + anN/2$, without changing any averages.

[73] R. L. Henderson. A uniqueness theorem for fluid pair correlation functions. *Physics Letters A*, 49(3):197 – 198, 1974.

[74] By "long range" we refer to systems for which $V(\vec{x})$ is not exactly zero for arbitrary large $\vec{x}$. In d spatial dimensions, for large distances, $|V(\vec{x})| \propto \exp(-|\vec{x}|/\lambda)/x^a$ with $0 \leq a \leq d$ and λ is a "screening length" which can in principle be arbitrarily large.

[75] By "charge neutrality", we mean that $\sum_{\vec{y}} \vec{S}(\vec{y}) = 0$ and, consequently, $\langle \vec{S}(\vec{x}) \cdot \sum_{\vec{y}} \vec{S}(\vec{y}) \rangle = 0 \implies \sum_{\vec{z}} G(\vec{z}) = 0$.

[76] Z. Nussinov, C. D. Batista, B. Normand, and S. A. Trugman. High-dimensional fractionalization and spinon deconfinement in pyrochlore antiferromagnets. *Phys. Rev. B*, 75:094411, Mar 2007.

[77] N.H. March and P. Tosi. *Atomic Dynamics in Liquids*. Dover Books on Physics and Chemistry. Dover, 1991.

[78] I. Dzyaloshinsky. A thermodynamic theory of weak ferromagnetism of antiferromagnetics. *Journal of Physics and Chemistry of Solids*, 4(4):241 – 255, 1958.

[79] Tôru Moriya. Anisotropic superexchange interaction and weak ferromagnetism. *Phys. Rev.*, 120:91–98, Oct 1960.

[80] Kliment I Kugel and D I Khomskii. The Jahn-Teller effect and magnetism: transition metal compounds. *Soviet Physics Uspekhi*, 25(4):231, 1982.

[81] Zohar Nussinov and Eduardo Fradkin. Discrete sliding symmetries, dualities, and self-dualities of quantum orbital compass models and $p+ip$ superconducting arrays. *Phys. Rev. B*, 71:195120, May 2005.

[82] Ran Budnik and Assa Auerbach. Low-energy singlets in the Heisenberg antiferromagnet on the Kagome lattice. *Phys. Rev. Lett.*, 93:187205, Oct 2004.

[83] Alexei Kitaev. Anyons in an exactly solved model and beyond. *Annals of Physics*, 321(1):2 – 111, 2006.

[84] J. F. Sadoc and R. Mosseri. *Geometrical Frustration*. Cambridge University Press, 1999.

[85] J. F. Sadoc and F. Mosseri. *Amorphous Materials*. American Institute of Metallurgical Engineering New York, 1983.

[86] D. R. Nelson. *Defects and Geometry in Condensed Matter Physics*. Cambridge University Press, 2002.

[87] Sadoc, J.F. Periodic networks of disclination lines : application to metal structures. *J. Physique Lett.*, 44(17):707–715, 1983.

[88] Sadoc, J.F. and Charvolin, J. Frustration in bilayers and topologies of liquid crystals of amphiphilic molecules. *J. Phys. France*, 47(4):683–691, 1986.

[89] David R. Nelson and Michael Widom. Symmetry, Landau theory and polytope models of glass. *Nuclear Physics B*, 240(1):113 – 139, 1984.

[90] David R. Nelson. Order, frustration, and defects in liquids and glasses. *Phys. Rev. B*, 28:5515–5535, Nov 1983.

[91] James P. Sethna. Frustration, curvature, and defect lines in metallic glasses and the cholesteric blue phase. *Phys. Rev. B*, 31:6278–6297, May 1985.

[92] Subir Sachdev and David R. Nelson. Statistical mechanics of pentagonal and icosahedral order in dense liquids. *Phys. Rev. B*, 32:1480–1502, Aug 1985.

[93] J. L. Lebowitz and J. K. Percus. Mean spherical model for lattice gases with extended hard cores and continuum fluids. *Phys. Rev.*, 144:251–258, Apr 1966.

[94] Here, we adhere to the prevalent practice of effectively setting $\beta = 1$ (with the temperature dependence relegated solely to the prefactor r of Eq.(3.30)).

[95] Shang-keng Ma. Critical exponents above T_c to $O(\frac{1}{n})$. *Phys. Rev. A*, 7:2172–2187, Jun 1973.

[96] Kenneth G. Wilson and Michael E. Fisher. Critical exponents in 3.99 dimensions. *Phys. Rev. Lett.*, 28:240–243, Jan 1972.

[97] C. B. Muratov. Theory of domain patterns in systems with long-range interactions of Coulomb type. *Phys. Rev. E*, 66(6):066108, Dec 2002.

[98] Z. Nussinov, arXiv:cond-mat/0105253 (2001) – in particular, see footnote [20] therein for the Ising ground states.

[99] John Stephenson. Ising model with antiferromagnetic next-nearest-neighbor coupling: Spin correlations and disorder points. *Phys. Rev. B*, 1:4405–4409, Jun 1970.

[100] John Stephenson. Range of order in antiferromagnets with next-nearest neighbor coupling. *Canadian Journal of Physics*, 48(18):2118–2122, 1970.

[101] Nelson Alves Jr. and Carlos S. O. Yokoi. Spin pair correlation of the ANNNI chain in a field. *Brazilian Journal of Physics*, 30:667 – 670, 12 2000.

[102] Walter Selke. The ANNNI model – theoretical analysis and experimental application. *Physics Reports*, 170(4):213 – 264, 1988.

[103] S A Brazovskii. Phase transition of an isotropic system to a nonuniform state. *Sov Phys JETP*, 41(1):85, 1975.

[104] Harry Westfahl, Jörg Schmalian, and Peter G. Wolynes. Self-generated randomness, defect wandering, and viscous flow in stripe glasses. *Phys. Rev. B*, 64:174203, Oct 2001.

[105] J. Schmalian and M. Turlakov, Phys. Rev. Lett. **93**, 036405 (2004).

[106] R. J. Elliott. Phenomenological discussion of magnetic ordering in the heavy rare-earth metals. *Phys. Rev.*, 124:346–353, Oct 1961.

[107] Michael E. Fisher and Walter Selke. Infinitely many commensurate phases in a simple Ising model. *Phys. Rev. Lett.*, 44:1502–1505, Jun 1980.

[108] R. B. Griffiths. *Fundamental problems in statistical mechanics VII.* H. van Beijeren, Amsterdam, North Holland, 1990. pp. 69–110.

[109] An initial and far more cursory treatment appeared in Z. Nussinov, arXiv:cond-mat/0506554 (2005), unpublished.

[110] See Eq. (C29) of Ref. [43].

[111] T R Kirkpatrick and D Thirumalai. Random solutions from a regular density functional hamiltonian: a static and dynamical theory for the structural glass transition. *Journal of Physics A: Mathematical and General*, 22(5):L149, 1989.

[112] G is a function of k^2 for rotationally symmetric systems. Similarly, for a reflection invariant system (invariant under $k_l \to -k_l$), G is a function of (k_l^2) when $k_{l' \neq l}$ are held fixed. The results described in Sec. 5.2.5 hold, *mutatis mutandis*, for any component k_l in such reflection invariant systems.

[113] S. Redner and H. E. Stanley. The R-S model for magnetic systems with competing interactions: series expansions and some rigorous results. *J. Phys. C*, 10(23):4765, 1977.

[114] S. Redner and H. E. Stanley. Helical order and its onset at the Lifshitz point. *Phys. Rev. B*, 16(11):4901–4906, Dec 1977.

[115] J Oitmaa. A high temperature series study of the annni model in two and three dimensions. *J. Phys. A*, 18(2):365, 1985.

[116] D Mukamel. Critical behaviour associated with helical order near a Lifshitz point. *J. Phys. A*, 10(12):L249, 1977.

[117] R. M. Hornreich, Marshall Luban, and S. Shtrikman. Critical behavior at the onset of $\vec{k}$-space instability on the λ line. *Phys. Rev. Lett.*, 35(25):1678–1681, Dec 1975.

[118] Kai Zhang and Patrick Charbonneau. Monte Carlo approach for studying microphases applied to the axial next-nearest-neighbor Ising and the Ising-Coulomb models. *Phys. Rev. B*, 83:214303, Jun 2011.

[119] P Bak. Commensurate phases, incommensurate phases and the devil's staircase. *Reports on Progress in Physics*, 45(6):587, 1982.

[120] We thank Michael Ogilvie for prompting us to think about this generalization.

[121] Carl M. Bender and Stefan Boettcher. Real spectra in non-Hermitian Hamiltonians having $\mathcal{PT}$ symmetry. *Phys. Rev. Lett.*, 80:5243–5246, Jun 1998.

[122] B.D. Josephson. Relation between the superfluid density and order parameter for superfluid he near tc. *Physics Letters*, 21(6):608 – 609, 1966.

[123] H. Thomas. *Nonlinear dynamics in solids*. Springer-Verlag, 1992.

[124] Dandan Hu, Peter Ronhovde, and Zohar Nussinov. Phase transitions in random Potts systems and the community detection problem: spin-glass type and dynamic perspectives. *Philosophical Magazine*, 92(4):406–445, 2012.

[125] Yves Pomeau and Paul Manneville. Intermittent transition to turbulence in dissipative dynamical systems. *Communications in Mathematical Physics*, 74:189–197, 1980.

[126] W. Klement, R. H. Willens, and Pol Duwez. Non-crystalline structure in solidified gold-silicon alloys. *Nature*, 187:869–870, 1960.

[127] M. H. Cohen and D. Turnbull. Composition requirements for glass formation in metallic and ionic systems. *Nature*, 189:131–132, 1961.

[128] W.H. Wang, C. Dong, and C.H. Shek. Bulk metallic glasses. *Materials Science and Engineering: R: Reports*, 44(23):45 – 89, 2004.

[129] Subir Sachdev and David R. Nelson. Theory of the structure factor of metallic glasses. *Phys. Rev. Lett.*, 53:1947–1950, Nov 1984.

[130] Daniel B. Miracle. A structural model for metallic glasses. *Nature Materials*, 3:697–702, Oct 2004.

[131] IMD website: `http://www.itap.physik.uni-stuttgart.de/~imd`.

[132] G. Kresse and J. Hafner. Ab initio molecular dynamics for liquid metals. *Phys. Rev. B*, 47(1):558–561, Jan 1993.

[133] G. Kresse and J. Furthmüller. Efficient iterative schemes for ab initio total-energy calculations using a plane-wave basis set. *Phys. Rev. B*, 54(16):11169–11186, Oct 1996.

[134] VASP website: `http://www.vasp.at`.

[135] P. W. Anderson. *Science*, 267(5204):1610, 1995.

[136] D. B. Miracle, W. S. Sanders, and O. N. Senkov. The influence of efficient atomic packing on the constitution of metallic glasses. *Philos. Mag.*, 83(20):2409–2428, Jul 2003.

[137] T. Schenk, D. Holland-Moritz, V. Simonet, R. Bellissent, and D. M. Herlach. Icosahedral short-range order in deeply undercooled metallic melts. *Phys. Rev. Lett.*, 89(7):075507, Jul 2002.

[138] K. F. Kelton, G. W. Lee, A. K. Gangopadhyay, R. W. Hyers, T. J. Rathz, J. R. Rogers, M. B. Robinson, and D. S. Robinson. First x-ray scattering studies on electrostatically levitated metallic liquids: Demonstrated influence of local icosahedral order on the nucleation barrier. *Phys. Rev. Lett.*, 90(19):195504, May 2003.

[139] M. E. J. Newman. The physics of networks. *Phys. Today*, 61(11):33–38, 2008.

[140] P. Ronhovde and Z. Nussinov. An improved Potts model applied to community detection. *Phys. Rev. E*, 81(046114), 2010.

[141] Marina Meilă. Comparing clusterings – an information based distance. *J. Multivariate Anal.*, 98:873–895, 2007.

[142] Leon Danon, Albert Díaz-Guilera, Jordi Duch, and Alex Arenas. Comparing community structure identification. *J. Stat. Mech.: Theory Exp.*, 9(9):P09008, 2005.

[143] L.-C. Valdes, F. Affouard, M. Descamps, and J. Habasaki. Mixing effects in glass-forming Lennard-Jones mixtures. *The Journal of Chemical Physics*, 130(15):154505, 2009.

[144] By "connected contours", we refer to contours whose links connect nearest neighbor sites. For general interactions, the individual links may have arbitrary length and weight. Albeit some notable differences, this is, essentially, reflected in our expansion where $V(\vec{x}-\vec{y})$ is, in general, a link connecting sites $\vec{x}$ and $\vec{y}$.

[145] J. Binney. *The Theory of Critical Phenomena: An Introduction to the Renormalization Group*. Oxford Science Publications. Clarendon Press, 1992.

[146] The general Hamiltonian that V encodes allows for (constant) on-site energies is a trivial generalization of Eq.(1): $H = \frac{1}{2}\sum_{\vec{x},\vec{y}} V(|\vec{x}-\vec{y}|)\vec{S}(\vec{x})\cdot\vec{S}(\vec{y})$ that also includes a sum over sites $\vec{x}=\vec{y}$ (i.e., allows for $V(\vec{x}=0)\neq 0$).

[147] Robert B. Griffiths. Correlations in Ising ferromagnets. I. *Journal of Mathematical Physics*, 8(3):478–483, 1967.

[148] M. Born and H. S. Green. A general kinetic theory of liquids I. the molecular distribution functions. *Proceedings of the Royal Society of London. Series A. Mathematical and Physical Sciences*, 188(1012):10–18, 1946.

[149] Jerome K. Percus and George J. Yevick. Analysis of classical statistical mechanics by means of collective coordinates. *Phys. Rev.*, 110:1–13, Apr 1958.

[150] Myron B. Salamon and Marcelo Jaime. The physics of manganites: Structure and transport. *Rev. Mod. Phys.*, 73:583–628, Aug 2001.

[151] B. Kalisky, J. R. Kirtley, J. G. Analytis, Jiun-Haw Chu, A. Vailionis, I. R. Fisher, and K. A. Moler. Stripes of increased diamagnetic susceptibility in underdoped superconducting $Ba(Fe_{1-x}Co_x)_2As_2$ single crystals: Evidence for an enhanced superfluid density at twin boundaries. *Phys. Rev. B*, 81:184513, May 2010.

[152] John R. Kirtley, Beena Kalisky, Lan Luan, and Kathryn A. Moler. Meissner response of a bulk superconductor with an embedded sheet of reduced penetration depth. *Phys. Rev. B*, 81:184514, May 2010.

[153] J. M. Tranquada, B. J. Sternlieb, J. D. Axe, Y. Nakamura, and S. Uchida. Evidence for stripe correlations of spins and holes in copper oxide superconductors. *Nature*, 375:561–563, 1995.

[154] K. Yamada, C. H. Lee, K. Kurahashi, J. Wada, S. Wakimoto, S. Ueki,

H. Kimura, Y. Endoh, S. Hosoya, G. Shirane, R. J. Birgeneau, M. Greven, M. A. Kastner, and Y. J. Kim. Doping dependence of the spatially modulated dynamical spin correlations and the superconducting-transition temperature in $La_{2-x}Sr_xCuO_4$. *Phys. Rev. B*, 57:6165–6172, Mar 1998.

[155] Steven R. White and D. J. Scalapino. Density matrix renormalization group study of the striped phase in the 2d $t-J$ model. *Phys. Rev. Lett.*, 80:1272–1275, Feb 1998.

[156] Jan Zaanen and Olle Gunnarsson. Charged magnetic domain lines and the magnetism of high-T_c oxides. *Phys. Rev. B*, 40:7391–7394, Oct 1989.

[157] Kazushige and Machida. Magnetism in la2cuo4 based compounds. *Physica C: Superconductivity*, 158(12):192 – 196, 1989.

[158] A. A. Koulakov, M. M. Fogler, and B. I. Shklovskii. Charge density wave in two-dimensional electron liquid in weak magnetic field. *Phys. Rev. Lett.*, 76:499–502, Jan 1996.

[159] M. P. Lilly, K. B. Cooper, J. P. Eisenstein, L. N. Pfeiffer, and K. W. West. Evidence for an anisotropic state of two-dimensional electrons in high Landau levels. *Phys. Rev. Lett.*, 82:394–397, Jan 1999.

[160] R.R. Du, D.C. Tsui, H.L. Stormer, L.N. Pfeiffer, K.W. Baldwin, and K.W.

West. Strongly anisotropic transport in higher two-dimensional Landau levels. *Solid State Communications*, 109(6):389 – 394, 1999.

[161] J Zaanen. High-temperature superconductivity: Stripes defeat the Fermi liquid. *Nature*, 404(6779):714–715, 2000.

[162] S. A. Kivelson, I. P. Bindloss, E. Fradkin, V. Oganesyan, J. M. Tranquada, A. Kapitulnik, and C. Howald. How to detect fluctuating stripes in the high-temperature superconductors. *Rev. Mod. Phys.*, 75(4):1201–1241, Oct 2003.

[163] G. Grüner. The dynamics of charge-density waves. *Rev. Mod. Phys.*, 60:1129–1181, Oct 1988.

[164] G. Grüner. *Density Waves In Solids*. Frontiers in Physics. Perseus Pub., 2000.

[165] Haijun Zhang, Chao-Xing Liu, Xiao-Liang Qi, Xi Dai, Zhong Fang, and Shou-Cheng Zhang. Topological insulators in Bi_2Se_3, Bi_2Te_3 and Sb_2Te_3 with a single Dirac cone on the surface. *Nat. Phys.*, 5:438–442, 2009.

[166] C. M. Varma, Z. Nussinov, and Wim van Saarloos. Singular or non-Fermi liquids. *Physics Reports*, 361(5-6):267 – 417, 2002.

[167] P Coleman, C Pépin, Qimiao Si, and R Ramazashvili. How do Fermi liquids get heavy and die? *Journal of Physics: Condensed Matter*, 13(35):R723, 2001.